OSLO METROPOLITAN UNIVERSITY
STORBYUNIVERSITETET

Master's Thesis

Master's Program in Biomedicine
August 2021

General control nonderepressible two (GCN2) as a therapeutic target for prostate cancer

Shanima Shanu Mirza

MABIO5900

60 credits

Faculty of Health Sciences
OSLO METROPOLITAN UNIVERSITY
STORBYUNIVERSITET

A thesis submitted for the degree of the Master's Program in Biomedicine, 60 credits

Title:

GCN2 as a therapeutic target for prostate cancer

By:

Shanima Shanu Mirza

Supervisors:

Dr. Beata Grallert, Dr. Alfonso Urbanucci and Dr. Nikolai Engedal

Department of radiation biology, Institute for Cancer Research,
The Norwegian Radium Hospital, OUH, Oslo, Norway

Faculty of Health Sciences,
Department of Life Sciences and Health
OsloMet – Oslo Metropolitan University
August 2021

OSLOMET
OSLO METROPOLITAN UNIVERSITY
STORBYUNIVERSITETET

Oslo universitetssykehus
Radiumhospitalet

ACKNOWLEDGMENTS

The project presented here was carried out at the Department of Radiation Biology, Institute for Cancer Research at the Norwegian Radium Hospital from August 2020 until August 2021 as a part of the master program in Biomedicine at Oslo Metropolitan University.

First and foremost, I would like to express my sincerest gratitude to my main supervisor Dr. Beata Grallert, for believing in me and giving me the opportunity to be part of her group to work on this exciting and innovative project. I am very thankful for all of your shared knowledge, good feedbacks, encouragement and enthusiasm you provided me from day one. My research would have been impossible without the support from you and the group.

I would also like to thank my co-supervisors, Dr. Alfonso Urbanucci and Dr. Nikolai Engedal. I am grateful for your support, shared knowledge, motivation and always taking time to answer questions.

I am very thankful to all the members of the research group for welcoming me and your willingness to help all the time, also making my time here pleasant and educational. Especially, thanks to Laura Marian Valencia Pesqueira, Julia Elisabeth Simensen and Lillian Lindbergsengen for sharing their laboratory experience and guidance.

Finally, I would like to thank my family and friends, especially my most tremendous gratitude toward my mamma, papa and brother, for great encouragement and support through this fun, exciting and demanding year. Lastly, a very special thanks go to my classmates and friends that went through this experience with me. We did it my friends ☺

Shanima Shanu Mirza

Oslo, August 2021

ABSTRACT

Background: Prostate cancer (PC) is the second most common cancer in men worldwide. Primary PC is treated by surgery, radiotherapy or high dose-rate brachytherapy and androgen deprivation therapy (ADT) – and this is usually very effective initially. However, most of the PC patients relapse after ADT and progress to castration-resistant prostate cancer (CRPC), which is not curable. General control nonderepressible 2 (GCN2) is a protein kinase, best known for its important role in the response to nutritional changes such as shortage of amino acids and glucose, as well as in other stresses. Since cancer cells are often in a hostile microenvironment, the standing view is that GCN2 is important for cancer cells to survive and thrive. However, the importance of GCN2 in the context of PC has not been studied.

Aim: This project aimed to explore the role and regulation of GCN2 in PC, as well as that of a known activator, GCN1, to address whether GCN2 might be an effective therapeutic target for the treatment of prostate cancer.

Methods: Standard molecular biology methods were used to assess mRNA and protein levels such as RT-qPCR and immunoblotting, respectively. Appropriate PC cell lines were maintained in culture and treated as necessary to address the specific questions described in results. Cell viability assays were performed to determine the functional consequence of inhibiting GCN2 in PC cell lines.

Results: We have shown that GCN2 is functional in PC-derived cell lines. We suggest that AR regulates GCN2 and GCN1 expression. Overexpressed MYC in PC seems to regulate GCN2, however not GCN1. Furthermore, we suggest that GCN2i decreases PC cell survival in an androgen-dependent manner.

Conclusion: Our findings suggest that GCN2 plays an important role in PC cells. Furthermore, these findings lead us to speculate that GCN2 inhibition should be considered as a new therapeutic strategy for PC.

SAMMENDRAG

Bakgrunn: Prostatakreft er den nest vanligste kreft hos menn over hele verden. Primær prostatakreft behandles med kirurgi, strålebehandling eller høy-doserate brachyterapi og kastrasjonsbehandling –og dette er vanligvis veldig effektivt i utgangspunktet. Imidlertid får de fleste prostatakreft pasientene tilbakefall etter kastrasjonsbehandling og framgang mot kastreringsresistent prostatakreft, noe som ikke er kurerbar. General control nonderepressible 2 (GCN2) er et protein kinase, best kjent for sin viktige rolle i respons til ernærings endringer som for eksempel mangel på aminosyrer og glukose, i tillegg til andre påkjenninger. Siden kreftceller ofte er i et fiendtlig mikromiljø, er den stående oppfatningen at GCN2 er viktig for at kreftceller skal overleve og trives. Imidlertid har betydningen av GCN2 i sammenheng med prostatakreft har ikke blitt studert.

Mål: Dette prosjektet hadde som mål å utforske rollen og reguleringen av GCN2 i prostatakreft, i tillegg til dens kjente aktivator, GCN1, for å ta for seg om GCN2 kan være et effektivt terapeutisk mål for behandling av prostatakreft.

Metoder: Standard molekylærbiologiske metoder ble brukt for å vurdere mRNA og proteinnivåer, slik som henholdsvis RT-qPCR og immunoblotting. Passende prostatakreft cellelinjer ble opprettholdt i kultur og behandlet som nødvendig for å adressere de spesifikke spørsmålene beskrevet i resultater. Cellelevedyktighets analyser ble utført for å bestemme den funksjonelle konsekvensen av å hemme GCN2 i prostatakreft cellelinjer.

Resultater: Vi har vist at GCN2 er funksjonell i prostatakreft cellelinjer. Vi foreslår at AR regulerer GCN2 og GCN1 uttrykk. Overuttrykt MYC i prostatakreft ser ut til å regulere GCN2, men ikke GCN1. Videre foreslår vi at hemming av GCN2 reduserer celleoverlevelsen til prostatakreft i en androgen avhengig måte.

Konklusjon: Våres funn antyder at GCN2 spiller en viktig rolle i prostatakreft celler. Videre våres funn fører til å spekulere at hemming av GCN2 burde betraktes som en ny terapeutisk strategi for prostatakreft.

ABBREVIATIONS

ADT	Androgen deprivation therapy
AF-1	Activation factor 1
AF-2	Activation factor 2
AR	Androgen receptor
ARE	Androgen response element
AR-V	AR spice variants
BSA	Bovine serum albumin
CRPC	Castration resistant prostate cancer
CSFBS	Charcoal stripped fetal bovine serum
DBD	DNA binding domain
DHT	Dihydrotestosterone
DMSO	Dimethyl sulfoxide
DNA	Deoxyribonucleic acid
DOX	Doxycycline
DTT	Dithiothreitol
EBRT	External beam radiation therapy
EDTA	Ethylenediaminetetraacetic acid
eIF2-α	Eukaryotic translation initiation factor 2 alpha
ER	Endoplasmic reticulum
EtOH	Ethanol
FBS	Fetal bovine serum
FOXA1	Forkhead box A1
G418	Geneticin
GCN1	General control nonderepressible 1
GCN2	General control nonderepressible 2
GCN2i	GCN2 inhibitor
GCN2-P	GCN2-phosphorylation
GCN2-T	GCN2-total
Gy	Gray
HR	Hinge region

HSP90	Heat shock protein 90
IRS	Integrated stress response
kD	Kilo Dalton
KLK3	Kallikrein Related Peptidase 3
mCRPC	Metastasis CRPC
MMS	Methyl methanesulfonate
mRNA	Messenger RNA
NKX3.1	NK3 homeobox protein 1
NOCA-1	Nuclear receptor activator 1
NOCA-2	Nuclear receptor activator 2
NOCA-3	Nuclear receptor activator 3
PAG	Polyacrylamide gel
PAGE	Polyacrylamide gel electrophoresis
PC	Prostate cancer
PCR	Polymerase chain reaction
PDL	Poly-D-Lysine
PIN	Prostatic intraepithelial neoplasia
PSA	Prostate specific antigen
qPCR	Quantitative PCR
ROS	Reactive oxygen species
RPMI	Roswell Park Memorial Institute Medium
RT-qPCR	Real time qPCR
SDS	Sodium dodecyl sulfate
UPR	Unfolded protein response
UV	Ultraviolet

TABLE OF CONTENTS

1. INTRODUCTION

1.1 Introduction to cancer

1.1.1 Cancer epidemiology

Noncommunicable diseases or chronic diseases are now responsible for most global deaths. In the 21st-century, cancer has been expected to be the leading cause of global death (1). According to World Health Organization, in 2020, cancer is responsible for approximately 10 million deaths globally each year, making it about 1 in 6 deaths due to cancer (2). Lung, female breast, and colorectal cancer are the respective top three cancer types that encounter one-third of the cancer incidence and mortality worldwide (1).

In 2017, cancer was the leading cause of mortality in Norway (3). According to the cancer registry in Norway, there were 34.979 new cancer cases in 2019. Prostate cancer accounts for 13,9%, breast cancer 10,7%, lung cancer 9,5%, and colon cancer 8,5%; these cancer types are the most frequent (4). Together these types of cancer account for approximately 50% of cancer cases in Norway, which corresponds to about 15.000 cancers (5).

1.1.2 Characteristics of cancer

The body of an animal is an ecosystem where individual members are cells. These cells are reproduced by cell division and organized into collaborative assemblies, and these assemblies are known as tissues and organs. These cells send, receive, and interpret an elaborate set of external signals within the tissues and organs to maintain their behavior, reflecting how they reproduce themselves, differentiate, and keep homeostasis (6). Cellular homeostasis is known to be controlled by the genetic information stored in the genome in the nucleus, known as deoxyribonucleic acid (DNA). Usually, cells proliferate and differentiate in the animal body when necessary. Once these cells grow old or become damaged, they enter a cellular senescence state or die, and new cells replace them (7). Thus, alteration in a cell's DNA can lead to deviations from the normal cellular hemostasis process, which can then cause excessive growth and induce pathology (7, 8).

In definition, cancer is a group of diseases characterized by unregulated cell growth and proliferation and invade surrounding tissues and colonize to other sites in the body (metastasis) (8, 9). Since malignant cells arise from normal cells, the cancerous disease can affect any part of the body; thus, a single mutation or alteration to the genome cannot define cancer development. Instead, cancer cells acquire various unique properties as they evolve, multiply and spread; these collections of asocial properties make these cells genetically or epigenetically unstable (10). Cancer characteristics or "Hallmarks of Cancer" are a systematic representation of the essential multistep process that leads to the transition of a normal cell towards a cancerous cell (11) (**Figure 1.1**). Hallmarks of cancer were initially organized into six original characteristics; these characteristics are distinctive and complementary capabilities that enable tumor growth and metastasis. More recently have Hanahan & Weinberg modified their concept to include new developments: two enabling hallmarks that are crucial to forming the six hallmarks and two emerging hallmarks that describe the composition and signaling interaction of tumor microenvironment (9, 11).

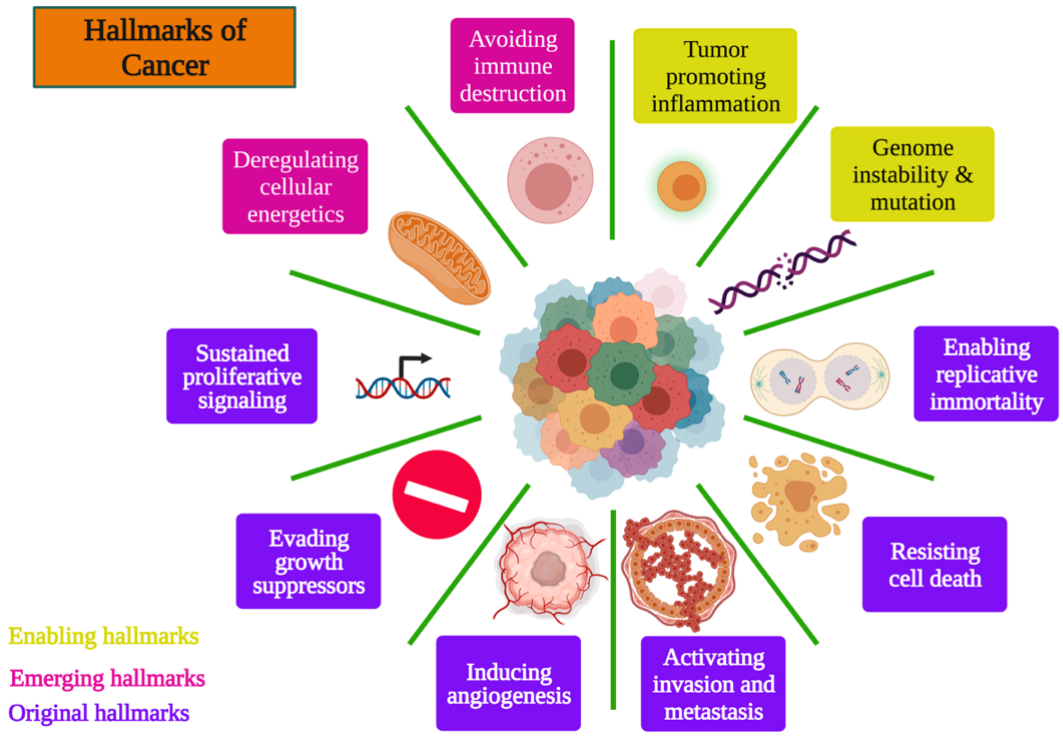

Figure 1.1 The hallmarks of cancer. Schematic representation of six original, two enabling, and two emerging hallmarks. Each hallmark represents a capability that enables tumor growth and metastasis. This figure is adapted from Douglas Hanahan and Robert A Weinberg's "Hallmark of Cancer: The Next Generation" (2011), drawn from BioRender.com.

One of the hallmarks of cancer is that cancer cells gain the ability to sustain proliferative signaling. Normal cells in tissues are dependent on growth signals from the surrounding environment that instruct them to enter cell growth and the cell division cycle. This process strictly controls the production and release of these growth signals. Remarkably cancer cells deregulate these signals and produce their own proliferation signals or manipulate surrounding normal cells to provide the signals (12). Cancer cells also gain the ability to evade the robust cellular programs including: proliferation suppressors or anti-proliferative signals, that negatively control cell proliferation to maintain cellular quiescence and tissue homeostasis (11). Typically, when cells are damaged or unhealthy, they are eliminated from the body by apoptosis, which is a type of "cell suicide" intrinsic to the cells. This process maintains tissue homeostasis, but cancer cells acquire resistance to programmed cell death by activating anti-apoptotic and cell survival programs (13, 14). Together with disruption of the cell senescence barrier mechanism, these three characteristics lead to another critical hallmark of cancer: limitless replicative potential.

Angiogenesis is the formation of new blood vessels. Angiogenesis is usually active during developing an embryo or healing wound since these blood vessels provide tissues with oxygen and nutrients, also remove metabolic wastes and carbon dioxide. Like normal tissues, tumor growth also requires oxygen, nutrients, and waste removal; thus, they activate the angiogenesis process by activating the angiogenesis switch (15). Eventually, growing tumors gain the ability to spread, a process known as metastasis; this process involves a set of events "invasion-metastasis-cascade." First, the primary tumor cells invade their local environment by epithelial-mesenchymal transition (EMT). EMT is the process that involves the conversion of sheets of closely connected epithelial cells into highly mobile mesenchymal cells. The second step is intravasation, which is the entry of cancer cells into blood or lymphatic vessels. Lastly, these cells eventually exit blood vessels and localize into a site distant from the original site (16, 17).

Genomic instability and mutations are one of the enabling characteristics, relevant for all cancers, especially mutations in tumor suppressors and proto-oncogenes. Tumor suppressor genes, also known as gatekeeper genes and function as proliferative breaks that keep cell behavior under control by suppressing inappropriate cell division, repairing DNA damage, or

induce cell death (apoptosis). In this manner, gatekeeper genes prevent a neoplastic cell population's appearance. In contrast, proto-oncogenes function as cell proliferation stimulators; upon alteration by DNA-damaging agents or viral genomes, these genes can be turned into oncogenes and abnormally stimulate proliferation (18, 19). Another enabling characteristic is tumor-promoting inflammation. Inflammation can contribute to tumor progression by providing bioactive molecules to the tumor microenvironment. These molecules can be growth factors, survival factors, pro-angiogenetic factors and various other molecules (11).

The two emerging hallmarks are: reprogramming energy metabolism and escaping immune detection. Cancer cells reprogram energy metabolism to keep up with uncontrolled cell growth and division and they evolved an alternative metabolic pathway known as Warburg effect. Warburg's effect on cancer cells reflects the dramatic change in glucose uptake and sugar metabolism (6, 11). Tumor cells can evade immune detection by exploiting various immune system factors (20).

All the mentioned carcinogenesis properties (figure 1.1) allow for diverse and genetically unique cancer types, where each tumor types exhibit a distinct fingerprint of genetic alteration and properties which results in tumor heterogeneity. Tumor heterogeneity leads to different prognosis and different responses to therapy. Thus, therapeutic targets or research into cancer treatments are equally diverse and challenging; however, increasing future clarification and molecular understanding of these characteristics can be utilized as a better therapeutic strategy and eventually cure cancer.

1.2 Prostate cancer

1.2.1 Epidemiology, incidence, and mortality

Prostate cancer (PC) is the second most common cancer in men worldwide, with an estimated incidence of 1.3 million new cases and 359 000 associated deaths in 2018 (1). In Norway, PC is still the most common cancer, and approximately 5000 men are diagnosed with PC in 2019 (4). Mortality and cancer incidences correlate with increasing age; three out

of four diagnosed cancer cases are over the age of 60 (5). Lifestyle, social, and environmental factors can also contribute to the disease's formation and outcome (4, 21).

1.2.2 Normal prostate and development of PC

The prostate is a male reproductive accessory gland located at the base of the balder and surrounding the urethra connected with the ejaculatory ducts and the urinary bladder's neck (22). The prostate consists of three glandular zones: central, peripheral, transition zone, and one non-glandular region of the anterior prostate. The non-glandular region consists of a fibromuscular stroma that provides structural support (23). The branching duct and acini, collectively known as the prostate gland, consist of four distinct cell types. These cell types include: prostate basal cells, luminal or glandular cells, neuroendocrine cells, and stromal cells that guide and support growth and differentiation of epithelium, along with a small population of stem cells (22, 24). The prostate is responsible for producing and storing seminal fluid, ensuring the survival, viability, and motility of spermatozoa (25). The prostate epithelium's other cell types, such as fibroblasts, immune cells, smooth muscle cells, endothelial cells, can influence the prostate's biological and clinical behavior (23). Lastly, one of the critical components for the normal development, growth, and maintenance of a normal prostate is dependent on the androgen signaling pathway, which acts through the androgen receptor (AR) (26).

PC initiates through a healthy cell's malignant transformation by a multistep process, and prostatic intraepithelial neoplasia (PIN) is the most common precursor. The PIN is defined by new abnormal tissue growth along the ducts. Formation of PIN is the result of accumulating somatic mutations in genes that regulate prostate cell growth, proliferation, death, and DNA damage response (27, 28). The formation of PIN, in turn, leads to neoplastic cells progress towards advanced prostate adenocarcinoma with a local invasion. Initially, advanced prostate adenocarcinoma metastasizes to the lymph nodes and eventually to distant organs, including the liver, lungs, and bones (29). In some cases, PC has an oligometastatic PC appearance, representing a transitional state between localized and widespread metastatic diseases, and encompasses various disease behavior. This type of cancer has a slow and late metastatic spreading to the pelvic area (30). Bone is the most frequent metastasis site for

PC and the interaction between PC cells, osteoblast, and osteoclast lead to new bone formation destruction (31, 32). Locally advanced prostate cancer is androgen-dependent and responds to androgen deprivation therapy (ADT); however, most of the patients relapse after ADT and progress towards castration resistance prostate cancer (CRPC), which eventually progress toward metastatic CRPC (mCRPC) (33, 34).

1.2.3 Diagnosis and PSA based test

The AR target gene prostate-specific antigen (PSA) is the most used PC biomarker in clinical practice and encoded by one of the androgens-regulated Kallikrein genes –kallikrein-related peptidase 3 (KLK3), which is a serine protease of the human kallikrein gene family (35). In normal tissues, PSA is produced by the prostate epithelium and secreted into the seminal plasma; thus, these epithelial cells are also the progenitor of prostate adenocarcinoma (35, 36). PSA has a significant functional role in the seminal coagulum's liquefaction that allows the release of sperm and prevents escape to blood circulation (35). In PC level of PSA increases and enters the blood circulation; thus, measurement of the serum PSA is widely practiced in screening programs of early PC and detecting recurring CRPC. Serum PSA levels are reported as PSA nanograms per milliliter (ng/mL) (35-37). Even though PSA is used as the most common biomarker for PC, it is not PC-specific rather prostate-specific; thus, it can also diagnose other prostate-related diseases (36). Other biomarkers include –C-met, B-cell lymphoma 2 (Bcl-2), glycoprotein A-80, apolipoprotein D (27).

The PC diagnosis is based on the microscopy evaluation of prostate tissue obtained by needle biopsy, where a pathologist examines the sample and determines a Gleason grade. Gleason grade is a score-based method that verifies the similarities of cancer cells to healthy tissue under the microscope. Thus, a less aggressive tumor (resemble more healthy tissue) has the lower Gleason grade, the more aggressive, the higher the grade (38, 39). Traditionally, clinicians have stratified the diagnosis into low, intermediate, and increased risk based on Gleason grade, PSA, and clinical stage.

1.3 Androgen receptor (AR) structure and function

1.3.1 AR structure

As mentioned earlier, AR plays a vital role in the development and function of the normal prostate. The AR transcription factor belongs to the evolutionary conserved nuclear receptor superfamily and a cytoplasmic protein, dependent on ligand binding. The gene is located in the X -chromosome at the locus Xq11-Xq12 and consists of eight exons, which constitute the four categorical AR domains. AR consists of three main functional domains – the N-terminal transactivation domain (NTD) comprising of exon 1, a central DNA binding domain (DBD) constitutes exon 2-3, and a C-terminal ligand-binding domain (LBD) spans between exons 4-8. The hinge region (HR) between DBD and LBD is essential for nuclear localization and degradation (40, 41). All of the mentioned functional domains are important for normal AR function (**Figure 1.2**). The NTD contains two transcriptional regulatory regions that include –activation function 1 (AF-1) and activation function 2 (AF-2) (41).

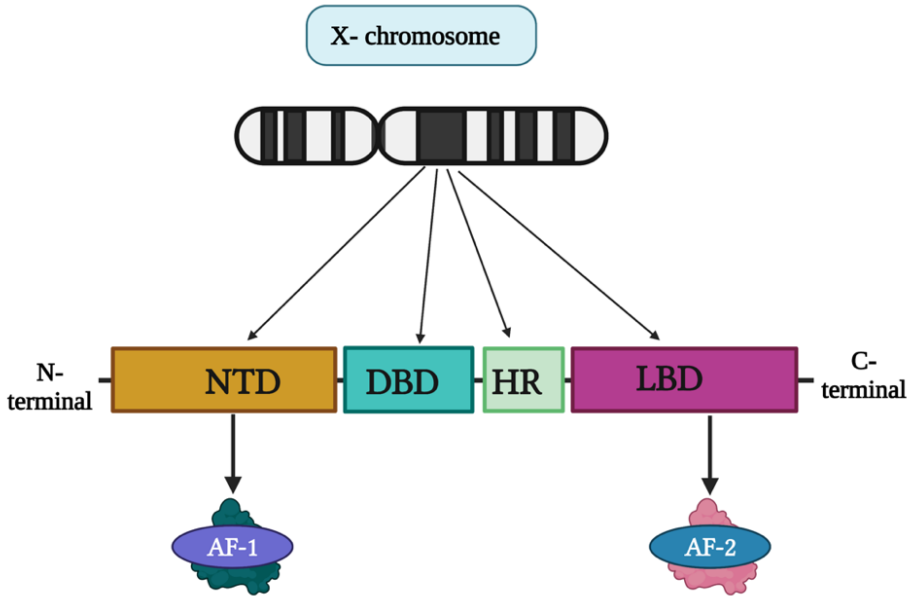

Figure 1.2 Schematic structure of AR. Simple schematic representation of the AR receptor, which has been mapped to the long arm of the X-chromosome. Usually, the LBD domain is connected to the DBD domain by flexible HR. The AF-1 is located in the NTD, and AF-2 is located in the LBD. This figure was adapted from "Androgen receptor: structure, role in prostate cancer and drug discovery," (41) drawn in BioRender.com.

1.3.2 Hormone stimulation

A large variety of small molecules interact with AR, and these molecules are identified as either agonists or antagonists (41). Generally, in the absence of androgen/hormone inactive version of AR is located in the cytoplasm and bound to a heat shock protein (HSP) so that it is incompetent to bind ligand (42). AR agonists such as testosterones (in their free form) are

converted into DHT by the 5α-reductase enzyme in the prostate cells. Androgen binding to LBD in AR leads to a conformational change of the LBD, which leads to AR homodimerization and dissociation from HSP, followed by translocation into the nucleus (**Figure 1.3**) (41, 43).

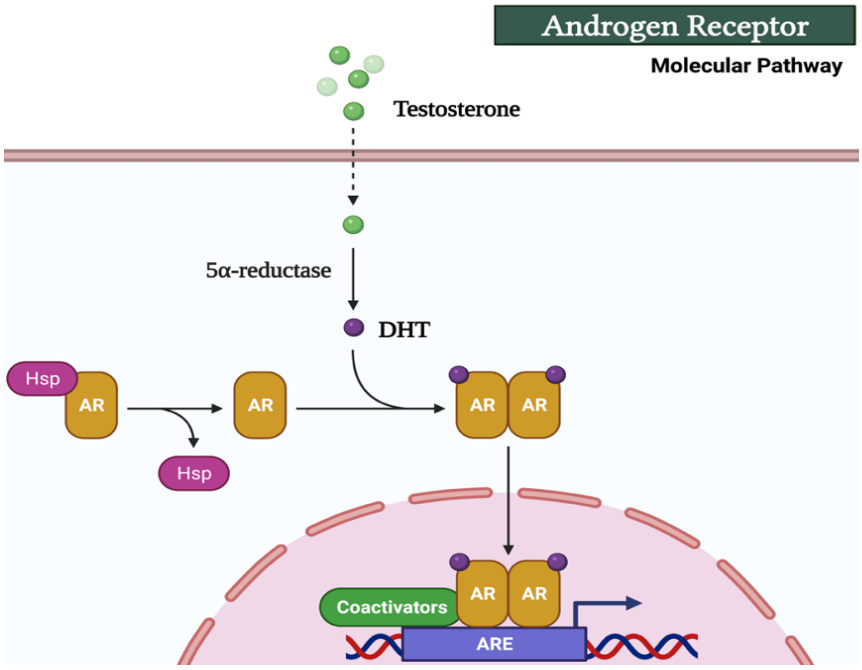

Figure: 1.3 The androgen-receptor signaling pathway. Testosterones diffuse into the cell membrane, which is then converted to DHT. DHT binds to AR and promotes the dissociation of HSP from AR, which leads to the dimerization and translocation of AR in the nucleus. Once inside the nucleus, AR binds to ARE in the promoter region of the target gene. This figure was adapted from and drawn from BioRender.com.

1.3.3 Chromatin binding

In the nucleus, AR binds a dimer to a specific genomic sequence known as an androgen response element (ARE) in its target genes' promoter and enhancer regions (figure 1.3). AR binds to and recruits various coactivators and regulatory element that forms a complex with AF-1 and AF-2 region of the AR (44). Coactivators and regulators recruited by AR such as – pCAF, CREB-binding protein, p300, and p160 family coactivators (SRC1, TIF2, SRC3, etc.) enable post-translation modification of histones by acetylation and methylation (44, 45). In addition to the histone acetylation, lysine-specific demethylase 1 also interacts with AR and relieves repressive histone marks through demethylase activity of mono and demethylated histone H3 at Lys 9 (H3K9). Post-translational modification of histones by AR leads to regulation of AR target gene, simultaneously demethylase activity leads to transcription of AR targeted gene (44, 45).

1.3.4 Activation of target genes

In addition to coactivators and coregulators, transcription factors also interact with AR on the genome to regulate gene expression; these transcription factors are known as collaborating factors. Forkhead box A1 (FOXA1) is the main transcription factor interacting with AR, in addition to FOXA1, GATA-binding factor 2, NK3 homeobox protein 1 (NKX3.1), and octamer transcription factor 1 were also identified as AR interacting transcription factors. With coactivators, regulators, and transcription factors, AR regulates the downstream gene expression with diverse functions of the ARE. These genes are involved in cell cycle progression, growth stimulation, proliferation, cell migration, and anti-apoptosis signaling (43, 46, 47).

1.3.5 AR in PC development

As mentioned earlier, AR's proper function and activity are heavily involved in maintaining prostate function, which similarly impacts PC development. AR, through the mutations in the regulation of transcription networks, genomic stability, and DNA repair, can lead to the formation of PC. The majority of deaths from PC is due to advanced-stage metastatic spread dependent on the AR. Through the conventional approach and next-generation sequencing, multiple studies have shown that most primary and metastatic prostate cancers harbor genomic alterations in the androgen signaling pathway (48). These genomic alterations include amplification and overexpression of AR, a mutation in AR, the gain of AR coactivators or loss corepressors, AR splice variants, which ultimately lead to CRPC. Thus, AR has, for a long time, been the main target in the treatment of advanced PC (49).

1.4 Castration resistance prostate cancer (CRPC)

1.4.1 Mechanism of resistance

As mentioned earlier, ADT treatment is an efficient treatment option of AR-dependent PC; however, tumor reoccurs after ADT, and the disease becomes lethal CRPC that can grow under low levels of androgen characteristic after castration. The development of CRPC is thought to be mediated through two main overlapping mechanisms: AR-dependent and AR-independent (50).

1.4.1.1 AR-dependent

I AR amplification and overexpression

AR overexpression is thought to be a significant cause of CRPC, and indeed, many studies have shown that increased AR expression is associated with CRPC progression. Increased AR expression in CRPC may be attributed to gene amplification, leading to increased transcription and translation of mRNA and decreased degradation due to more AR protein levels. Thus, transcriptional upregulation is an essential mechanism of increased AR expression (49, 51). However, overexpression of AR can also be a spontaneous reaction to castration since androgen tends to suppress AR transcription in prostate epithelial cells (52). Regardless of the molecular mechanisms of AR overexpression, AR amplification is the most frequent genetic alteration reported, approximately in 50% of CRPC. In contrast, AR amplification is rarely detected in untreated primary PC, suggesting that AR amplification is an adaptive response to ADT (53, 54). Studies have identified AR amplification in circulating tumor cells and circulating tumor DNA obtained from CRPC patients, which has been associated with therapy resistance to antiandrogens (51, 55).

II AR mutation

AR mutations such as point mutations are rare in untreated primary PC; however, AR mutation is common in CRPC patients, approximately 15% to 30% (53, 56). These point mutations appear to affect the ligand specificity of AR; the most known point mutation of AR is the T877A mutation. The T877A mutation alters the stereochemistry of the binding pocket and results in the loss of the agonist. This alteration allows other nuclear hormones such as –estrogen, progesterone, cortisol, cortisone, and antiandrogens can activate AR (57). Several different mutations have been identified; their mutations were located in the LBD of the AR, including: L701H, V715M, V730M, and H874Y. These mutations enhance AR sensitivity to other steroids (53). Recent studies have shown that circulating tumor DNA from CRPC patients contains genomic DNA with the AR mutations described above. The detection of point mutations by sequencing could be a biomarker for patients at risk of developing CRPC (55).

III AR splice variants

For more than two decades, it has been known that AR has splice variants (58), and AR splice variants (AR-Vs) are also involved in CRPC progression. More than twenty variants of AR-Vs have been identified; most of these variants lack LBD and remain constitutively active (59). PC cells express full-length AR and AR-Vs; both are androgen-independent. One of the most widely studied AR-V variants in PC is AR-V7, lacking the LBD domain. Thus, cells expressing AR-V7 have a selective advantage in an androgen-depleted environment due to AR being constitutively active in a ligand-independent manner (59). Another AR-V is ARv567e, which also lacks LBD, and its expression has been associated with only malignant PC tissues. The expression of AR-V7 and/or ARv567e is associated with poor survival (60, 61). These two are the major AR-Vs other splice variants, including AR-V1 –AR-V14; however, the molecular function behind these splice variants are unknown.

IV Gain of coactivator and loss of corepressor

AR directly interacts with the AR coactivator and forms a complex that enhances the opening of the chromatin structure and recruits transcriptional machinery to the target gene. AR coactivator SRC family plays an important role in CRPC progression, includes – nuclear receptor coactivator -1(NOCA-1), nuclear receptor coactivator -2(NOCA-2) and nuclear receptor coactivator -3(NOCA-3). A study has suggested that PC aggressiveness is associated with NOCA-1 expression; suppressing the coactivator leads to a reduction in growth and altered AR target gene regulation in PC (62). NOCA-2 is amplified both in primary and metastatic PC; during androgen deprivation, NOCA-2 activates the PI3K pathway, leading to metastasis and the development of CRPC (63, 64). NOCA-3 is overexpressed in CRPC and negatively correlates with PTEN expression. NOCA-3 is essential for the development of CRPC due to enhancing Akt activity and S6K1 expression in CRPC (65). Another coactivator, Tip60, also plays a role in CRPC progression; Tip60 promotes AR translocation in the nucleus and the proliferation of PC cells (66).

V Changes in androgen biosynthesis

In the adrenal gland, cytochrome p450 enzymes, CYP11A1, and CYP17A1 can synthesize DHEA and androstenedione; normal cells can convert these weak adrenal androgens into testosterone and DHT. However, CRPC overexpresses these converting enzymes that include

–Aldo-keto reductase family 1 member C3 (AKR1C3) and 3β-hydroxysteroid dehydrogenase type 1 (HSD3β1). Overexpression of these enzymes leads to enough production of DHT to activate AR (67, 68). CRPC can also be independent of circulating androgen by synthesizing a significant amount of androgen from cholesterol (69).

1.4.1.2 AR-independent

The AR-independent mechanism involves mechanisms that do not directly affect the androgen signaling pathway. Some various components/pathways can lead to the progression to CRPC in an AR-independent manner. Numerous studies have demonstrated that over-expression of c-MYC in PC leads to androgen-independent PC growth. In PC, overexpression of c-MYC leads to partially reprogramming of AR chromatin, leading to CRPC (70). The PI3K-AKT-mTOR pathway is well known for its regulative role in all major cellular processes, including cell growth, development, proliferation, protein synthesis, and programmed cell death. Preclinical model studies have shown that the PI3K/Akt pathway activation is critical for CRPC development (71). PTEN suppresses PI3K/Akt pathway, and approximately 40% of PC has loss of PTEN through deletion or mutation (72). Mutations in DNA repair pathways can also lead to CRPC; several independent genomic studies revealed that 15%-35% of mCRPC contain DNA repair defects. These mutations include breast cancer genes 1 and 2 (BRACA1/2), ATM serine/threonine kinase (ATM), ATR serine/threonine kinase (ATR), and RAD51 (73, 74). Genomic alteration in other pathways such as the TGF-β/SMAD4 pathways, FOXO signaling, WNT signaling, glucocorticoid signaling, NF-κB signaling can lead to the development of CRPC (29, 50).

1.5 Therapies available today

As mentioned earlier, PC diagnosis is based on the microscopy evaluation of prostate tissue, where clinicians stratify the diagnosis into low, intermediate, and high risk based on Gleason grade, PSA, and clinical stage. Thus, based on the stage of the disease and the fitness of the patient indicates which PC treatment is available and suitable for the patient (37, 38). Today the main/common PC treatments include radical prostatectomy, radiotherapy, chemotherapy, immunotherapy, ADT, and systematic AR target treatments.

1.5.1 Prostatectomy

Radical retropubic prostatectomy is a surgical procedure in which the prostate gland and its surrounding tissues are removed, which is the primary treatment for men with LAPC. Surgery can lead to the complete removal of cancer; additionally, radiation therapy is considered if needed. The complete removal of the prostate leads to a reduction in serum PSA level; thus, detecting cancer relapse gets more manageable due to increased serum PSA level (75-77).

1.5.2 Radiation therapy

External beam and internal radiation therapy are the two main types of radiation therapy. External beam radiation therapy (EBRT) is radiation delivered from a distant source outside the patient's body and directed into the cancer site. Depending on the tumor stage, clinicians use different levels of radiation. Multiple studies have demonstrated that a higher dose of radiation treatment improves disease control for patients with localized PC and have established the modern standard EBRT for PC, which lies between 75,6 and 81,0 Gy of radiation separated into hypo-fractions of 1.8-2 Gy daily for 7-9 weeks (78, 79). Brachytherapy involves the solid or liquid implantation of radiation sources as close as possible to the tumor site. These radioactive materials slowly release radiation to the cancerous site; the placement of the material can be temporary or permanent. Radium 223 (Ra 223), which emits alpha particles, has shown great survival benefits in mCRPC (80).

1.5.3 Chemotherapy

Chemotherapy uses cytotoxic drugs to destroy cancer cells; historically, chemotherapy for advanced PC was viewed as ineffective and toxic, without a significant effect on survival (81). However, over the years, chemotherapeutic treatments, especially docetaxel, were the first chemotherapeutic agent that demonstrated survival benefits for mCRPC patients (82). Docetaxel cytotoxic function occurs through binding to microtubules, which prevents depolymerization. Depolymerization of the microtubules prevents AR trafficking and together with other mechanisms lead to apoptosis through Bcl-2 phosphorylation (81, 83). Docetaxel improved the understanding of drug effect on CRPC, which lead to the production

of another semisynthetic taxane chemotherapeutic –cabazitaxel. Cabazitaxel inhibitor is the third generation taxane that has also been shown to prolong survival in mCRPC (83).

1.5.4 Immunotherapy

Over the years, more and more studies have been suggesting immunotherapy as one of the available treatment options for PC. Prostate cancer cells express several immunogenic antigens, including PSA, which has been the target for antigen-based vaccines (84). Therapeutic cancer vaccine –Sipuleucel-T is a vaccine generated from a patient's peripheral immune cells produced via leukopheresis, has shown therapeutic benefits to patients. The ultimate goal of the vaccine is to activate immune cells to produce a sustained antitumor immune response (81, 85, 86). Another vaccine therapy is the PSA-TRICOM vaccine – prostvac, which consists of a recombinant vector as a primary vector, followed by multiple booster vaccinations with a recombinant fowlpox vector –to enhance T cell response (86, 87). Other immunotherapy options include –CTL4-4 inhibition, PD-1/PD-L1 inhibition and CTL4-/PD-1 combination.

1.5.5 Hormone deprivation therapy (ADT)

As mentioned above, the development of PC is androgen-dependent, and ADT is the most widely used systematic treatment for advanced PC; this therapy aims to reduce androgen. There are several types of ADT, including –surgical methods or medical methods to lower the androgen level. Surgical castration involves removing the prostate. The medical process involves –luteinizing hormone-releasing hormone agonist, a drug that decreases the amount of testosterone made by the testicles (88, 89). There is strong evidence that the combination of ADT and radiotherapy improves outcomes, including survival of patients with high-risk LAPC compared with radiotherapy alone (90). Multiple studies have suggested that patient receiving ADT alleviate symptoms and prolong survival with PC, but side effect can lead to serious consequence for the patient's overall health and well-being. Studies have shown that ADT is associated with an increased risk of skeletal fracture, diabetes, and cardiovascular-related death (91, 92).

1.5.6 Systematic AR targeted treatment

New treatments involve targeting the AR because of the crucial role of AR in the development and progression of PC; drugs have focused on inhibiting the AR to prevent the AR from acting as a transcription factor (93). Evidence suggests that binding of these drugs can induce a conformational change that prevents AR from nuclear translocation and transcription. The drug's effectiveness can be noted by a decrease in the amount of serum PSA (93, 94).

1.5.6.1 Directly targeting the AR

Drugs directly targeting the AR include –enzalutamide, ARN-509, bicalutamide. Enzalutamide is also known as MDV3100, Xtandi® is a multi-targeted second-generation AR inhibitor. Enzalutamide exhibits three mechanisms of action: 1) prevents ligands from binding to AR, 2) prevents AR translocation into the nucleus, and 3) inhibits AR-mediated transcription of target genes by preventing binding of AR to DNA (50, 81). ARN-509 has similar effects as enzalutamide; however, some studies suggest that ARN-509 is more effective and potent antiandrogen than enzalutamide. Also, a lower dose is needed for treatment with ARN-509 than enzalutamide; this is advantageous for patients due to a smaller chance of possible side effects (95, 96). Lastly, the non-steroidal agent bicalutamide, which acts through binding to an allosteric site on the AR, induces a conformational change of the AR coactivator binding site and, thus inhibits transcription AR (97, 98).

1.5.6.2 Indirectly targeting the AR

Drugs that indirectly target AR are ketoconazole, abiraterone acetate, orteronel, Lupron. Abiraterone acetate (Zytiga®) selectively and irreversibly blocks androgen biosynthesis by inhibiting cytochrome P450 17A1 (CYP17A1), which is needed for the production of androgen (50, 99). Like abiraterone acetate, ketoconazole is another inhibitor of the cytochrome P450 pathway; however, this drug is not so commonly used as before. Studies suggested that ketoconazole is not a highly specific inhibitor; wide ranges of side effects are associated with this drug (100). Orteronel, also known as TAK-700, is also a CYP17A1 inhibitor; however, orteronel is more selective than abiraterone acetate (101, 102). Lupron is an LHRH agonist, which decreases the amount of follicle-stimulating hormone and luteinizing hormone (these hormones are involved in androgen synthesis), thus prevents

androgen synthesis (103). It has been shown that combining Lupron with other agents such as bicalutamide, can prevent harmful side effects (104).

1.5.6.3 Targeting heat shock protein

More and more studies show that heat shock proteins have a role in the AR signaling pathway, especially heat shock protein 90 (HSP90). HSP90 is a chaperon that regulates the function of multiple proteins, including AR and other oncogenes; HSP90 stabilizes the AR in the cytoplasm (105, 106). PC treatments that target heat shock protein involve methoxychalcones, a specific type of molecule that can prevent the dissociation of the HSP90-AR complex, thus preventing the nuclear translocation of the AR (107).

1.5.6.4 Natural agents

In addition to synthesizing drugs, drugs isolated from natural products have also affected PC significantly. Soy isoflavones, green tea, and selenium are examples of few natural compounds that can reduce cancer malignancy by inhibiting AR (108). BR-DIM is a formulated version of 3,3'-diindolylmethane, a natural agent that can potentially inhibit the growth and tumor characteristics of PC cells (109).

As mentioned above, all the mechanisms that lead to the progression of CRPC and eventually leads to mCRPC are the reasons for resistance to therapy. Intense molecular research is needed within the AR pathways and mechanisms; thus, improving the understanding of these AR resistance mechanisms and exploiting the knowledge when designing the next generation of AR targeting agents will be the key to designing more effective therapies.

1.6 The integrated stress response –IRS

As mentioned above, homeostasis is essential for normal cells' survival and functioning. Normal cells can exhibit changes due to disturbance in cellular homeostasis. Cells have evolved different pathways to deal with intrinsic and extrinsic stressors. During cellular stress, genes that promote tolerance-and-survival proteins are upregulated (110). One such pathway is –the integrated stress response (ISR), which consists of four kinases (**Figure 1.4**). The ISR pathway is activated in eukaryotic cells in response to various kinds of extrinsic

stress, including hypoxia, amino acid deprivation, glucose deprivation, and viral infection, also by intrinsic stress, such as endoplasmic reticulum (ER stress) (111). In the activated IRS pathway, the core event is the phosphorylation of eukaryotic translation initiation factor 2 alpha (eIF2-α) by one of four serine-threonine kinase members (112). These kinases include protein kinase double-stranded RNA-dependent (PKR), PKR-like ER-kinase (PERK), heme regulated inhibitor (HRI), and general control non-derepressible-2 (GCN2).

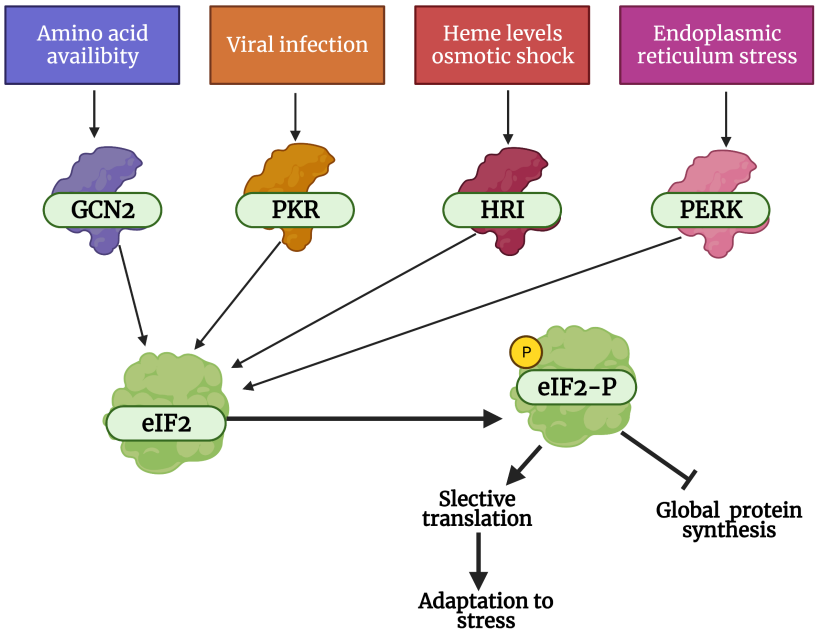

Figure 1.4 The integrated stress response signaling pathway. Amino acid deprivation, viral infection, heme deprivation, and ER stress activate GCN2, PKR, HRI, and PERK kinases, respectively. These kinases phosphorylate eIF2-α that leads to a decrease in global protein synthesis and initiates selective translation, which promotes cellular recovery. This figure is adapted from: "Integrated stress response" (111) and drawn in bioRender.com.

1.7 GCN2: structure and function

GCN2 or EIF2AK4 is a large protein and highly conserved from yeast to humans, a sensor of amino acid availability and regulator of gene expression changes in response to amino acid deprivation (113, 114). GCN2 contains five conserved distinct domains that include a pseudo-kinase domain, RWD (RING finger-containing proteins, WD-repeat containing proteins and yeast DEAD (DEXD)-like helicases) domain in N-terminus, a histidyl-tRNA synthesis (HisRS)-related domain, a catalytic active kinase domain and a C-terminal domain (CTD), (**Figure 1.5**) (115). Activation of GCN2 occurs by binding of uncharged tRNAs to the HisRS domain during starvation for amino acids (116-118). Upon binding to uncharged tRNA GCN2 undergoes a conformational change from the autoinhibitory state to dimerize form,

which activates its protein kinase catalytic domain. The catalytic activity of GCN2 also requires an interaction between the kinase and pseudo-kinase domains (114, 115).

Figure 1.5 Domain organization of GCN2. Simple schematic representation of five conserved domains of GCN2, which provides insights into activation mechanisms. RWD domains are known for being involved in protein-protein interactions. In the case of GCN2, the one of the known interacting protein is GCN1, which is an activator (115). The CTD is involved in ribosome binding. This figure is adapted from: "Towards a model of GCN2 activation" (115), drawn in bioRender.com.

The alpha subunit of the eIF2-α is phosphorylated by activated GCN2, which contains both phosphorylation and RNA binding sites. The GTP-bound forms of eIF2-α delivers initiator methionyl tRNA (Met-tRNA$_i^{Met}$) to the ribosome; phosphorylation by GCN2 converts eIF2-α to a competitive inhibitor of eIF2B, which leads to a reduction of global protein synthesis (119). Simultaneously, phosphorylation of eIF2-α leads to translational upregulation of selected mRNAs, including the mRNA encoding the transcription factor 4 (ATF4) to promote recovery from nutrient deprivation (112, 120).

Given that GCN2 activation leads to dramatic changes in cells' gene expression, strict regulation of GCN2 activity is essential for the cell and the organism. Several molecules are known to control GCN2 activity. Multiple of these molecules are conserved from yeast to mammals, suggesting that cells have a complex network of molecules that maintain the GCN2 function (119). These regulatory molecules regulate GCN2 activity either by directly bind and regulate GCN2 or regulates GCN2 activity indirectly by binding to GCN2 binding proteins or control GCN2 by an unknown mechanism so that GCN2 is only functional when necessary (119). Among all these regulatory molecules, one of them is GCN1, which acts as a positive activator of GCN2 (121).

1.7.1 Activator of GCN2

General control nonderepressible 1 (GCN1) is a large cytoplasmic protein, virtually found in all eukaryotic cells, and the role of GCN1 has been extensively studied in budding yeast (122). In yeast, it has been shown that GCN1 is necessary for the activation of GCN2; it binds

to the ribosome and GCN2 through distinct regions (122). Residues within the C-terminus GCN1 activates GCN2 by directly binding to the RWD of the protein kinase GCN2. Mutation in this specific amino acid of GCN1 disables the activation of GCN2 in vivo (122, 123). It has been recently established that in mammalian GCN1 is essential for activation of GCN2-dependent response to stress induced by amino-acid starvation and ultraviolet (UV) irradiation, GCN1 is necessary for cell proliferation and development; these GCN1 actions are GCN2-dependent (123, 124).

1.7.2 GCN2 activation via other types of stress

Multiple studies over the years have shown that, in addition to amino-acid starvation, various other types of stress conditions can lead to the activation of GCN2. These stresses include –ultraviolet (UV) irradiation, nutrient starvation, mitochondrial/oxidative stress, ER stress, toxin, and viral infection (125).

1.7.2.1 UV

Nucleic acids can be severely damaged by UV irradiation, and damage to DNA, mRNA, rRNA, or tRNA can dramatically change cellular physiology. Thus, organisms have evolved highly conserved repair mechanisms that can be activated in response to such conditions and other environmental stresses (126). A study suggests that stress caused by UV elicits an inhibition of general translation in mammalian cells by activating the eif2a kinase GCN2 (127). Another study reported that GCN2 is activated in DNA-PK (DNA damage checkpoint kinase) dependent on UVB-irradiation in mammalian cells. Thus, in human cells, GCN2 activation in response to some stresses might be linked to DNA damage through DNA-PK activity (128).

1.7.2.2 Starvation

The general amino acid control pathway maintains the amino acid level during starvation, and this is conserved from yeast to mammals (129). Starvation for nutrients compounds other than amino acids can also activate GCN2. For example various studies have shown that limitation to glucose in yeast leads to activation of GCN2, which then leads to activation of eIF2-α −GCN4 (ATF4 in mammals) pathway (129).

1.7.2.3 Mitochondrial or oxidative and ER stress

Protein homeostasis is vital for maintaining a normal cell's characterization; in eukaryotic cells, protein folding is facilitated by compartment-specific folding machinery in the cytosol known as ER. Maintenance of the mitochondrial metabolic function relies upon the mitochondrial proteome; chaperons in the mitochondrial matrix are responsible for protein folding into their functional conformation (130). Thus, the accumulation of misfolded or unfolded mitochondrial proteins leads to dysfunctional mitochondria, leading to mitochondrial stress. Reactive oxygen species (ROS) accumulate during mitochondrial stress in addition to upon exposure to various agents; GCN2 responds to accumulation of ROS and activates the GCN2 pathway (130, 131). Transmembrane and most secreted proteins are folded and matured in the ER's lumen. ER senses the accumulation of unfolded proteins in its lumen, which leads to ER stress. Accumulation of misfolded proteins in ER leads to the activation of unfolded protein response (UPR). Multiple studies suggest that both PERK and GCN2 function cooperatively regulate eIF2-α phosphorylation after activation of UPR (132, 133).

1.7.2.4 Toxin and viral infection

GCN2 can be activated during infection, bacterial or viral growth. This can be attributed to its role in starvation responses, since bacterial growth can lead to a nutrient shortage in the infected tissue (114). Human immunodeficiency virus type 1 (HIV) causes persistent infection in human cells, which leads to AIDS. This virus types heavily depends on the host cells' protein synthesis machinery to produce viral proteins –translation reduction. HIV infection accomplishes it by activating GCN2 (134). Inhibition of amino acid uptake or damage of the plasma membrane by pore-performing toxins (PFT), such as α -toxins, can also cause amino acid starvation. It has been shown that the initiation of autophagy as a defense mechanism against PFT requires GCN2, thus amino acid starvation leads to autophagy partly through activation of GCN2 (135).

Other stress mechanisms are also known to activate GCN2, such as osmotic stress and methyl methanesulfonate (MMS) treatment (125). As mentioned earlier, the molecular mechanism for activating GCN2 involves binding to uncharged tRNAs and leads to

conformational change. However, it is not well understood how all these different mechanisms might lead to the accumulation of uncharged tRNAs or there are other mechanisms that can activate GCN2 (114). In fact, recent study describes that a particular structure on the ribosome can activate GCN2, and they suggested that ribosome stalling can be a mechanism leading to GCN2 activation. Ribosome stalling process occurs upon damage to RNA for example by MMS, ROS and UV (136).

1.7.3 GCN2 in cell cycle progression

Proper control of cell division is vital for all organisms, and normal cells go through a multistep cell cycle process that is highly regulated, the cell cycle include: G1, S, G2 and M phase. Several inhibitory mechanisms called cell cycle checkpoints regulate correct cell division; these checkpoints include: G1 checkpoint, G2 checkpoint and metaphase checkpoint. G_1 is a critical phase in the cell cycle since, during G_1, cells decide whether to enter into a new cell division or not. Thus, a complex regulatory network ensures that cell enters S phase in a timely manner (137).

Studies have shown that GCN2 has a role in cell-cycle progression –delays G1/S transition. It is well established that damage to DNA delays the cell cycle progression at the G_1/S transition, and it has been shown that entry into S-phase is delayed in a GCN2 dependent manner in MMS treated budding yeast cells (138, 139). The pre-replication complex (pre-RC) formation is a mandatory step in preparation for DNA replication; pre-RC is formed when the Mcm complex is loaded onto chromatin (140). This process is delayed in a GCN2-dependant manner in fission yeast in response to UV, oxidative damage by H_2O_2, and alkylation by MMS (137, 141). However, it is unclear whether the cell cycle effects are mediated through translational regulation of selected proteins, general downregulation of translation, or phosphorylation of other substrates than eIF2-α (125).

1.8 The role of GCN2 in cancer

As mentioned above, cancer is a collection of very complicated diseases, and the tumor microenvironment plays an essential role in cancer progression. The ability of cancer cells to adapt to cell-intrinsic and extrinsic stresses through the IRS pathway is vital for cancer cell

development. Multiple studies have shown that GCN2 is essential for cancer cells to survive and thrive in a hostile microenvironment; the following sections describe some examples of the role of GCN2 in tumorigenesis.

1.8.1 MYC-GCN2 role in cancer development

Tumor growth and survival depend on altered rates of protein synthesis, the c-MYC is a proto-oncogene and a transcription factor, when overexpressed, causes an increase in protein synthesis (142, 143). Increased protein synthesis will increase the demand for amino acids and other intermediates, resulting in intrinsic stress, which can activate the ISR pathway through GCN2, which then maintains metabolic and protein homeostasis (142, 143). For example, it has been shown that the loss of the tumor suppressor gene adenomatous polyposis coli (APC) occurs almost universally in colorectal tumors. Loss of APC increases global translation and leads to MYC's overexpression, which leads to the phosphorylation of eIF2α via GCN2 kinase. Thus, it creates a negative feedback loop that limits protein synthesis to prevent MYC-dependent apoptosis in APC deficient colorectal cancerous cells (142). Another study has shown that the GCN2-eIF2α-ATF4 pathway plays a critical role in cell adaption and survival during MYC-dependent lymphoma tumor growth and progression (143). During tumor progression, ATF4 activation in a GCN2-dependant manner couples MYC-dependent translational activity to biogenetic demands by co-regulating translation initiation factor 4E-binding protein 1 (4E-BP1), which is a negative regulator of translation (143).

1.8.2 Angiogenesis

The GCN2-AFT4 pathway is also involved in promoting angiogenesis, thus promoting cancer cell growth. Tumor cells promote angiogenesis to overcome the stress associated with hypoxia by stimulation of endothelial growth factor (VEGF). It has been shown that VEGF expression is remarkably increased in response to amino acid deprivation through activating the GCN2-ATF4 pathway *in vitro* (144, 145). This suggestion was supported by observing GCN2 knock-down in tumor cells, which reduced tumor growth and angiogenesis in vivo (144).

1.8.3 Warburg effect

Today, various ongoing studies provide evidence that the GCN2 pathway plays an essential role in the Warburg effect. Pyruvate kinase is the critical enzyme that switches from oxidative phosphorylation to aerobic glycolysis; several isoforms of this enzyme exist. Most cancer cells display high glycolytic activity by expressing the less active pyruvate kinase isoform –pyruvate kinase muscle 2 (PKM2) (146). Findings suggest that tumor cells utilize serine-dependent regulation of PKM2 and the GCN2-ATF4 pathway to modulate glycolytic intermediates' flux to support cell proliferation (146). Another study has shown the importance of GCN2 activation in the regulation of mitochondrial H^+-ATP synthesis through selective translation (147). Thus, GCN2 activation is essential for reprogramming cancer-cell metabolism, which supports cell survival and growth.

1.8.4 Immunology

Various ongoing studies suggest that GCN2 has a role in T-cell response in the tumor microenvironment. Research indicates that GCN2 response to amino acid starvation prevents T-cell functionality by allowing T-cells to respond to the conditions created by indoleamine 2,3-dioxygenase (IDO), which leads to proliferative arrest and induction of anergy (148). However, another study shows that GCN2 is required for survival, proliferative fitness, and migration of $CD8^+$T-cell in nutrient-deficient tumors (149, 150). These inconsistent findings suggest that GCN2 has pleiotropic effects in T-cells that require further investigation.

Suggestions from all these different studies make it easier to see why GCN2 is an attractive target for cancer therapy, however there are still a lot is unknown. Thus, intense molecular research is needed within GCN2 and GCN2-dependant pathways, when designing drug targeting GCN2 and will be the key to designing more effective therapies for cancer in future.

AIMS OF THE STUDY

In spite of the emerging view that GCN2 is a promising target in cancer therapy, nothing is known about the role of GCN2 in prostate cancer. Thus, the main goal of this study is to investigate the role and regulation of GCN2 in prostate cancer, with the long-term goal of revealing whether GCN2 will be an effective therapeutic target for the treatment of prostate cancer.

In this Thesis we aimed to:

1. Verify if GCN2 is androgen-regulated in prostate cancer.
2. Investigate if GCN1 is essential for GCN2 activation in prostate cancer.
3. Determine if there is any interplay between MYC and GCN2 in prostate cancer.
4. Address whether treatment with GCN2 inhibitor (GCN2i) is effective in prostate cancer cells.

3. METHODS

This chapter describes the experimental approaches used in this work. A complete list of equipment and reagents used in this thesis are listed in Appendix A: Materials

3.1 Cell culture methods

3.1.1 Cell line models

In this study following eight prostate cancer derived cell lines were used: LNCaP-parental, LNCaP-C4-2 (hereafter referred to as C4-2), LNCaP-C4-2B (hereafter referred to as C4-2B), LNCaP-MYC, LNCaP-pcDNA3.1 (hereafter referred as pcDNA3.1), LNCaP-ARhi (hereafter referred as ARhi), LNCaP-Res-A (hereafter referred as RES-A), and LNCaP-Res-B (hereafter referred as RES-B). Additionally, HeLa cells were used as a control cell line. The pcDNA3.1 and ARhi cell lines were used more extensively. An overview of the cancer cell lines is provided in **table 3.1** and further described below:

Table 3.1 Overview of the cancer cell lines. Positive status is shown as +, negative status is shown as –, overexpression is shown as +++, and the approximate doubling time of the cells in the culture are given in hours. Dox: doxycycline.

Cell line	Cancer type	Origin	Doubling time (h)	AR status	c-MYC status
HeLa	Cervical cancer	Cervical tumor	24	-	+
LNCaP	Prostate cancer	Lymph node metastasis	60	+	+
C4-2	Prostate cancer	LNCaP subline	48	+	+
C4-2B	Prostate cancer	LNCaP cell xenograft	48	+	+
pcDNA3.1	Prostate cancer	Transfected LNCaP	60	+	+
ARhi	Prostate cancer	Transfected LNCaP	60	+++	+
RES-A	Prostate cancer	LNCaP + enzalutamide	60	+	+
RES-B	Prostate cancer	LNCaP + RD-162	60	+	+
LNCaP-MYC	Prostate cancer	Transfected LNCaP	60	+	+
LNCaP-MYC + Dox	Prostate cancer	Transfected LNCaP	60	+	+++

LNCaP or LNCaP-parental

Originally LNCaP cells were isolated from a metastatic of human prostatic adenocarcinoma (151). These cells are androgen sensitive and express AR and PSA mRNA in response to androgen; they also contain a T877A missense mutation in the LBD of the AR coding sequence. T877A missense mutations lead to less specific affinity to androgen, instead allow binding to a number of other steroid compounds (57). Over the years, multiple LNCaP sublines have been established with typical selective strategies for more specific studies.

C4-2 and C4-2B

C4-2 cell lines are androgen-independent LNCaP subline. The C4 was established by injecting LNCaP and human osteosarcoma mesenchymal stem cells under the skin of an intact mouse. These mice were then castrated to develop an androgen independent tumor; subsequently, the tumor was extracted, and the C4 line was established in culture. C4 was then injected under the skin of a castrated mouse to generate a second-generation cell line: C4-2 (152, 153) with subsequent monitoring for metastasis (154). Several metastases were detected, including lymph node and bone metastasis; these bone metastasis cells were isolated and termed C4-2B. C4-2B cells grow either intact or castrated mice; they also express AR and PSA in response to androgen (152, 154).

LNCaP-MYC

LNCaP-MYC cells are isogenic for MYC overexpression and are derived from LNCaP cells. LNCaP-MYC cells were established based on a "Tet-on-Tet off system" that modulates the expression of a gene of interest by either adding or removing tetracyclines. Tetracyclines are a diverse family of chemical compounds, and one of the derivatives is doxycycline (dox) (155). The c-MYC was amplified from an IMAGE clone and inserted by IN-fusion advantage homologous fusion at the BamH1 restriction site of the lentiviral pLVX-Tight-Puro vector (156). The plasmids were maintained by 2 μg/ mL puromycin and 200 μg/ mL geneticin (G418). Expression of the c-MYC oncogene is only activated in the presence of a transcriptional activator, in this case, doxycycline. MYC overexpression is inducible using 2 μg/ mL doxycycline (156, 157).

LNCaP-pcDNA3.1 and LNCaP-ARhi

LNCaP cells were also transfected with either empty pcDNA3.1 vector or pcDNA3.1 vector with wild-type AR coding region, cells were selected with 400 μg/mL G418, and several clones were expanded. LNCaP-pcDNA3.1 cells were established by transfection into an androgen responsive LNCaP cell with an empty pcDNA3.1 vector, and transfected cells were selected with 400 μg/mL G418. Then northern blot analysis and RT-PCR were used to determine the AR mRNA level. Subsequently, multiple clones were overexpressing AR mRNA, thus generating LNCaP-ARhi cells. LNCaP-ARhi cells contain both mutated AR and wild type AR, which leads to 13-fold higher AR expression and 4-6 higher protein levels than LNCaP-pcDNA3.1 (158, 159).

LNCaP Res-A and LNCaP Res-B

LNCaP cells were treated with first-generation nonsteroidal antiandrogen (NSAA) enzalutamide to generate anti-androgen resistant cell line RES-A. LNCaP cells were passaged with increasing concentrations of enzalutamide for 9.5 months. RES-B cells were generated by passing LNCaP cells with continuous treatment with 10 μM of second generation NSSA RD-162 for 13 months. Both cell lines were maintained in the same media as LNCaP cells containing 10 μM enzalutamide (160). In this study, RES-B cells were used in multiple experiments, but due to technical issues, data for RES-B are not shown (Appendix B). However, experiments using this cell line are suggested for future work.

3.1.2 Aseptic technique in the cell lab

The aseptic technique is designed to use practices and procedures to prevent contamination. This technique requires strict rules to minimize the risk of infection, simultaneously creates a barrier between microorganisms in the environment and the sterile cell culture. The aseptic technique is mandatory when performing cell culture work (161).

Procedure:

All the experiments involving cell culture were performed in a mammalian cell lab on a laminar air flow bench. Lab coats and gloves were always worn. Before working with cell culture, the laminar air flow bench was sprayed with 70% ethanol. All the equipment used

for cell culture and experiment were sterile; moreover, bottles and reagents were never left open inside the laminar air flow bench longer than necessary.

3.1.3 Cell culturing

Cell culturing is a method where cells harvested from an animal or plant are grown *in vitro* under controlled conditions. This method requires strict maintenance of the controlled conditions that mimic the cells' natural conditions. Thus, the cells must be supplied with nutrients such as amino acids, carbohydrates, vitamins, minerals, necessary growth factors, and hormones through a medium. Moreover, proper management of physical conditions such as temperature and gas composition are controlled by specialized incubators. To avoid contamination, handling and storage of cell cultures are performed under sterile conditions (162).

Procedure:

In this study, all the mammalian cell cultures were cultivated in Roswell Park Memorial Institute (RPMI) 1640 medium. RPMI 1640 medium both with and without phenol red was used. The medium was supplemented with additional nutrients, including 10% regular fetal bovine serum (FBS) or 10% Hyclone FBS with low antibodies and high growth factors, referred to as complete media. Glutamax is an alternative supplement to L-glutamine that provides Gln with increased stability (163) and is also added. For some of the cell culture, media puromycin and geneticin (G418) was added to maintain the plasmids of the cell lines. In addition, 1% penicillin streptomycin (PS) was added to the medium to prevent bacterial infection. **Table 3.2** represents the culturing conditions of each cell line used in this study.

Table 3.2 Cell lines and the growth media used for their culture.

Cell lines	Medium and additives	Special additives
HeLa	RPMI, 10% FBS, 1% PS	
C4-2	RPMI, 10% FBS, glutamax, 1% PS	
C4-2B	RPMI, 10% FBS, glutamax, 1% PS	

LNCaP-MYC	RPMI, 10% FBS, glutamax,	2 μg/mL puromycin, 200 μg/mL G418
LNCaP parental	RPMI, 10% FBS, glutamax	
LNCaP Res A	RPMI, 10% FBS, glutamax,	10 μM enzalutamide
LNCaP Res-B	RPMI, 10% FBS, glutamax,	10 μM enzalutamide
LNCaP-pcDNA3.1	RPMI, 10% Hyclone FBS, glutamax,	200 μg/mL G418
LNCaP-ARhi	RPMI, 10% Hyclone FBS, glutamax,	200 μg/mL G418

Cultivated cells were grown in a T75 flask, plates, or dishes depending on the experiment and were performed under a sterile condition in a laminar air flow bench. All the cells were cultivated in an autoflow IR direct heat CO_2 incubator with HEPA filter ISO class 5 VWB18 water bath (VWR) at the standard conditions of 37° C with 5% of CO_2 and O_2. Furthermore, to prevent overgrowth, these cells were checked 2-3 times a week.

3.1.4 Cell subculturing

Cell subculturing or cell passaging involves medium removal and transfer of cultivated cells from the previous culture into a fresh growth medium. This enables the cultured cell lines in a continuously dividing phase under controlled conditions. Passaging is performed when the cells are in the log phase, as indicated in **Figure 3.1**; this is necessary when performing research experiments for extended periods. As overgrowth of the cultured cells can reduce cell division ability, simultaneously increased the risk of mutations (162).

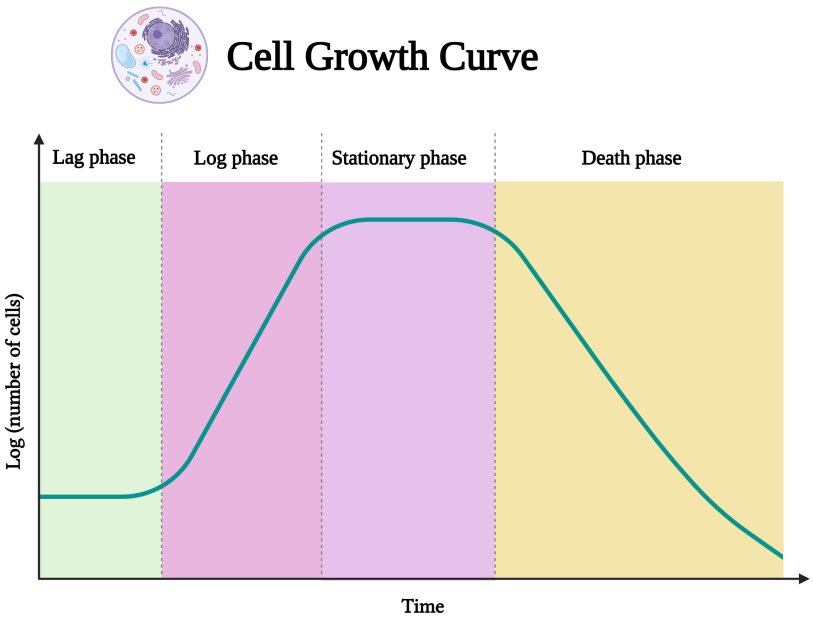

Figure 3.1 Growth curve of cultured cells. Cultured cells should be passaged during the log phase growth, which is also known as exponential growth and is characterized by 70-80% confluency. This figure was adapted and drawn from Biorender.com.

Adherent cells are enzymatically detached from the surface of the cultured flask by Trypsin-EDTA, which is widely used due to digestive strength. During subculturing, cells must be washed before adding Trypsin-EDTA, Phosphate Buffer Saline (PBS) is a widely used balanced salt solution and rinse chelators from the culture. FBS contains a1-antitrypsin that inactivates the Trypsin-EDTA; thus, the media must be removed, and cells must be washed with PBS before treatment with Trypsin-EDTA (162). Cell lines used in this study were sub-cultured according to **table 3.3**.

Table 3.3 Overview of cell lines and sub-cultivation requirements. Represents all the volume in mL for the T-75 flask.

Cell line	Dilution factor	Trypsin	Media (cell suspension)	Media (without cell suspension)
HeLa	1:8	1	6	10
C4-2	1:6	1	6	11
C4-2B	1:6	1	6	11
LNCaP-MYC	1:5	1	6	12
LNCa parental	1:5	1	6	12
LNCaP Res A	1:3	1	6	12
LNCaP Res-B	1:3	1	6	12

LNCaP pcDNA3.1	1:4	1	6	12
LNCaP ARhi	1:4	1	6	12

Procedure:

Aseptic technique was used during the whole process, and splitting was performed under the laminar air flow bench. The cell culture media was aspirated prior to washing with pre-warmed PBS (approximately 2 mL per 10 cm^2 cultured surface area) at 37° C. PBS was removed and pre-warmed Trypsin-EDTA (approximately 0.5 mL per 10 cm^2) at 37° C was added to the culture flask and incubated for 5-10 minutes at 37° C in the humidified incubator until the cells had visibly detached. Pre-warmed culture media was added to inactivate Trypsin-EDTA and repeatedly pipetted to prevent cell aggregation. According to passaging factor, a fraction of cell suspension was transferred to a new flask containing fresh medium and cultured at 37° C and 5% CO_2 in a humidified incubator.

3.1.5 Seeding of cells

Different experiments require cell solutions with a specific cell concentration. To achieve this, cells in suspension are counted and diluted to attain the desired cell concentration for seeding. Trypan blue is a dye that stains the dead cells, thus makes sure that live and dead cells are counted separately in the Countess™ II Automated Cell Counter (Invitrogen) (164). The desired cell numbers are obtained using the formula presented in the **equation. 3.1**.

Equation 3.1: cell seeding formula:

$$\frac{Desired\ number\ of\ \frac{cells}{dish}}{Counted\ cell\ \frac{cells}{mL}} = mL\ of\ cell\ solution\ to\ use$$

Procedure:

Aseptic technique was used during the whole process, and passaging was performed in the laminar air flow hood. The cell suspension was obtained as described in section 3.1.4, 10 μL of 0,4% trypan blue was mixed well with 10 μL of cell suspension by pipetting up and down multiple times. Then 10 μL of the trypan-blue stained was loaded into the loading area of the Countess™ II Automated Cell Counting Chamber slide (Invitrogen). The concentration

and percentage number were given by the counter machine, which was noted, and equation 3.1 was used to appropriately dilute the cell suspension to the desired concentration.

3.2 Snap freeze

Snap-freeze is a technique that allows rapid freezing and preservation of tissue, cells, or samples. Snap-freezing reduces water crystal formation, reduces actions of proteases and nuclease to inhibit degradation of molecules such as RNA, thus maintain the integrity of tissues, cells, or samples (165).

Procedure:

For cell dishes, media was removed before snap-freezing at -80° C, prior to snap-freeze, samples were correctly labeled with the date, name, and other information.

3.3 Ionizing Radiation

Radiation exists all around us, and radiation biology describes the interaction between radiation and living matter (166). According to the biological effect, radiation is categorized in two forms: non-ionizing and ionizing. The **figure 3.2** shows the electromagnetic spectrum, ranging from a frequency below 3 gigahertz to above 3 exahertz. Non-ionizing radiation are frequencies below ultraviolet (UV). In this study, we only focused on the ionizing form of radiation. Ionizing radiations are seriously harmful to biological materials because they form ions which is an electrically charged particle and transfer the energy to the cells of the tissue they pass through. Upon direct interaction with DNA, this ionizing radiation causes DNA damage (167, 168).

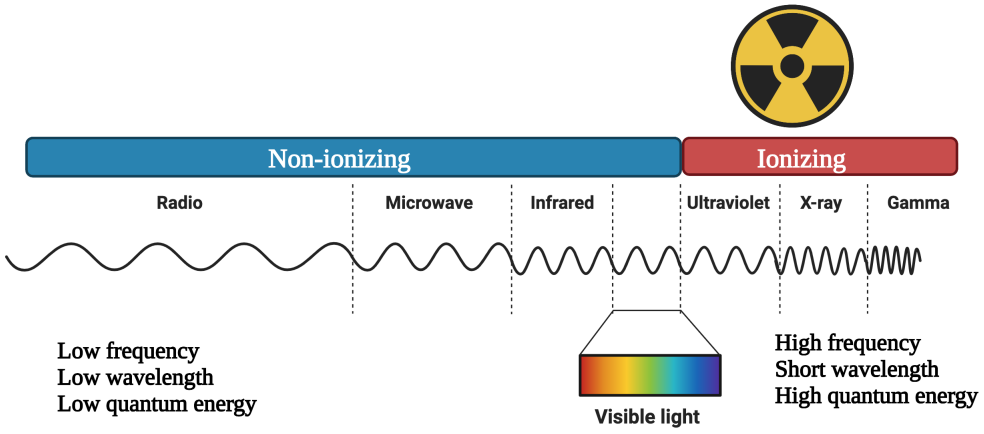

Figure 3.2 Schematic representation of the electromagnetic spectrum. Shows both non-ionizing and ionizing radiations. This figure was adapted from the article "5G Radiation and COVID-19: The Non-Existent Connection" and drawn in Biorender.com.

3.3.1 Ultraviolet radiation

Ultraviolet (UV) irradiation is a method that uses electromagnetic radiation that can penetrate the cell membrane and cause damage to DNA. UV electromagnetic radiation has a shorter wavelength than visible light and a longer wavelength than X-ray (169). In this study, the UV method was performed under a fume hood with a UV lamp and protection glass and have radiated cells with UV-C with a radiation dose of 20 J/m^2. UV radiation dose duration was measured according to **equation 3.2**.

Equation 3.2 UV-radiation dose time:

$$Time = \frac{Dose \times 1000}{Intensity\ detected}$$

Procedure:

The fume hood with a UV lamp and protection glass was turned on, and the radiation intensity was measured by a radiometer (Ultraviolet products, San Gabriel, CA, USA). The medium was removed from the dishes and radiated for a time calculated according to equation 3.2. After radiation, the medium was placed back very quickly, and the cells were incubated for 1 hour.

3.3.2 X-ray radiation

X-rays are photon beams with low radiation charge and lower mass; like other ionizing radiation, x-ray also causes damage to DNA. X-rays are generated by a device that excites electrons, and the doses are measured in the unit Gray (Gy) (168). In this study, X-ray experiments were performed with the x-ray generator Faxitron® Cabinet X-ray System, model CP-160, 160kV, 6.3mA.

Procedure:

Cells were taken out of the incubator 48 hours after seeding and placed in Faxitron® Cabinet X-ray System and irradiated with 1 Gy. The cells were then placed back in the incubator for further.

3.4 Starvation assay

The starvation assay involves amino acid starvation of the desired cells for a certain amount of time. In this study, we have used a salt-based starvation medium with BSA provided by Dr. Beata Grallert.

Procedure:

Cells were seeded in 35 mm dishes coated with poly-D-Lysine (PDL), which is a chemically synthesized extracellular matrix and aids cells for better attachment to the dish surface (170). Cells were taken out of the incubator 36 hours after seeding; the media was carefully removed and replaced with starvation media. The dishes were placed back in the incubator for 2 hours at 37° C before snap-freeze at -80° C (section 3.2).

3.5 Hormone treatment

In this study, we have experimented with steroid hormones, and to see the effect of the hormone *in vitro,* we had to replace RPMI media with phenol red (red media) with RPMI media without phenol red (white media). White media with charcoal stripped FBS (CS-FBS) was used, which removes hormones, growth factors, and cytokines (171), since our goal was to remove molecules that would inhibit androgen uptake.

Procedure:

Aseptic technique was used during the whole process, and passaging was performed under the laminar air flow bench. The cell suspension was obtained as described in section 3.1.4, and desired cell numbers were obtained by cell counter machine (section 3.1.5). Then the cell suspension was centrifuged in Allegra® X-14 Series Benchtop Centrifuge for 5 minutes. The supernatant was removed, and pre-warmed whited media was added; cell aggregation was prevented by pipetting multiple times up and down. The cells were then seeded in 35 mm dishes coated with PDL and incubated for 48 hours. After 48 hours, 10 nM DHT was

added and placed back in the incubator at 37° C in the humidified incubator for further growth.

3.6 Protein methods

Immunoblotting, or protein blotting, also known as western blotting, is a rapid and sensitive assay that detects proteins based on specific-antibody recognition. Immunoblotting involves protein extraction, separation of proteins in sodium dodecyl sulfate (SDS) polyacrylamide gel, transfer of proteins to a solid support or membrane (polyvinylidene difluoride –PVDF membrane), and lastly, detection and visualization of proteins by an antibody specific to the protein of interest, which is then detected by an HRP-conjugated secondary antibody and chemiluminescent substrate (172). The schematic representation of western blotting is shown in **figure 3.3**.

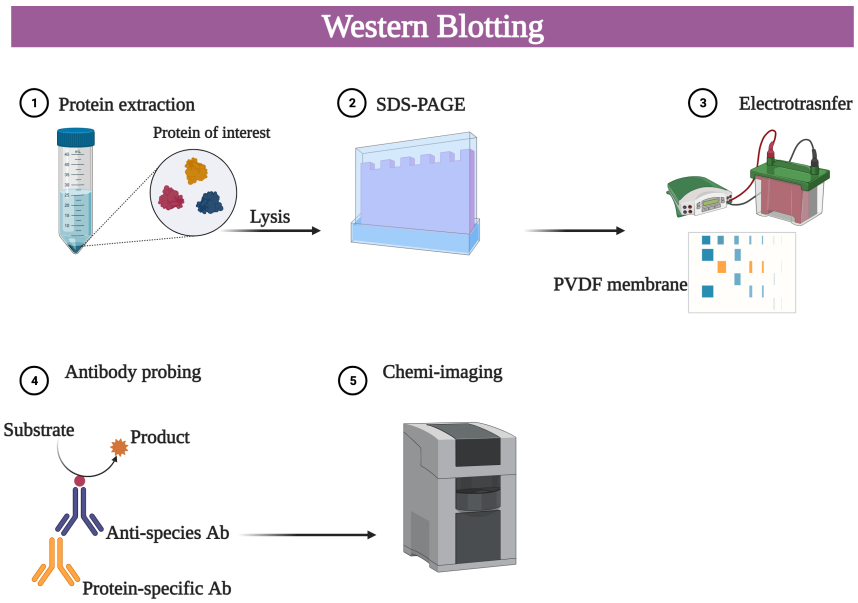

Figure 3.3 Schematic representation of western blot. This figure was adapted from and drawn in Biorender.com.

3.6.1 Protein extraction

Protein extraction involves isolating proteins from cells or tissues via lysis by disrupting cell membranes (figure 3.2) (172). Laemmli sample buffer was used for protein extraction, which contains necessary components for membrane degradation and protein stabilizer. Lammeli sample buffer includes components such as sodium dodecyl sulfate (SDS), which denatures protein and give them negative charge so that protein can be separated based on size, also contain glycerol increases the density of the sample so that it can be loaded better in the

sample well. In addition, the sample buffer contains bromphenol blue dye, which makes the lysate visible during loading in the well; moreover, it includes Dithiothreitol (DTT), which reduces the intra and inter-molecular disulfide bonds (173).

Procedure:

Pre-warm laemmli sample buffer 2x was directly added to the cell dishes or frozen cell dishes. The frozen cell dishes were kept on ice during the whole procedure. Cell scarper was used to scrape the cells from the cell dish surface and pipetted in 1 ml labeled Eppendorf tube. The cell scraper was washed in water and 70% ethanol and dried completely before using to prepare another sample.

3.6.2 Protein measurements

Protein measurement is the method of measuring protein concentration of the cell lysate to ensure equal protein is loaded during the protein separation (section 3.7.3). Quantification of the protein is a colorimetric detection, which was done by Pierce™ BCA Protein Assay Kit. In alkaline environments, amino acids such as cysteine, tryptophan, and tyrosine in a protein reduces Cu^{2+} to Cu^{+}. The reduced Cu^{+} reacts with bicinchoninic acid (BCA) containing reagent and results in a purple-colored complex. The absorbance of the purple-colored complex is measured at 562 nm in a Multiscan™ FC microplate photometer (Thermo Scientific). The absorbance is linear with increasing protein concentration. A standard curve is generated by measuring absorbance values Bovine Serum Albumine (BSA) (174). **Table 3.4** shows the compounds needed for the BCA assay.

Table 3.4 BCA protein assay reaction setup. SC: standard curve dilution

Reagents	**Wells in the 96- well plates**						
	Blank	**SC1**	**SC2**	**SC3**	**SC4**	**SC5**	**Sample**
BSA, 2 μg/mL (μL)	-	1	2	3	4	8	-
Milli-Q H_2O (μL)	50	49	48	47	46	42	49
Sample solution (μL)	-	-	-	-	-	-	1
Total volume (μL)	50	50	50	50	50	50	50

Procedure:

BCA protein assay reaction was set up according to table 3.4, and BCA working solution was made by diluting Reagent B 50-fold in Reagent A. 100 μL BCA working reagent was added to each well and incubated at 37° C for 30 minutes. After incubation, the absorbance of the standard and samples was measured at 562 nm in a Multiscan™ FC microplate photometer, a statistical method was performed to obtain protein concentration (section 3.9).

3.6.3 Protein separation

Protein separation is a method where proteins are separated through sodium dodecyl-sulfate polyacrylamide gel electrophoresis (SDS-PAGE) based on molecular weight (figure 3.3). Sample buffer (from section 3.7.1) contains DTT and SDS, which linearize the protein and disrupt disulfide bonds so that the proteins can separate solely based on the molecular weight by electrophoresis. Polyacrylamide gel (PAG) consists of a three-dimensional acrylamide polymer network and a cross-linker, which is neutrally charged. The linearized negatively charged proteins migrate toward the positively charged through PAG under the influence of the electric field. Smaller proteins migrated faster than larger proteins in PAG (175).

Procedure:

Eppendorf tubes with cell lysates and sample buffer were boiled in a heating block at 95°C for 5 minutes. BIO-RAD gel chamber was assembled with desired gel, and the chamber was filled with 1X running buffer. The desired amount of protein was loaded in the PAG, and 8 µL of Precision Plus Protein™ Dual color molecular weight standard was loaded in one well. SDS-PAGE was running at 180-200 V for 30-60 minutes depending on PAG percentage and the size(s) protein(s) of interest.

3.6.4 Protein transfer

Protein transfers is a vital step, where the separated protein in PAG must be transferred to a solid support matrix so that proteins can be detected by immunodetection methods (figure 3.3). In this study, the PVDF membrane was used and had high binding affinity proteins.

PVDF membrane binds to proteins by dipole and hydrophobic interaction, moreover, provides better retention of absorbed proteins than other supports (176). **Figure 3.4** shows the PVDF membrane and PAG assembly.

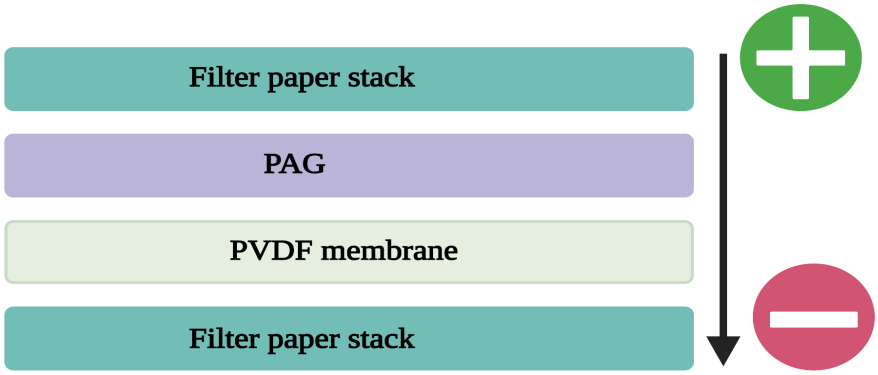

Figure 3.4 Western blot transfer assembly. The composition of the protein transfer elements inside the Trans-Blot® Turbo™ transfer system and the black arrow represent the direction of protein transfer. The figure was drawn in BioRender.com.

Procedure:

The PVDF membrane was activated by soaking in 96% ethanol for 30 seconds. Then the membrane was soaked in Milli-Q H_2O until the membrane was hydrophilic. Two stacks of filter paper were soaked in transfer buffer and assembled according to the figure 3.4. Assembled PVDF membrane and PAG was transferred in the semi-dry Trans-Blot® Turbo™ transfer cassette. A roller removed air bubbles and excess liquid before selecting the desired transfer program from the Trans-Blot® Turbo™ transfer system.

3.6.5 Immunodetection

PVDF membrane bound protein can be detected by immunodetection, where proteins are detected and visualized by binding specific antibodies (figure 3.3). The membrane must be treated with non-ionic detergents such as non-fat dry milk or BSA so that unreacted membrane sites are blocked for antigen binding. The primary antibody binds to the protein of interest, and the secondary antibody binds to the primary antibody; secondary antibody is an enzyme conjugated antibody specific to the primary antibody. In this study, we have used horseradish peroxidase (HRP) conjugated enzyme. Lastly, a substrate is added that reacts to HRP and produces detectable chemiluminescence, which can be imaged by ChemiDoc™ MP imaging system.

Procedure:

After protein transfer, PVDF membrane was blocked with blocking buffer containing either 5% skim milk powder or 5% BSA and incubated for 1 hour at room temperature. Primary antibody was added and incubated at 4°C overnight. The day after primary antibody was collected and stored for future use. Then the membrane was washed with tris buffered saline with tween (TBS-T) 5 minutes 3 times. Secondary antibody was added and incubated at room temperature for 1-2 hours. After incubation, secondary antibody was removed, and the membrane was washed with TBS-T for 5 minutes 3 minutes. TBS-T was removed and 3-5 mL combined substrate of A and B 1:1 by Immunobilon® Western Chemiluminescence Substrate was added. ChemiDoc™ MP imaging system was used to visualize the chemiluminescence signal, and the data was analyzed by the Image lab Software (BIO-RAD).

3.6.6 Stripping

Performing western blot on the same samples multiple times to test different antibodies is very time-consuming and expensive. Furthermore, when comparing signals, it can be important that it is done on the same blot so that there are no differences deriving from loading or other issues. Also, it can be useful when detecting proteins of the same or similar sizes. Stripping is a process that removes antibodies that are present in the PVDF membrane; thus, one membrane can be stripped multiple times and probed for new antibodies (177).

Procedure:

Stripping buffer was added to the PVDF membrane to cover the membrane and incubate for 15 minutes at 37° C. After incubation, washed with TBS-T for 5 minutes 3 times. Then blocked for 1 hour with blocking buffer containing either 5% skim milk powder or 5% BSA. Immunodetection procedure from section 3.7.5 was performed after incubation with blocking buffer.

3.7 Gene expression

Quantitative polymerase chain reaction (q-PCR) is one of the methods used to analyze transcript levels. qPCR involves extraction and measurement of RNA, synthesis of

complementary DNA (cDNA) by reverse transcription, and amplification of cDNA using polymerase chain reaction (PCR) (178).

3.7.1 RNA extraction

RNA extraction is a method that successfully isolates intact RNA and consists of four steps: effective disruption of cells, denaturation of nucleoproteins, inactivation of RNase activity, and removal of DNA and RNA proteins (179). The ReliaPrep™ RNA Cell Miniprep System kit was used to extract RNA. This kit provides different enzymes that breakdown cell components and aids the nucleic acid bind to the column by disrupting water molecules with chaotropic salts. Furthermore, the kit provides RNAase-free DNAase I that digest contaminating genomic DNA. Multistep washing further purifies the total RNA from contaminating salts, protein, and other cellular components (179).

Procedure:

RNA extraction was performed under RNA LAF hood and rinsed with RNAaseZap. The cells were harvested using 250 µL BL+ TG buffer and pipetted multiple times to shear the DNA. The cell lysate was collected and transferred into the minicolumn in collecting tubes. 85 µL of 100% isopropanol was added to the minicolumn and vortexed for 5 seconds. The cell lysate with isopropanol was then centrifuged at 1000 rpm for 30 seconds. The liquid in the collection tube was discarded, and 500 µL of RNA Wash solution was added to the minicolumns and centrifuged at 1000 rpm for 30 seconds. 30 µL of DNAase I incubation mix was added and incubated at room temperature for 15 minutes. After incubation, 500 µL of RNA Wash solution was added and centrifuged at 1000 rpm for 30 seconds, the liquid in the collection tube was discarded. 300 µL of RNA Wash solution was added to the minicolumns and centrifuged at 1000 rpm for 2 minutes. The ReliaPrep™ Minicolumn was transferred to an elution tube, and 30 µL of Nuclease-free water was added, subsequently centrifuged at 1000 rpm for 1 minute. The minicolumn was discarded, and the elution tube containing purified RNA was labeled and put on ice.

3.7.2 RNA measurement

RNA measurement provides information about both the quality and quantity of the extracted RNA before further experiments. The quality and quantity of the RNA were measured in NanoDrop™ 2000 (TermoFisher) spectrophotometer. The NanoDrop spectrophotometer is designed to measure nucleic acid concentrations of the samples based on their absorbance. The purity of DNA and RNA is assessed by the ratio absorbance at 260 nm and 280 nm. A ratio of approximately 2,0 is generally accepted as "pure" for RNA, and a ratio below that indicates the presence of protein, phenol, or other contaminants that absorb strongly at or near 280 nm (180). NanoDrop™ 2000 (TermoFisher) spectrophotometer measured RNA concentrations in µg/µL unit.

Procedure:

NanoDrop™ 2000 was started and the «measurement of nucleic acid» program was chosen. 2 µL of RNAase-free water was loaded into the lower measurement pedestal before closing the sample arm. RNA measurement program was chosen by clicking Ok on the program. The lower pedestal was wiped with filter paper and loaded with 2 µL nuclease-free water used in section 3.7.1. Nuclease-free water was calibrated as a blank. For all the samples following the blank, 2 µL was loaded and measured; at each loading, the pedestal was clean with filter paper.

3.7.3 cDNA synthesis

cDNA synthesis is the process where DNA is produced from RNA by reverse transcription, which is then used as templates for a variety of applications for RNA studies. In this study, we qScript® cDNA Synthesis Kit (Quantabio) was used for cDNA synthesis. The kit is capable of reverse transcription up to 2 µg of RNA into cDNA. The qScript Reaction Mix (5X) contains all the necessary components, including random primers, which are oligonucleotides with random sequences and are not limited to the requirement of 3´ end poly A-tail. Moreover, the kit contains a reverse transcriptase enzyme. The primers bind to the reverse transcriptase enzyme, which adds nucleotides complementary to the mRNA (181). In this study, a volume equivalent to 2 µg of RNA was taken and diluted with nuclease-free water. **Table 3.5** shows the composition of solutions for cDNA synthesis in qScript® cDNA Synthesis Kit.

Table 3.5 Compositions of solutions for reverse transcription. Varied variables represent as: –.

qScript Reaction mix	Volume added
RNA	- µL
Nuclease-free water	- µL
qScript Reaction Mix (5X)	4.0 µL
qScript RT	1.0 µL
Final volume	**20 µL**

Procedure:

Master mix according to table 3.5 was prepared in PCR Eppendorf tube on Eppendorf® PCR Cooler. The tubes were vortexed for 5 seconds and centrifuged for 10 seconds. Then the Eppendorf tubes were placed in DNA Engine Tetrad® 2 Thermal Cycler (BIO-RAD) with recommended conditions and incubated for 45 minutes. After cDNA synthesis, the products were diluted 1:10 with Milli-Q H_2O and snap frozen at -80° C.

3.7.4 RT-PCR

Real time PCR (RT-PCR) is a form of quantitative PCR and provides both absolute and relative quantification. This is possible by detecting and quantifying the amplified DNA in the real time by the fluorescence reporter molecule included in the reaction mixture. The PerfeCTa® SYBR® Green Super Mix kit was used for RT-PCR in this study. The kit contains SYBR green I dye probe, and this dye display relatively little fluorescence, but when it binds to DNA, its fluorescence increases more than 1000-fold. In addition, the kit also contains Taq-DNA polymerase that contains a monoclonal antibody, which inactivates polymerase by binding to it, and the unmodified Taq polymerase is only activated in the initial PCR denaturation at 95ºC. This process enables specific and efficient primer extension(182, 183). **Figure 3.5** shows the general steps involved in RT-PCR.

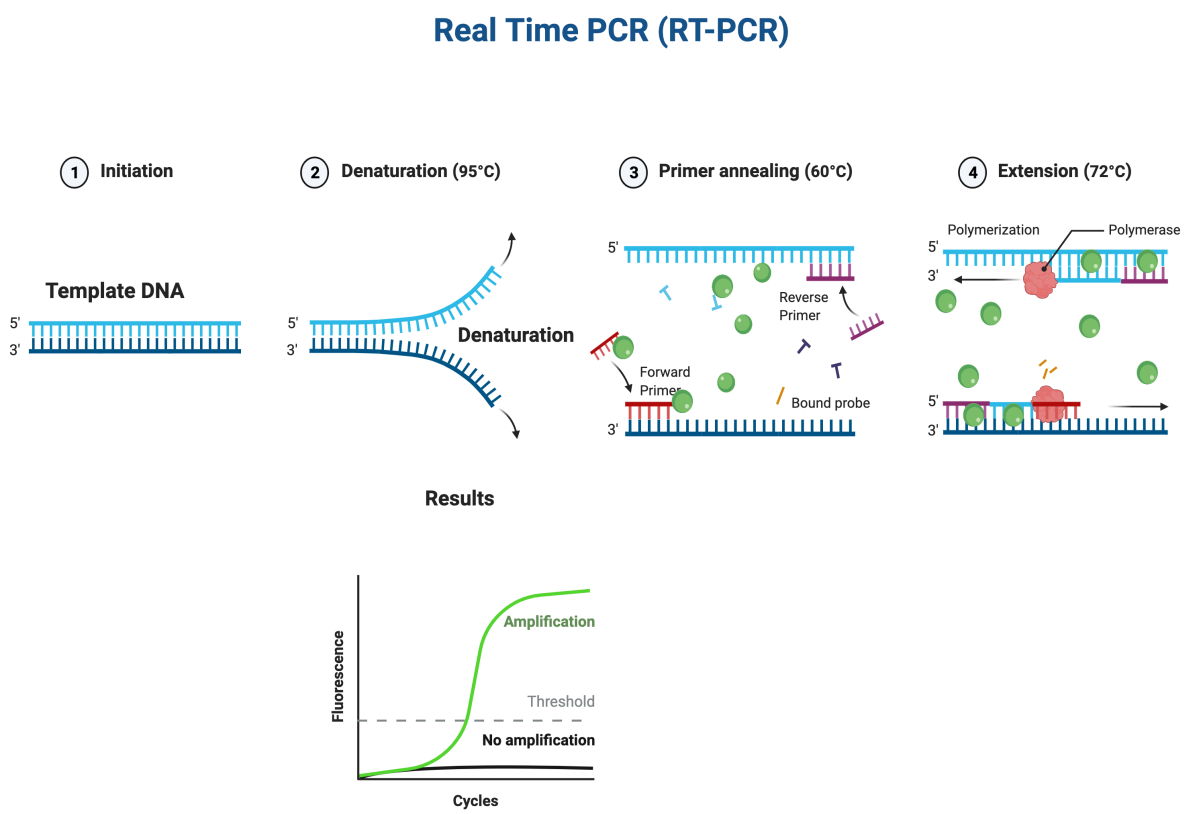

Figure 3.5 Schematic representation of general RT-PCR. The template DNA represents cDNA; once primers bind to single stand DNA after denaturation, they provide the starting point for DNA polymerase. During elongation process, SYBR Green I fluoresce only when bound to dsDNA. This figure was adapted from and drawn in BioRender.com.

In this study, we have used relative quantification to measure the cDNA present in the samples, and the value was referred to as the transcriptional level (183). For the quantitative method standard curve is necessary; the standard curve was prepared by mixing universal RNA (Clontech Laboratories, Inc., Mountain View, CA, USA) and total RNA of LNCaP cells in a ratio of 1:5. A serial dilutions was prepared after cDNA synthesis and correspond to 1000, 200, 40, 8, 1.6, and 0.32 µg of RNA. In addition, for better understanding and comparison of the observed values, a reference gene or housekeeping gene was used (TBP) (183). CFX Connect Real-Time PCR Detection System (BIO-RAD) was used to quantify cDNA. The system uses a threshold cycle to calculate the quantity of DNA present in the samples. **Table 3.6** shows the composition of the reaction mix for qPCR used in this study.

Table 3.6 Composition of reaction mix for qPCR

qScript Reaction mix	Volume added

PerfeCTa SYBR Green Super Mix (2X)	5 µL
Forward primer	0,25 µL
Reverse primer	0,25 µL
Nuclease-free H_2O	3,5 µL
Template	1 µL
Final volume	**10 µL**

Procedure:

Master mix according to table 3.6 was made except template (section 3.7.3) and added 9 µL of the master mix to 96 well plates; the 96 plate was placed on Eppendorf® PCR Cooler during the whole process. After adding 1 µL of the template the plate was sealed with plastic film. The plate was spined down by a centrifuge for 10 seconds. The plate was then incubated in CFX Connect Real-Time PCR Detection System (BIO-RAD). After incubation the data was exported to excel for analysis.

3.8 Presto blue assay

PrestoBlue™ Cell Viability Reagent is used for cell viability assays, PrestoBlue™ Cell Viability Reagent is a resazurin-based solution. Metabolically active cells reduce resazurin to resorufin, and this compound has a red color with high fluorescence. Thus, the reduction process is very quick, providing a quantitative measure of viability and cytotoxic values. The fluorescence was measured by Modulus™ Microplate Multimode Reader with a maximum absorbance of approximately 570 nm (184, 185).

Procedure:

Cells were seeded in a black 96 well plate with a transparent bottom and incubated for 48 hours. 11 µL of presto blue reagent was added to the wells and incubated at 37° C for 20 minutes. The plate was inserted into Modulus™ Microplate Multimode Reader and fluorescence was measured. The data were saved for further analysis.

3.9 Statical analysis

All the statical analysis of this study was performed using Microsoft-Excel 2016 software. Most of the experiments of this study needed the normalization of the data. The formula that was used:

Equation 3.3: Normalize value

$$\frac{Mesured\ value\ to\ be\ normalized}{Value\ of\ the\ reference}$$

For each analysis, an evaluation of the most suitable formula was used. For all the average values, standard deviation, and standard error, basic equations were used, and the equations are given below:

Equation 3.4 Arithmetic mean values:

$$\frac{sum\ of\ all\ the\ values}{number\ of\ terms}$$

Equation 3.5 Standard deviation (SD):

$$\sigma = \sqrt{\frac{\sum(x_i-\mu)^2}{N}},$$

Where σ = population standard deviation, N = the size of the population, x_i = each value from the population and μ = the population mean.

Equation 3.6 Standard error of the mean (SEM):

$$SE = \frac{\sigma}{\sqrt{n}},$$

Where SE = standard error of the sample, σ = sample standard deviation, and n = number of samples.

For the precision of the presented data, the error bars were used in the form of $\pm$SEM or $\pm$SD, and the following formulas were used to propagate the error bars.

Equation 3.7 For addition or subtraction:

$$\sigma x = \sqrt{\sigma_a^2 + \sigma_b^2}$$

Where x = A+ B or x =A-B.

Equation 3.8 For multiplication or division:

$$\sigma x = X\sqrt{\frac{\sigma_a^2}{a^2} + \frac{\sigma_b^2}{b^2}}$$

Where X = A/B or X = A* B

BCA assay

Obtained absorbance values from the BCA assay were transferred to Microsoft Excel, where a linear regression equation was used to estimate the protein concentration.

Equation 3.9 Linear regression equation**:**

$$y = ax + b$$

Where y is the measured absorbance values, x is the protein concentration, a is the slope of the line, and b is the line's y-axis intercept.

T-test

The t-test was performed on Microsoft excel 2016, and for this study, we have used a two-tail test to find significant differences.

4. RESULTS

The results of this study are explained as follows:

- First, verify the functionality of GCN2 in PC, subsequently regulation of GCN2 by AR nuclear receptor.
- Second, GCN1 necessity in PC cell lines expressing the basal level AR and overexpressing AR.
- Third, determine whether MYC regulates GCN2 expression in the PC cell line, which overexpresses MYC. Additionally, the importance of GCN1 in that very same cell line.
- Forth, address the functional consequence of inhibiting GCN2 in prostate cancer cell line overexpressing AR.

4.1 GCN2 functionality in PC

GCN2 has been shown to play an important role in several different cancers and few of them have been described. However, nothing is known about the role of GCN2 in PC. Therefore, we first aimed to investigate whether GCN2 is functional in selected PC-derived cell lines using established methods to assess whether GCN2 can be activated.

4.1.1 Activation of GCN2 in C4-2 by UV irradiation

Upon activation GCN2 auto-phosphorylates, which allows us to assess the activity. HeLa as control cell and C4-2 as PC-derived cell were chosen for this experiment. To test whether GCN2 is functional, we stressed C4-2 and HeLa cells by UV irradiation at 20 J/m^2, which is known to activate GCN2 (114). **Figure 4.1** shows the GCN2-P protein levels in the cell lines and their response to UV irradiation.

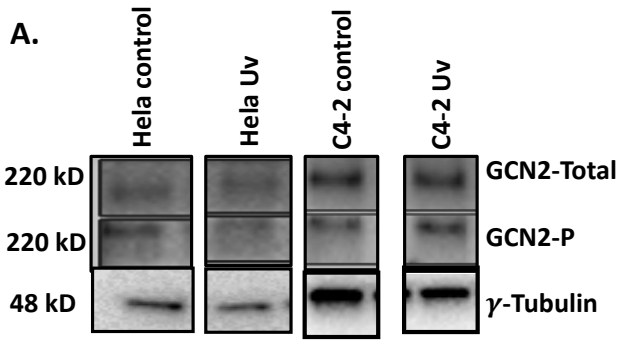

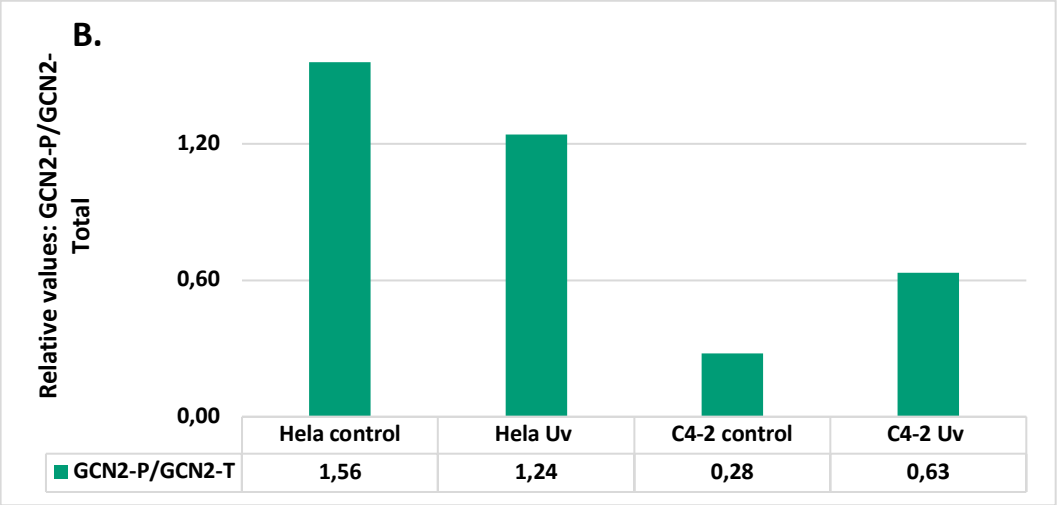

Figure 4.1 Western blot and quantification of GCN2 phosphorylated in HeLa and C4-2 cell lines after UV irradiation. A) Western blot image representation of GCN2-total and GCN2-P result in the HeLa and C4-2 cell lines induced by UV irradiation. Both GCN2-T (GCN2-total) and GCN2-P (GCN2-phosphorylated) have the same size of approximately 220 kD, and γ – tubulin as loading control has a size of about 48 kD. **B)** Bar graphs representing GCN2-P levels normalized to GCN2-T in the HeLa and C4-2 cell lines. These bar graphs represent the mean relative values of two independent biological replicates.

GCN2 phosphorylation (GCN2-P) is induced in C4-2 cell lines after UV irradiation and much the same for HeLa cell lines (figure 4.1 A). Protein amount after quantification by densitometry where GCN2-T is normalized to the γ – tubulin loading control tubulin and then GCN2-P is normalized to the GCN2-T, GCN2 activation after UV irradiation in the C4-2 cell line is a visible, almost 2,3-fold increase compared to control (figure 4.1 B). Interestingly, at the UV doses used in the assay less GCN2-P was detected in HeLa cells after UV irradiation, approximately 1,3 -fold decrease compared to the control. Thus, we could not observe GCN2 activation in response to UV irradiation in HeLa cells, but we could determine that GCN2 is functional in C4-2 cells upon being subjected to stress such as UV.

4.1.2 Activation of GCN2 in C4-2 by starvation

We investigated further the functionality of GCN2 when cells are exposed to another type of stress namely amino acid starvation which is known to activate GCN2. HeLa and C4-2 cells were grown in regular media for 36 hours, then the regular media was replaced with salt-based starvation media and incubated for 2 hours. Then protein was extracted and assessed GCN2 activation by immunoblotting. **Figure 4.2** shows the GCN2-P protein levels in these cell lines in starvation media.

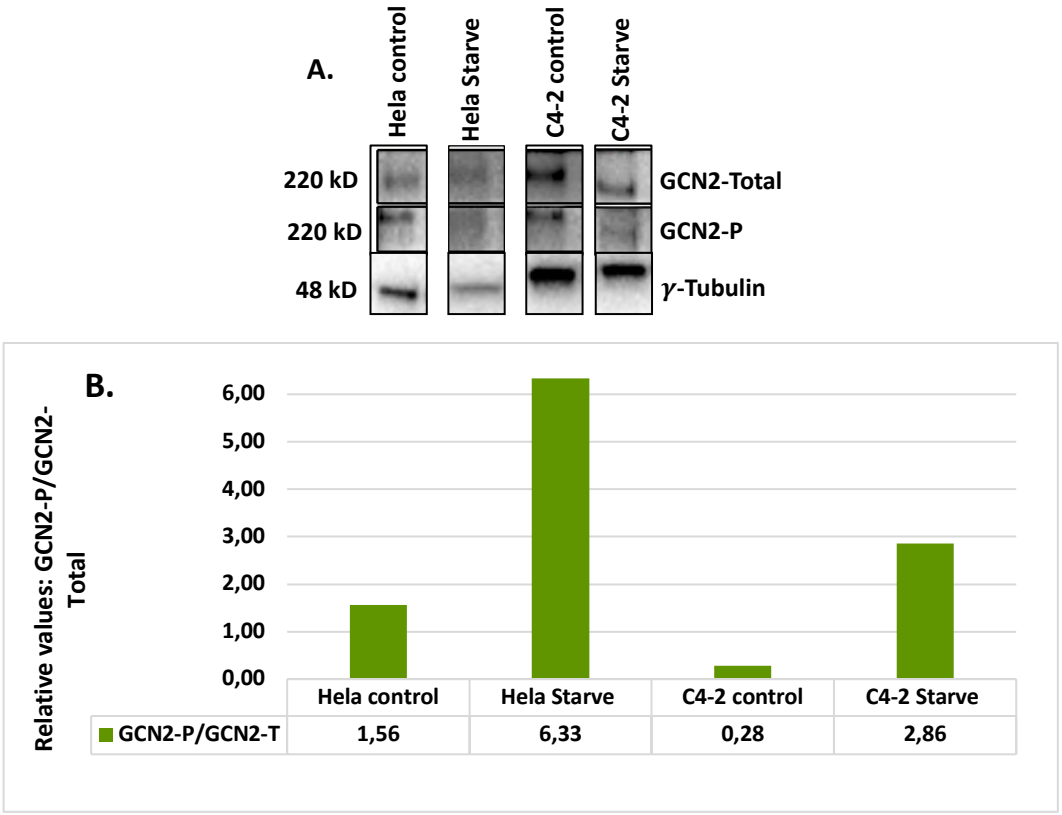

Figure: 4.2 Western blots and quantification of GCN2 phosphorylation in HeLa and C4-2 cell lines after amino-acid starvation treatment. A) Western blot image representation of GCN2-total (GCN2-T) and GCN2-phosphorylation (GCN2-P) result in the HeLa and C4-2 cell lines induced by starvation media. **B)** Bar graphs representing GCN2-P levels normalized to GCN2-T in the HeLa and C4-2 cell lines. These bar graphs represent the mean relative values of two independent biological replicates.

The presence of GCN2 protein bands could not be assessed clearly via visual inspection in C4-2 and HeLa cell lines after starvation treatment (figure 4.2 A). However, after quantification by densitometry in which GCN2-T is normalized to the γ – tubulin loading control and GCN2-P normalized to GCN2-T, an increase in GCN2-P levels could be seen both in HeLa and C4-2 cells (figure 4.2 B). In C4-2 cells we detected almost 10,2 -fold increase compared to control, while in HeLa cells the GCN2-P level increased approximately 4,1-fold compare to the control. We therefore concluded that GCN2 is activated after amino acid starvation treatment and functional in both C4-2 and HeLa cell lines.

4.2 GCN2 expression regulated by AR

Experiments described in section 4.1 suggested that GCN2 is functional in PC not only after UV irradiation but also under amino acid starved condition. Thus, the goal of the following experiments was to verify whether AR regulates GCN2 expression in PC.

4.2.1 Investigating GCN2 activation in PC cell line models

The following experiment aimed to determine levels of GCN2-P, in absence of stressors, in PC cell lines in normal culture conditions. The cell lines for this experiment include: C4-2, C4-2B, LNCaP parental (also known as LNCaP), LNCaP-Res-A cells.

As C4-2 are derivatives of LNCaP cells grown in castrated mice, we cultured these cells not only in RPMI with phenol red supplemented with full fetal bovine serum (red media) but also in RPMI phenol-red-free media with charcoal stripped fetal bovine serum (white media). This allows comparison of GCN2 levels in LNCaP-Res-A cells presence and absence (castrate levels) of androgens. To compare levels of GCN2 in cells, which grow in 10 μM enzalutamide, with parental lines, LNCaP were grown in regular red media, treated either with DMSO or with enzalutamide for 48 hours. **Figure 4.3** shows the GCN2-P protein levels of PC cell lines models.

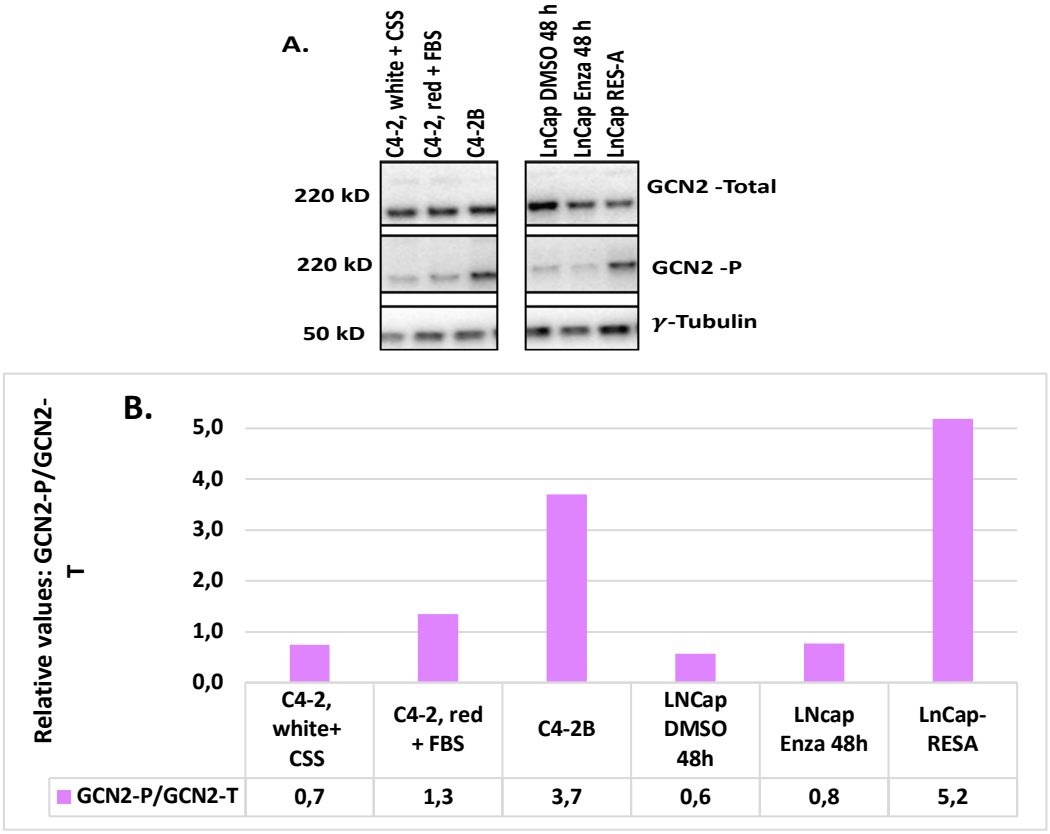

Figure 4.3 GCN2 functionality in different PC cell lines. A) Representative western blot image of GCN2-phosphorylation (GCN2-P) and GCN2-total (GCN2-T) in four different PC cell lines **B)** Bar graph represents GCN2-P levels in four different PC cell lines and represents two technical replicates' mean relative values.

The western blot image shows that GCN2-P band is visible in all the cell lines. C4-2B and LNCaP-Res-A have the most visible band (figure 4.3 A). Figure 4.3 B shows protein quantification by densitometry where GCN2-P normalized to GCN2-T and GCN2-T is normalized to the γ – tubulin loading control. LNCaP Res-A cells show the highest GCN2-P level, almost 8,7-fold more than LNCaP treated with DMSO and 6,5-fold more than LNCaP treated with enzalutamide. The second highest GCN2-P level is present in C4-2B cell lines, compare to C4-2 cells both in white and red media. C4-2 cell in red media has higher GCN2-P level than white media, almost 2-fold more GCN2-P. The data suggests that GCN2 is functional in all the cell lines presented in this experiment.

4.2.2 AR and MYC bind to the *GCN2/EIF2AK4* gene locus

The previous experiments hinted at a relationship between androgen signaling and GCN2 activation, also suggested that GCN2 might be regulated by AR in PC. We first retrieved publicly available ChIPseq data depicting profiles of AR and MYC binding to chromatin from Barfeld et al. (2017) (157) and visualized these on USCS human genome version 19 (hg19) (**Figure 4.4**) (186).

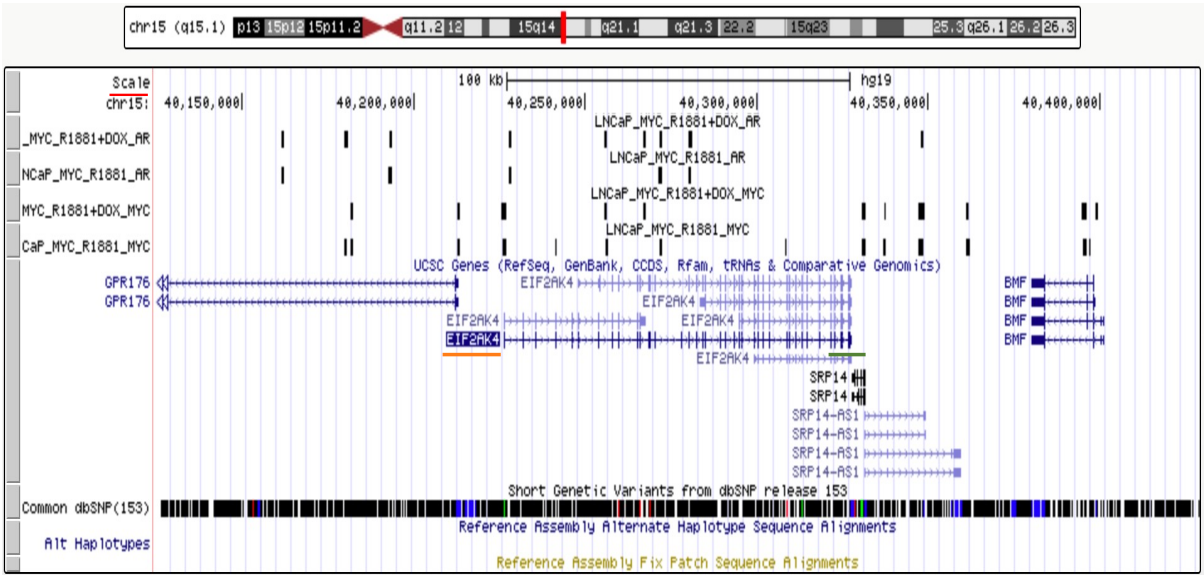

Figure: 4.4 ChIPseq data visualization of MYC and AR binding sites on the *GCN2/EIF2AK4* gene locus. The upper navigation bar indicates the position within the chromosome 15 for the expanded visualization of the *GCN2/EIF2AK4* gene locus below. The scale annotation on the left side (red color underline) shows the enlarged version of the red bar that is 100 Kb. The numbered black straight lines indicate the positions of reference nucleotides in chromosome 15. The interval between each line represents 50000 base pairs. The black bars represent genomic intervals for AR binding sites and MYC binding sites in the respective genomics tracks (labelled in the left-hand side of the figure and

on top of each of them) from Barfeld et al., 2017 (157). The four tracks represent LNCaP-MYC cells treated with hormone (R1881) or doxycycline (DOX; to induce overexpression of MYC) plus hormone (R1881+DOX), prior ChIPping for AR (_AR) or MYC (_MYC). Transcription start site of *EIF2AK4* is underlined in orange while transcription termination site is in green indicating transcription starts from the left to right direction.

The *GCN2/EIF2AK4* gene locus show several MYC and AR binding sites both proximal and distal to the gene. In particular, AR shows several intronic binding sites while MYC binding seems to sit at the transcription start site or promoter region. This data indicates that *EIF2AK4* expression might be under the control of both AR and MYC in PC cells.

4.2.3 *EIF2AK4* and *KLK3* mRNA expression in pcDNA3.1 and ARhi cells

Given the hypothetical regulation of *EIF2AK4* by AR, we first verified whether AR regulates *EIF2AK4* expression at the transcriptional level. To explore this, RT-PCR was performed in LNCaP-pcDNA3.1 and LNCaP-ARhi cells which are an isogenic AR-overexpression model (187). Thereafter referred as pcDNA3.1 and ARhi cells.

We measured *EIF2AK4* expression after 4, 6, and 24-hours stimulation with 10nM DHT (**Figure 4.5)**. We also measured *KLK3* expression levels, which is known to be highly induced by AR (187). The specific primers were previously tested and verified in the groups; sequence and graphs provided in (Appendix A material and appendix C: GCN2 and GCN1 primers).

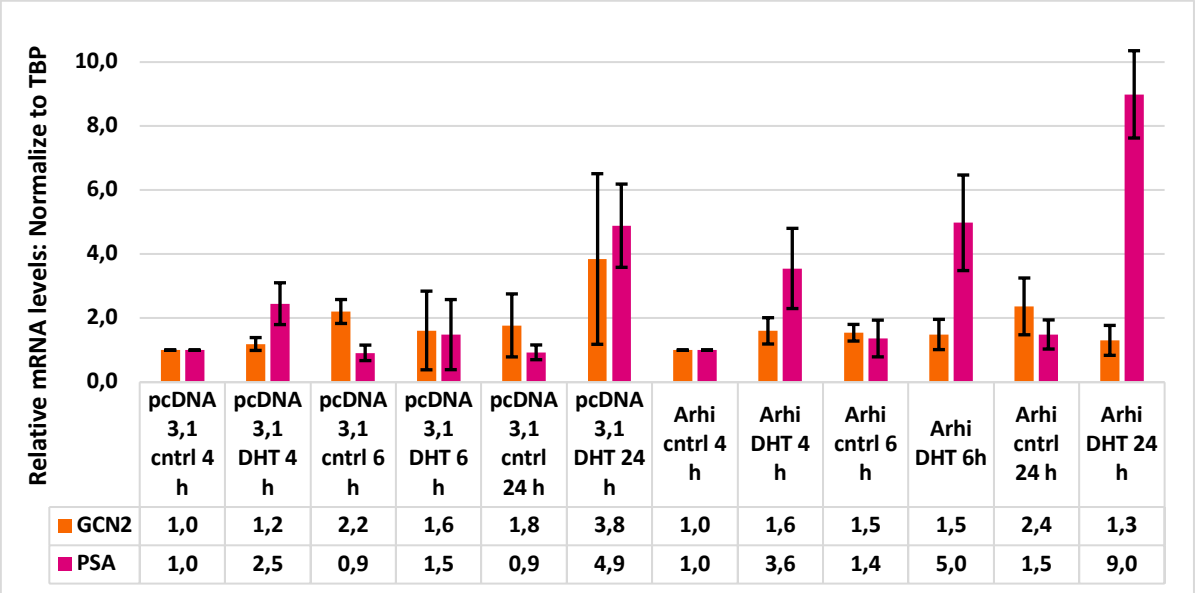

Figure 4.5 Gene expression of *EIF2AKA* and *KLK3* in LNCaP-pcDNA3.1 and LNCaP-ARhi cells. pcDNA3.1 as the control cell line and ARhi as the AR overexpressing cells were seeded in PDL coated

35 mm dish and grown in white media with CSFBS for 48 hours. After 48 hours, these cells were either treated with 10 nM DMSO or 10 nM DHT, and the total RNA was then collected at three different time points, 4, 6, and 24 hours, respectively and refers to the duration of the DHT treatment. The standard procedure of RNA isolation and cDNA synthesis was performed for each of the cell lines for all three independent biological replicates. Bar graphs represent relative mRNA levels of *EIF2AK4* and *KLK3*, normalized to *TBP* and then normalized to 4-hour control in each cell line at different time points. Error bars was calculated using the standard error of the mean (SEM) method of technical duplicates and independent biological triplicates.

Relative mRNA levels of *EIF2AK4* increased in pcDNA3.1 cell treated with DHT for 4 and 24 hours. *EIF2AK4* mRNA level peaked in pcDNA3.1 cells treated with DHT for 24 hours at approximately a 2-fold compared to control. pcDNA3.1 cell treated with DHT for 6 hours has a decrease in *EIF2AK4* mRNA level, about 1,3-fold decrease compare to control. *KLK3* mRNA level has increased in all the DHT treated time points than the control. ARhi cells treated with DHT for 4 hours show an increase in *EIF2AK4* mRNA level compared to control, an approximately 2-fold increase. *EIF2AK4* mRNA level is similar both for control and 6 hours DHT treated ARhi cells. The level of *EIF2AK4* mRNA level has decreased about 2-fold in 24 hours DHT treated ARhi cells compared to control. In ARhi cells, *KLK3* expression increased in all the time points of DHT treatments compared to control, especially at 24 hours, approximately 9-fold. This data indicates that *EIF2AK4* expression is regulated by androgens, but in the context of AR overexpression *EIF2AK4* regulation seems to fall of direct AR control.

4.2.4 GCN2 protein levels in hormone treated pcDNA3.1 and ARhi cells

Next, we aimed to verify whether AR not only regulates GCN2 at transcription level but also at the protein level. To this end we assessed protein levels of GCN2, GCN2-P, and the ISR components including: eIF2-α and ATF4 in the AR overexpression model (pcDNA3.1 and ARhi cells) upon stimulation with 10 nM DMSO or 10 nM DHT for 48 hours (**Figure 4.6**).

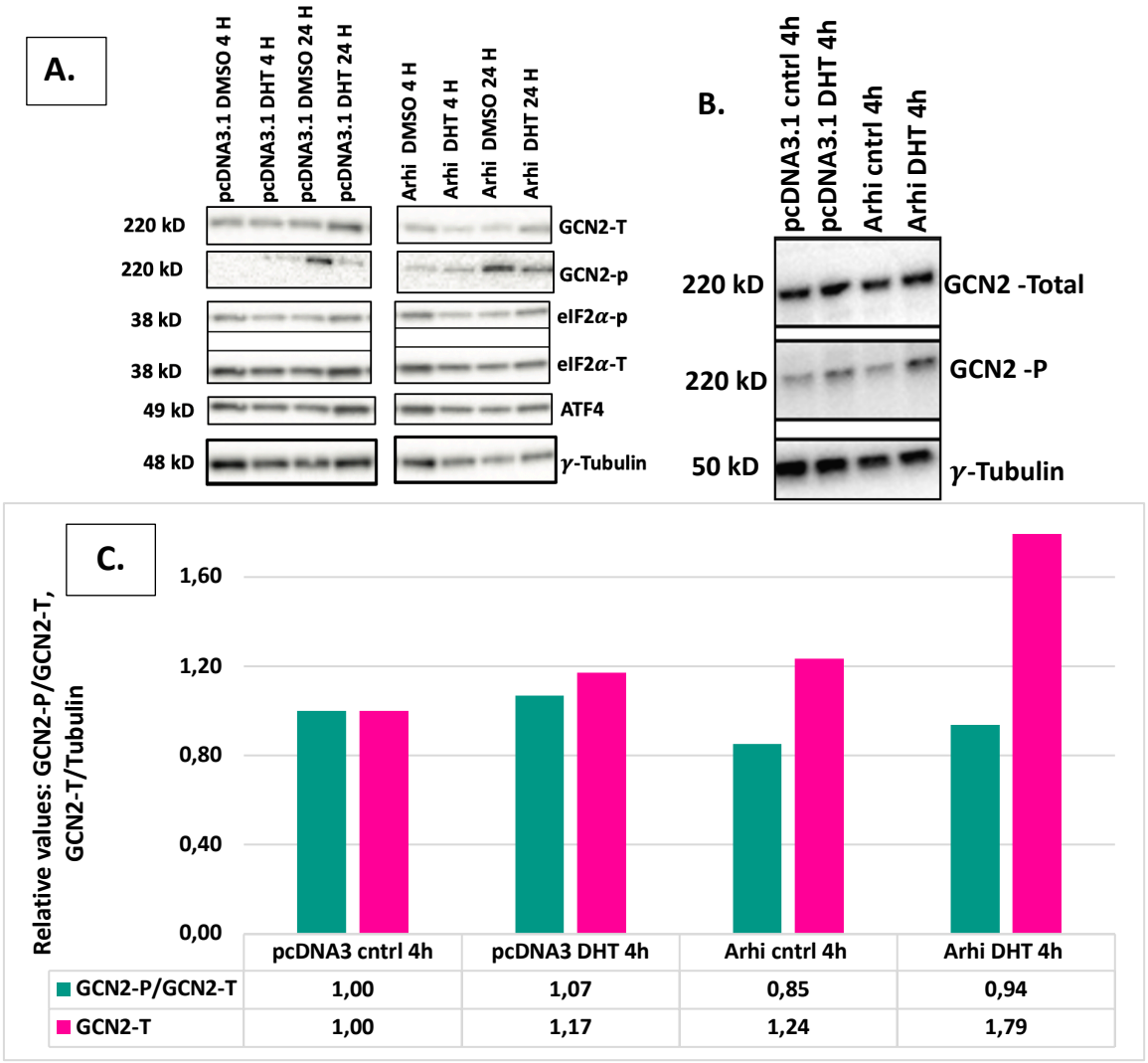

Figure 4.6 Hormone and AR control of GCN2 levels and activation. A) Representative western blot representation of several protein including: GCN2-total (GCN2-T, 220 kD), GCN2-phosphorylation (GCN2-P, 220 kD), eIF2-α-total (38 kD), eIF2-α-phospho (38 kD) and ATF4 (49 kD). **B)** Western blot image of GCN2 functionality of pcDNA3.1 and ARhi cells treated with DMSO and DHT for 4 hours **C)** Graph bar representation of western blot image in B), mean relative values are of two technical replicates. All the values are normalized to pcDNA3.1 control 4 hour.

The Western blot analysis shows that GCN2 total seems to be stimulated by androgens in both cell lines (Figure 4.6 A-C). GCN2-P increases upon 4 hours stimulation with androgens (Figure 4.6 A-B) but seems to increase further after 24h (Figure 4.6 B) although in this case, 24h stimulation with androgens induce decreased phosphorylation in both cell lines after DHT treatment (Figure 4.6 B). eIF2-α is phosphorylated similarly in both cell lines, and the western blot image also shows that ATF4 is present in all the cell lines in all conditions and cell lines (figure 4.6 A).

Figure 4.6 B suggests that GCN2 is activated in both cell lines after treatment with DHT and untreated samples. Quantification by densitometry where GCN2-T is normalized to the γ – tubulin loading control and then normalized to pcDNA3.1 control 4 hour shows that GCN2-T protein level increases when treated with DHT compared to untreated samples in both cell lines, approximately 1,2-fold increase (figure 4.6 C). Protein quantification where GCN2-P normalized to GCN2-T and then normalized to pcDNA3.1 control 4 hour shows that increased level of GCN2-T protein leads to increase level of GCN2-P in all the samples. Thus, the data suggests that AR regulates GCN2 at the protein level and androgens somewhat control phosphorylation of GCN2.

4.3 GCN1 as an activator of GCN2 in PC

GCN1 is a positive co-activator of GCN2, and recently it has been shown that GCN1 is essential for activation of GCN2 in mammalian cells (124). Thus, we investigated whether GCN1 is necessary for GCN2 activation in PC cells.

4.3.1 AR and MYC bind to the *GCN1/GCNL1* gene locus

We first determined whether we could detect binding of AR and MYC in publicly available ChIPseq data depicting profiles of AR and MYC binding to chromatin from Barfeld et al. (2017)(157) in LNCaP-MYC cells and visualized these on USCS human genome version 19 (hg19) (**Figure 4.7**) (186). We could find several MYC and AR binding sites in the GCNL1 gene.

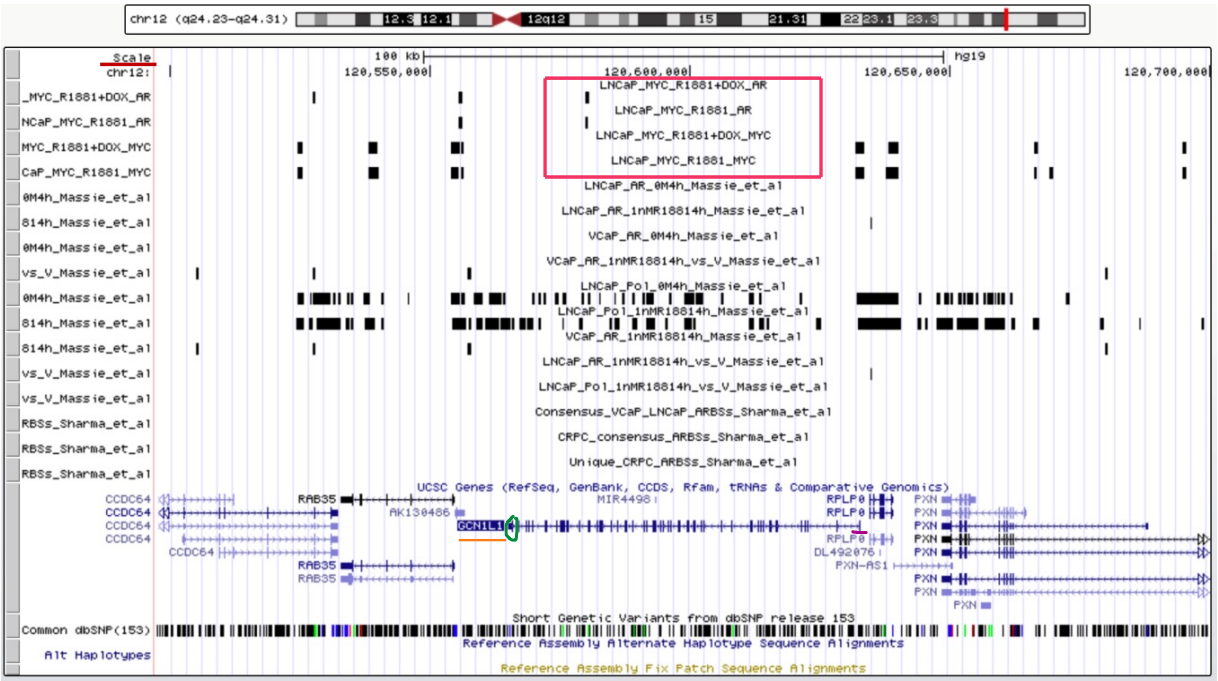

Figure 4.7 ChIPseq data visualization of MYC and AR binding sites on the *GCN1/GCNL1* gene locus. The upper navigation bar indicates the position within the chromosome 12 for the expanded visualization of the *GCN1/GCNL1* gene locus below. The scale annotation on the left side (red color underline) shows the enlarged version of the red bar that is 100 Kb. The numbered black straight lines indicate the positions of reference nucleotides in chromosome 12. The interval between each line represents 50000 base pairs. The black bars represent genomic intervals for AR binding sites and MYC binding sites in the respective genomics tracks (labelled in the left-hand side of the figure and on top of each of them) from Barfeld et al., 2017 (157). The four tracks represent LNCaP-MYC cells treated with hormone (R1881) or doxycycline (DOX; to induce overexpression of MYC) plus hormone (R1881+DOX), prior ChIPping for AR (_AR) or MYC (_MYC) (pink-square). Transcription start site of *GCNL1* is underlined in pink while transcription termination site is circled in green and underlined in orange indicating transcription starts from the right to left direction.

The figure shows LNCaP-MYC cells treated with both R1881 and doxycycline has AR binding site in the exon of the GCN1/GCNL1 gene (LnCap_MYC_R1881+DOX_AR). This is similar for LNCaP-MYC cells treated only with the R1881 (LnCap_MYC_R1881_AR). LNCaP-MYC cells treated with both R1881 and doxycycline has MYC binding site in the promoter region of the *GCN1/GCNL1* gene (LnCap_MYC_R1881+DOX_MYC) and similar for LNCaP-MYC cells treated only with the R1881 (LnCap_MYC_R1881_MYC). This data indicated that GCN1 might also be controlled by both MYC and AR.

4.3.2 *GCNL1* and *EIF2AK4* mRNA expression in pcDNA3.1 and ARhi cells

Next, we investigated whether AR regulates GCN1 at the transcriptional level. To explore this, we designed specific primers for *GCNL1* and optimized and performed RT-PCR in pcDNA3.1 and ARhi cells to assess *GCNL1* expression upon hormone stimulation (**Figure 4.8**). We have also measured *EIF2AK4* expression after 4, 6, and 24-hours stimulation with 10nM DHT. The specific primers sequence and graphs provided in (Appendix A material and Appendix C: GCN2 and GCN1 primers).

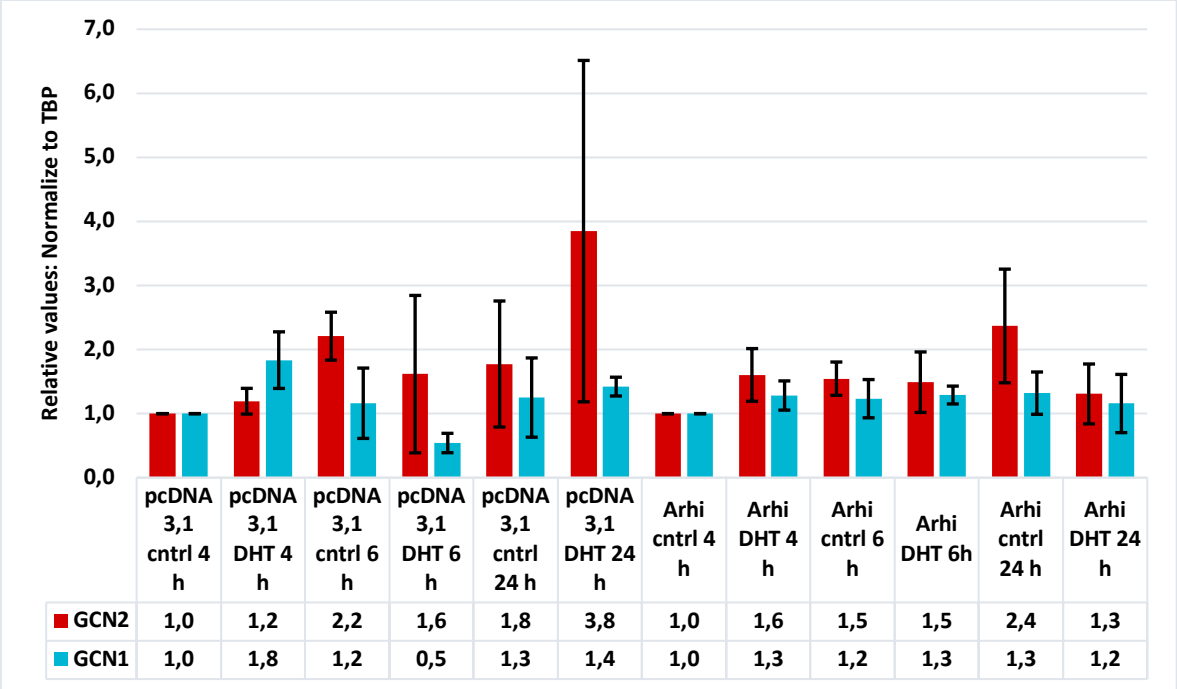

	pcDNA 3,1 cntrl 4 h	pcDNA 3,1 DHT 4 h	pcDNA 3,1 cntrl 6 h	pcDNA 3,1 DHT 6 h	pcDNA 3,1 cntrl 24 h	pcDNA 3,1 DHT 24 h	Arhi cntrl 4 h	Arhi DHT 4 h	Arhi cntrl 6 h	Arhi DHT 6h	Arhi cntrl 24 h	Arhi DHT 24 h
GCN2	1,0	1,2	2,2	1,6	1,8	3,8	1,0	1,6	1,5	1,5	2,4	1,3
GCN1	1,0	1,8	1,2	0,5	1,3	1,4	1,0	1,3	1,2	1,3	1,3	1,2

Figure 4.8 Gene expression of *GCNL1* and *EIF2AK4* in LNCaP-pcDNA3.1 and LNCaP-ARhi cells. pcDNA3.1 as the control cell line and ARhi as the AR overexpressing cells were seeded in PDL coated 35 mm dish and grown in white media with CSFBS for 48 hours. After 48 hours, these cells were either treated with 10 nM DMSO or 10 nM DHT, and the total RNA was then collected at three different time points, 4, 6, and 24 hours, respectively and refers to the duration of the DHT treatment. The standard procedure of RNA isolation and cDNA synthesis was performed for each of the cell lines for all three independent biological replicates. Bar graphs represent relative mRNA levels of *GCNL1* and *EIF2AK4*, normalized to *TBP* and then normalized to 4-hour control in each cell line at different time points. Error bars was calculated using the standard error of the mean (SEM) method of technical duplicates and independent biological triplicates.

Relative mRNA levels upon induction of pcDNA3.1 and ARhi cells with DHT shows increase *GCNL1* mRNA level both in pcDNA3.1 and ARhi cells that resemble the trend observed for GCN2. pcDNA3.1 cells treated with DHT for 4 and 24 hours show an increase in *GCNL1* expression compared to untreated control samples except at 6 hours. The highest *GCNL1* mRNA level was observed in pcDNA3.1 cells treated with DHT for 4 hours; approximately a

1,8-fold increase compared to control. pcDNA3.1 cells treated with DHT for 6 hours had decreased *GCNL1* mRNA level, about a 2,4-fold decrease compared to control. *GCNL1* expression in ARhi cells seems to increase upon treatment with DHT for 4 hours and remain at the same level during all the other time point in presence and absence of hormone. Similarly, to the results obtained for *EIF2AK4, GCNL1* genes seems to be androgen regulated but AR overexpression impacts the hormonal regulation of the gene.

4.3.3 GCN1 protein levels and regulations in PC cells

The purpose of the following experiments is to verify whether AR regulates GCN1 protein amount in PC. Furthermore, we also want to verify the level of GCN1 in various PC cell lines under normal culture conditions.

4.3.3.1 GCN1 is hormone dependent in PC cells

To investigate whether GCN1 protein level is regulated by AR, pcDNA3.1 and ARhi cells were seeded in PDL coated 35 mm dish and grown in white media with CSFBS for 48 hours. After 48 hours, these cells were either treated with 10 nM DMSO or 10 nM DHT; the cells were then harvested at three different time points, 4 hours, 6 hours, and 24 hours respectively. Then protein was extracted and assessed GCN1 protein level by immunoblotting. **Figure 4.9** shows GCN1 presence in these cell lines.

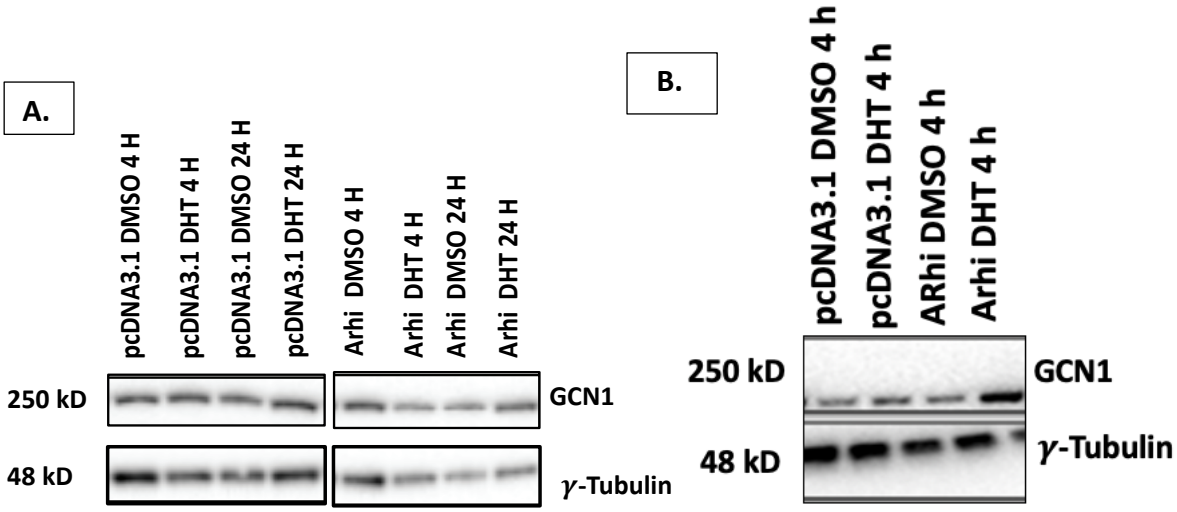

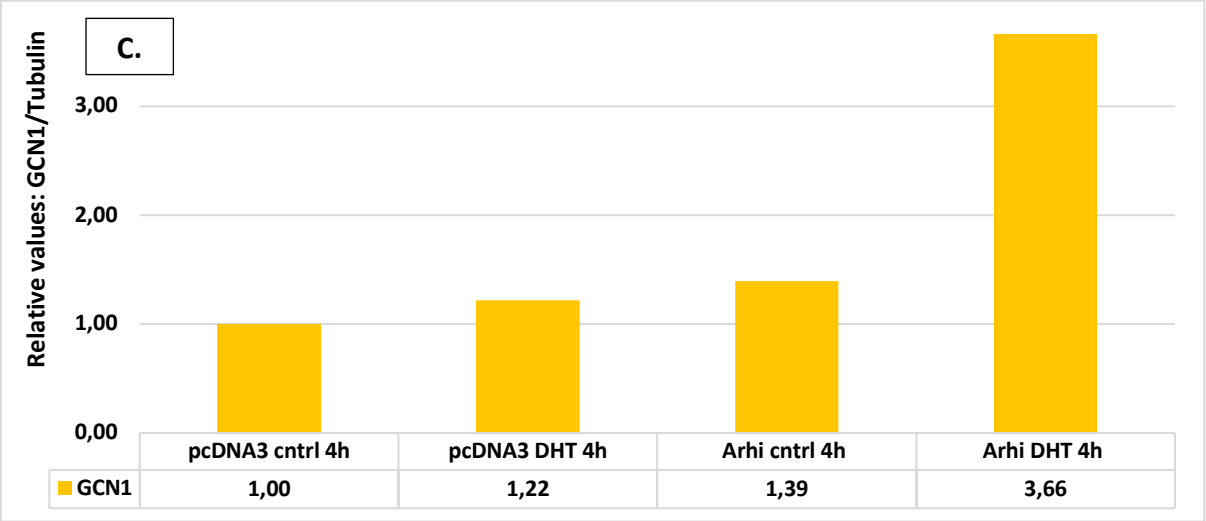

Figure 4.9 Quantification and western blot image of GCN1 in LNCaP-pcDNA3.1 and LNCaP-ARhi cells. A) Shows that GCN1 has a size of approximately 250 kD and γ – tubulin as loading control has a length of about 48 kD. **B)** Western blot image of GCN1 presence in pcDNA3.1 and ARhi cells treated with DMSO and DHT for 4 hours **C)** Graph bar representation of western blot image B) mean relative values of GCN1/Tubulin and normalized to pcDNA3.1 control 4 hour. All the relative values are of two technical replicates.

Western blot shows that GCN1 protein band is visible in both cell lines after DHT and DMSO treatment at 4 and 24 hours (figure 4.9 A). This is similar for the second western blot image representing 4 hours (figure 4.9 B). After quantification by densitometry, where GCN1 is normalized to the γ – tubulin loading control and then normalized to pcDNA3.1 control 4 hour (figure 4.9 C) shows more protein level in DHT treated cells than control. In pcDNA3.1, 1,2-fold more proteins in DHT sample and approximately 2,6-fold more protein in ARhi cells treated with DHT. This data seems to resemble the trend observed for GCN1 data from figure 4.8 at the same time points. Thus, it can be suggested that GCN1 protein level is regulated by AR and androgen.

4.3.3.2 GCN1 protein level in different PC cell lines

The previous experiment suggested that GCN1 is regulated by AR, we wanted to further investigate if GCN1 is present in various PC cell lines included: C4-2, C4-2B, LNCaP parental (also known as LNCaP), LNCaP-Res-A cells. As C4-2 are derivatives of LNCaP cells grown in castrated mice, we cultured these cells not only in RPMI with phenol red supplemented with fetal bovine serum (red media) but also in RPMI phenol-red-free media with charcoal stripped fetal bovine serum (white media). This allows comparison of GCN1 levels in LNCaP-Res-A cells presence and absence (castrate levels) of androgens. To compare levels of GCN1

in cells, which grow in 10 μM enzalutamide, with parental lines, LNCaP parental was grown in regular red media, treated either with DMSO or with enzalutamide for 48 hours. **Figure 4.10** shows the GCN2-P protein levels of PC cell lines models.

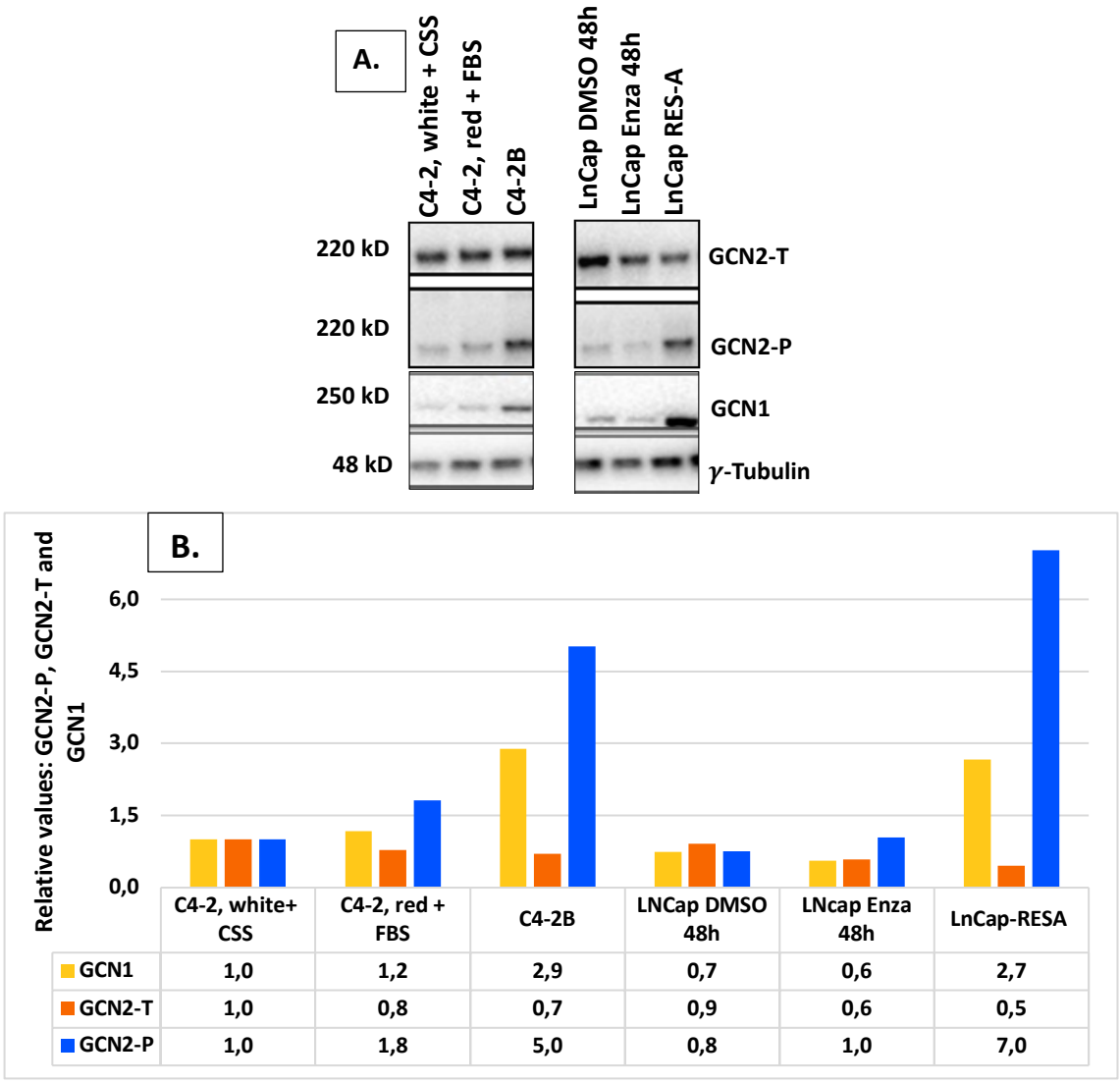

	C4-2, white+ CSS	C4-2, red + FBS	C4-2B	LNCap DMSO 48h	LNcap Enza 48h	LnCap-RESA
GCN1	1,0	1,2	2,9	0,7	0,6	2,7
GCN2-T	1,0	0,8	0,7	0,9	0,6	0,5
GCN2-P	1,0	1,8	5,0	0,8	1,0	7,0

Figure 4.10 GCN1 levels in various PC cell lines. A) Western blot image of GCN1, GCN2-total (GCN2-T), and GCN2-phosphorylation (GCN2-P) in four different PC cell lines. **B)** Bar graph represents relative values of GCN1, GCN2-P (GCN2-P/GCN2-T), and GCN2-T in four different PC cell lines. All the values are normalized to C4-2, white media with charcoal stripped fetal bovine serum. These bar graphs represent the mean relative values of two technical replicates.

The western blot image shows that GCN1 is present in all the cell lines, Res-A has the most visible band intensity (figure 4.10 A). Figure 4.10 B, quantification by densitometry where GCN1 is normalized to the γ – tubulin loading control and then normalize to C4-2 white media sample shows that C4-2B and LNCaP-Res-A cells had the highest GCN1 protein level. Overall, the protein itself is present in all the samples.

4.4 The interplay between GCN1, GCN2, and MYC in PC cell lines

ChIPseq dataset described in sections 4.2.1 and 4.3.1 indicated that MYC regulates both GCN2 and GCN1 expression in PC. Upon stimulation, with doxycycline, LNCaP-MYC cells overexpress approximately 3-fold more c-MYC protein (157). Thus, these cells were suitable for investigating the suggestion that MYC regulates both GCN1 and GCN2 expression in PC. To investigate the interplay between GCN1, GCN2, and MYC in PC, LNCap-MYC cells were seeded, and then these cells were either treated with 2 μg/mL doxycycline for 5 hours or untreated (control). Then protein was extracted, and immunoblotting was performed. **Figure 4.11** represents the presence of GCN1 and GCN2 activity in LNCaP-MYC cells after treatment with doxycycline.

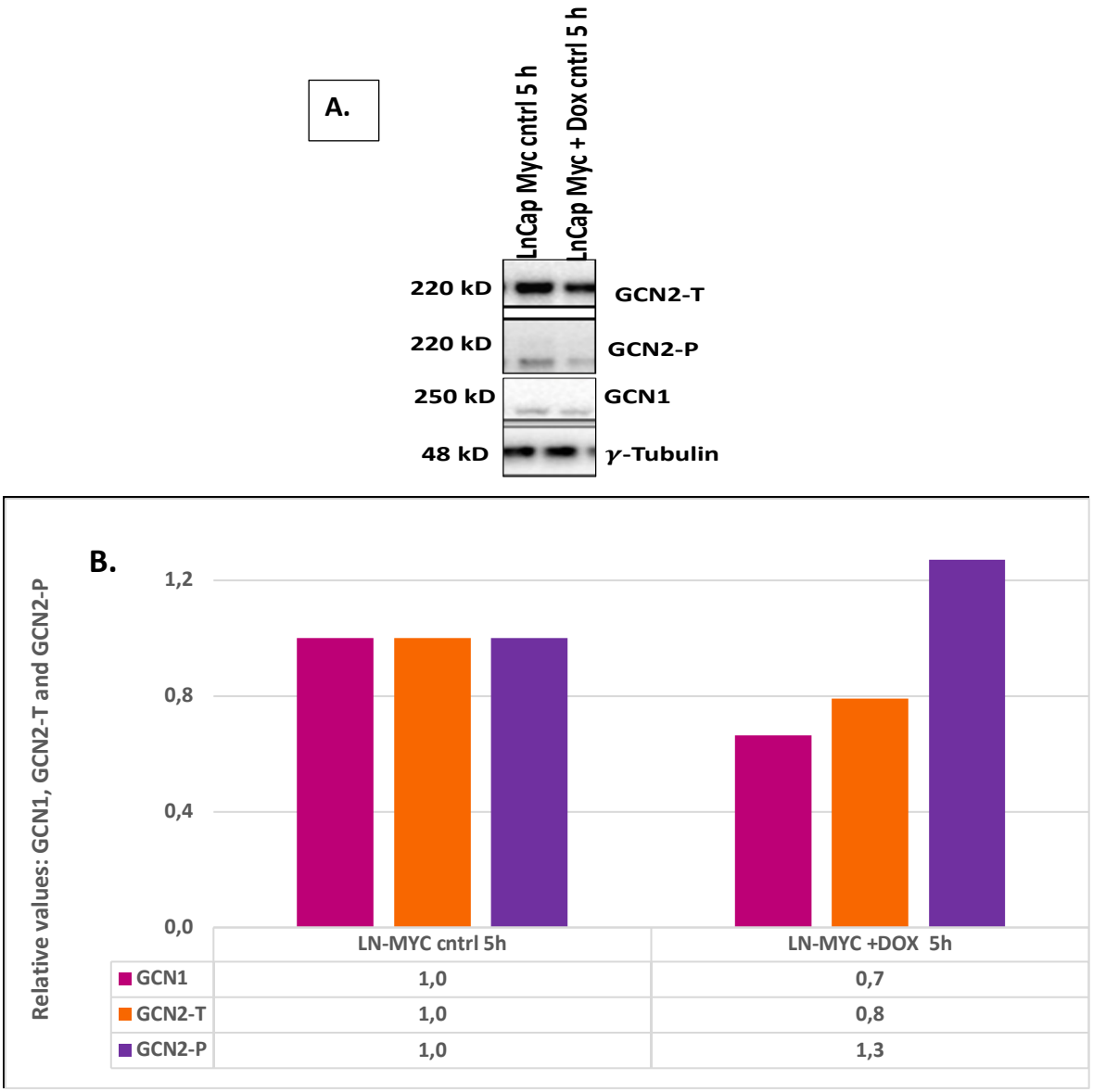

Figure: 4.11 Regulation of GCN2 and GCN1 protein by MYC in LNCaP-MYC cells. A) Western blot image represents prominent protein band of GCN1, GCN2-total (GCN2-T), and GCN2-

phosphorylation (GCN2-P) in LNCaP-MYC cell line and γ – tubulin as the loading control. **B)** Bar graphs representing levels of GCN1, and GCN2-T normalized to γ – tubulin; and GCN2-P levels normalized to GCN2-T in LNCaP-MYC cell line. All the values are normalized to LNCaP-MYC control 5-hour sample. These bar graphs represent the mean relative values of two technical and independent biological replicates.

From the western blot, GCN1 and GCN2-P is detectable both in LNCaP-MYC control and LNCaP-MYC treated with doxycycline (figure 4.11 A). From the quantification (figure 4.11 B), approximately 1,3-fold increase in GCN2-P level in LNCaP-MYC cells treated with doxycycline compared to control. The quantification also indicates an approximately 1,4-fold decrease in GCN1 protein level in LNCaP-MYC cells treated with DOX compared to control. Thus, it can be stated that GCN2-P is regulated by MYC in LNCaP-MYC cells, however, same cannot be stated for GCN1 protein level.

4.4.1 Measuring GCN1 protein level using known methods

Next, we wanted to further investigate whether GCN2 activation after amino-acid starvation or UV is regulated by a MYC-dependent change in GCN1 levels. Thus, the following experiment aimed to address whether either GCN2, GCN1 or protein levels of both increase in the LNCaP-MYC cell line overexpressing MYC using UV and amino-acid starvation.

4.4.1.1 Measuring GCN1 protein level by UV

LNCaP-MYC cells were seeded in PDL coated 35 mm dishes, 2 μg/mL doxycycline was added to half of the dishes and incubated for 36 hours. After 36 hours, these cells were UV irradiated at 20 J/m^2, protein was extracted, and immunoblotting was performed. **Figure 4.12** shows GCN1 protein level measurement in LNCaP-MYC cells irradiated with UV.

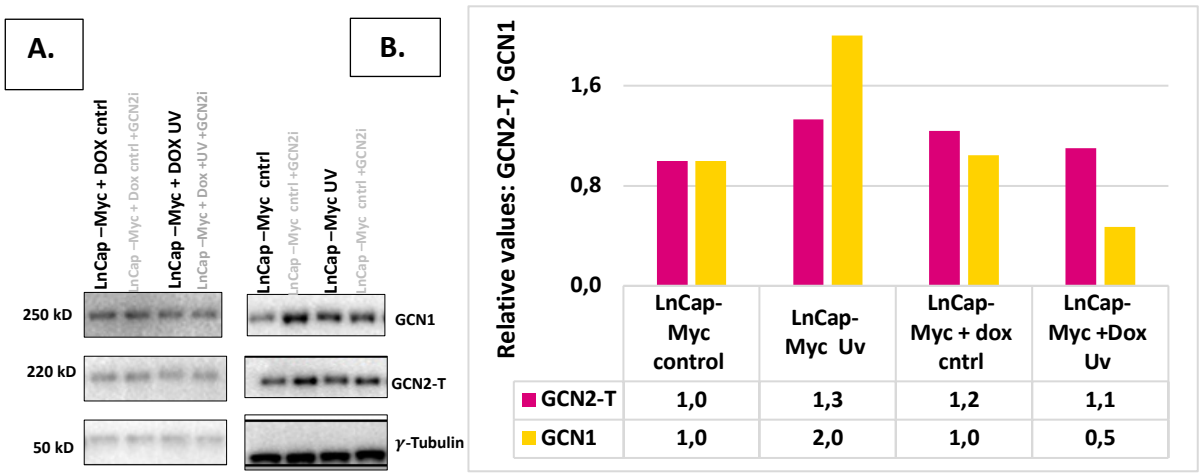

Figure 4.12 GCN1 and GCN2 protein levels upon exposure to UV in LNCaP-MYC cells. Western blot (please omit bands labelled in gray) shows GCN1 and GCN2-total (GCN2-T) protein in LNCaP-MYC cell line and γ – tubulin as the loading control. **B)** Bar graphs representing GCN1 and GCN2 protein levels normalized to γ – tubulin in LNCaP-MYC cell. All the values are normalized to MYC control sample. These bar graphs represent the relative values from one experiment.

Changes in GCN1 protein levels are very subtle in LNCaP-MYC UV untreated and treated samples and the bands are fainted in the DOX-treated samples (figure 4.12 A). However, from the quantification (figure 4.12 B), approximately 4-fold more GCN1 protein is present in LNCaP-MYC cells irradiated with UV compared to LNCaP-MYC treated with DOX and UV irradiated. GCN2-T protein is approximately 1,2-fold more in LNCaP-MYC UV samples compared to LNCaP-MYC in presence of DOX. These results indicate that after 36 hours treatment with DOX, MYC might, if anything, limit GCN1 levels in response to UV, a similar trend can be seen for GCN2-T.

4.4.1.2 Measuring GCN1 protein level by starvation

Next, we wanted to address if MYC induces similar changes in levels of GCN1 and GCN2 total proteins when the LNCaP-MYC cells are exposed to stress caused by amino acid starvation. LNCaP-MYC cells were seeded in PDL coated 35 mm dishes, two μg/mL doxycycline was added to half of the dishes and incubated for 36 hours, then withdrew normal media and replaced with salt-based starvation media and incubated for two hours. Then protein was extracted, and immunoblotting was performed. **Figure 4.13** shows GCN1 protein level measurement in LNCaP-MYC cells treated with starvation media.

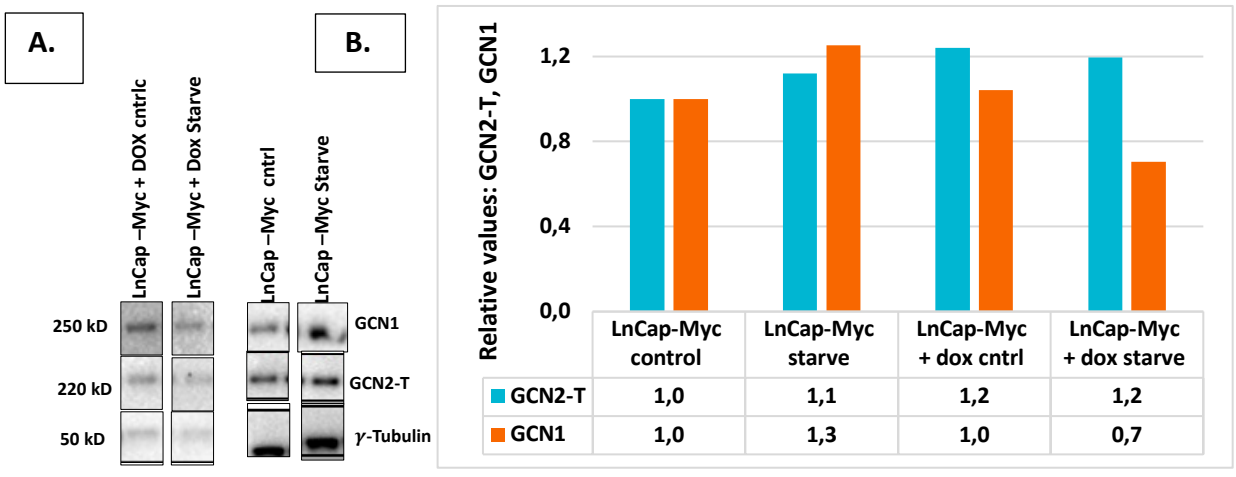

Figure 4.13 GCN1 and GCN2 protein levels upon amino acid starvation in LNCaP-MYC cells. Western blot image representation of GCN1 and GCN2-total GCN2-T protein in LNCaP-MYC cell line

and γ – tubulin as the loading control treated with starvation media. **B)** Bar graphs representing GCN1 and GCN2 protein levels normalized to γ – tubulin in LNCaP-MYC cell. All the values are normalized to MYC control sample. These bar graphs represent the relative values from one experiment.

Changes in GCN1 protein levels are very subtle in LNCaP-MYC starvation untreated and treated samples and the bands are fainted in the DOX-treated samples (figure 4.13 A). From the quantification (figure 4.13 B), approximately 1,9-fold more GCN1 protein is present in LNCaP-MYC cells in response to starvation compared to LNCaP-MYC treated with doxycycline and starved. This indicates that MYC might limit GCN1 levels in response to starvation. In contrast, GCN2-T protein is slightly upregulated in consequence of both amino acid starvation and also upon overexpression of MYC. Taken together the data indicates that GCN2, but not GCN1 levels might be affected by MYC. Moreover, stressor such as UV and amino acid starvation are able to upregulate both levels of GCN1 and GCN2, but MYC overexpression suppresses GCN1 levels.

4.5 Functional consequences of inhibiting GCN2

As stated earlier, GCN2 is a stress response kinase and known to play an essential role in the tumor microenvironment. GCN2 pathway might be activated in tumor cells; thus, we wanted to address the functional consequence of inhibiting GCN2 in PC cell lines in this section. We hypothesized that treating these cells with an inhibitor for GCN2 would prove the dependency of these cells from the pathway and that inhibition of GCN2 in PC cells could lead to poor cell survival. AR overexpressed cell lines were used in the following experiments to explore this proposition.

4.5.1 Optimization of cell seeding density

Cell viability assay was performed to assess the appropriate cell numbers for the remaining experiments to verify the theory. Since the cell viability assay was conducted over several days, our goal was to not exceed 60-70% confluency. pcDNA3.1 (as control cell line) and ARhi cells were seeded at a seeding density of 8000, 6000, and 4000 cells per well in 96-well plates; and incubated for 36 hours. After 36 hours, presto blue reagent was added and incubated for 20 minutes before measuring the fluorescence. This procedure was

performed for four days. **Figure 4.14** shows the three different seeding densities of pcDNA3.1 and ARhi cells.

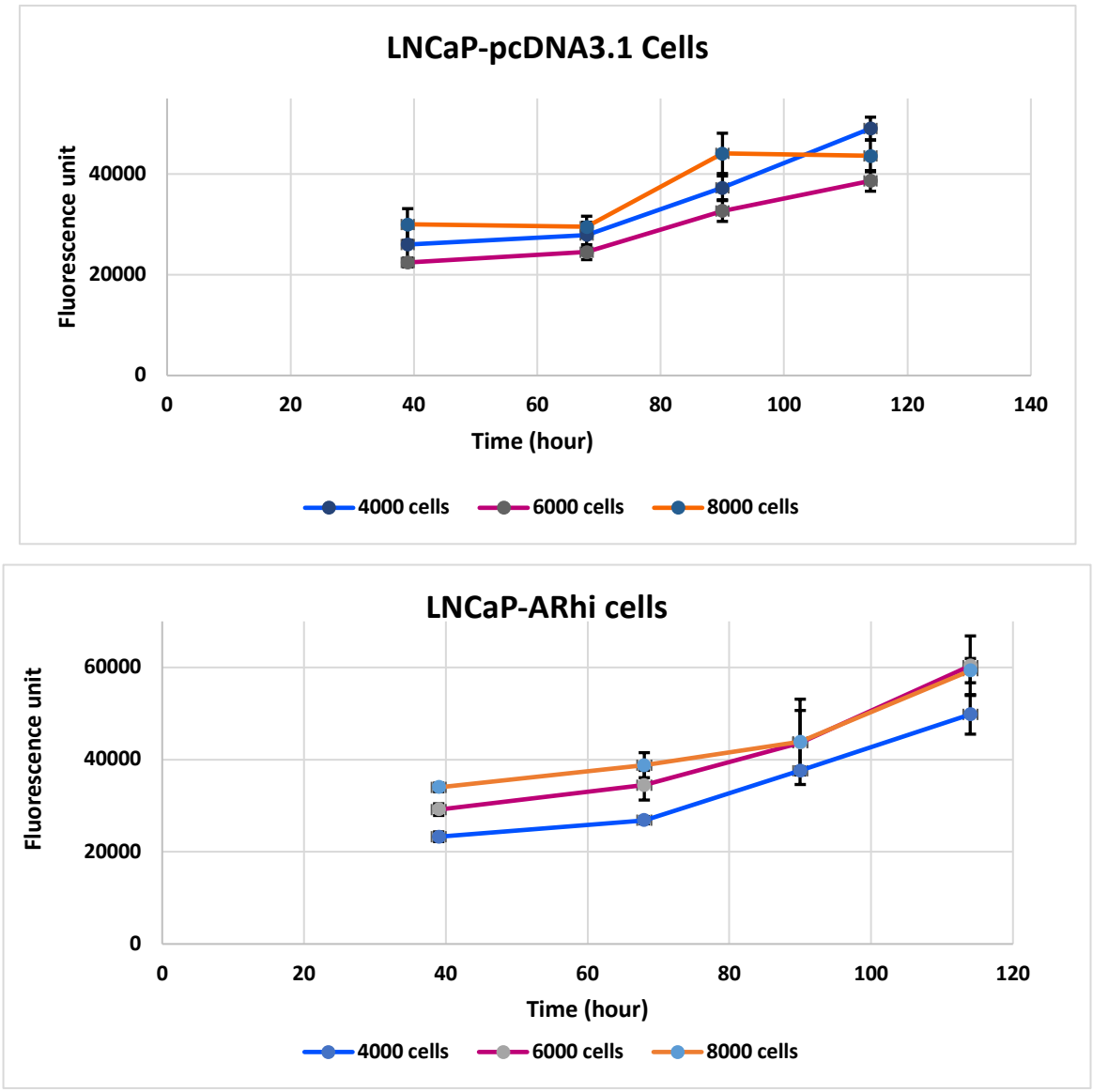

Figure 4.14 Optimization of seeding density of LNCap-pcDNA3.1 and LNCaP-ARhi cells. The Scatter plot shows the fluorescence intensity representing the growth curve of these cell lines. The fluorescence value of the medium was subtracted as background from all the values. Standard error was calculated using technical triplicates and added accordingly.

The presto blue assay shows exponential growth continued during the course of the experiment where lower cell numbers were seeded. In the pcDNA3.1 cell line the curve reached a plateau during the experiment where 8000 cells were seeded. For ARhi cells over the course of 120 hours, 6000 cells are the appropriate cell number. We decided upon 6000 cells for further cell viability assay based on the seeding density of ARhi cells.

4.5.2 GCN2i combined with X-ray

The following experiment aimed to determine the viability of cells when treated with GCN2i. In addition to that, we also investigated whether GCN2i and x-ray in combination have a synergistic effect on cell viability. 6000 pcDNA3.1 and ARhi cells per well were seeded in 96 well plates. After 48 hours, 3 μM DMSO, 3 μM and 10 μM GCN2i was added accordingly and incubated for 2 hours. Subsequently, half of the cells were radiated with X-ray at 1-Gray (Gy), and cell viability was measured using the presto blue reagent. This measurement was performed over the course of 4 days. **Figure 4.15** shows the cell viability of pcDNA3.1 and ARhi cells treated with GCN2i and irradiated with X-ray.

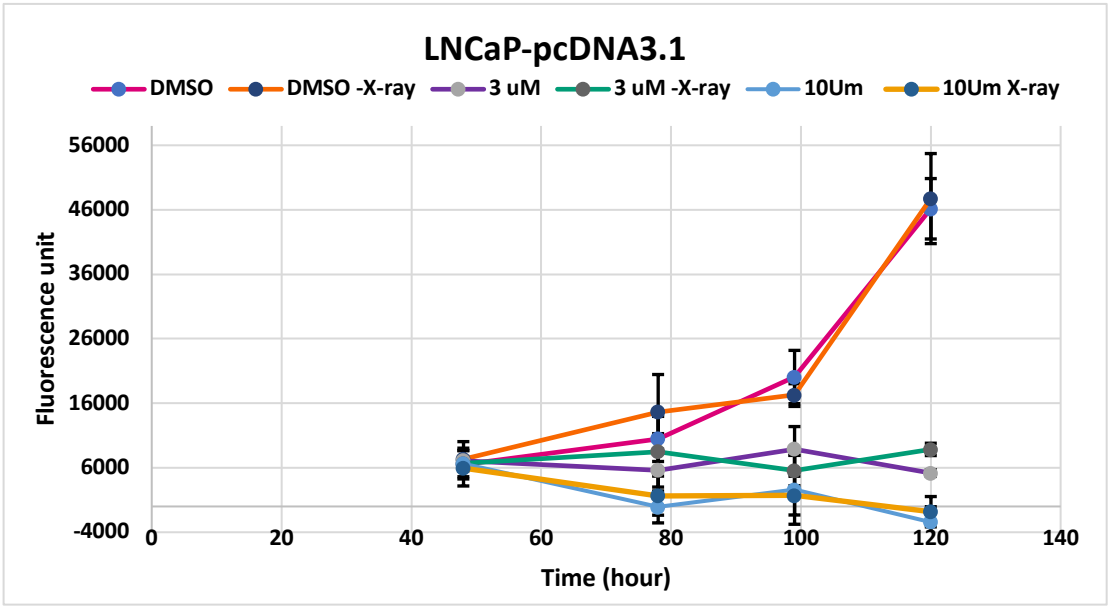

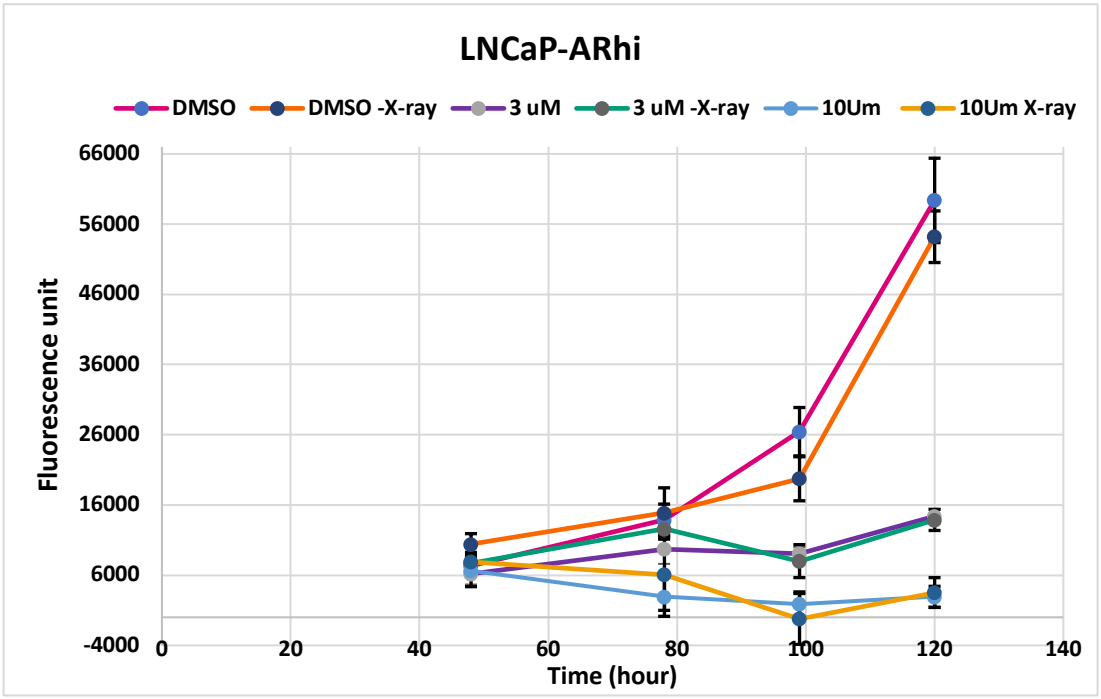

Figure 4.15 Titration curves measuring the dose-response of GCN2i combined with 1-Grey in LNCaP-pcDNA3.1 and LNCaP-ARhi cells. The Scatter plot shows cell viability that corresponds to fluorescence measurement. The fluorescence value of the medium was subtracted as background from all the values. The error bars were calculated using technical triplicates.

Both pcDNA3.1 and ARhi cells treated only with DMSO grow exponentially and similarly as expected. The dose of 1 Gy X-ray irradiation did not have significant effect alone. Also, in both cell lines treated with 3 μM GCN2i and GCN2i combined with X-ray shows very little change in growth curve, indicating that GCN2i at 3μM is already too toxic alone to be able to assess any potential synergy between the effect of the radiation and the drug. When cells were exposed to GCN2i at 10 μM the fluorescent signal decreased, suggesting a reduced number of viable cells. Overall, GCN2i seems to affect cell viability in a dose dependent manner, but the concentration of GCN2i used was overly high to observe any synergistic effect with radiation.

4.5.3 Dose and time-dependent survival of pcDNA3.1 and ARhi cells

Data from the previous experiment suggested that GCN2i concentration was too high, and it was too toxic to observe any synergistic effect on cell survival. Thus, the following experiment aimed to assess cell viability with finer titration of GCN2i, that will show the actual functional consequence of inhibiting GCN2. pcDNA3.1 and ARhi cells were seeded in 96 well plates, respectively, and incubated for 48 hours. Subsequently, 3 μM DMSO, 3 μM, one μM, 300 nM, and 100 nM GCN2i was added accordingly and incubated for 2 hours. Cell viability was measured using the presto blue reagent. Fluorescence was measured over the course of 4 days. **Figure 4.16** shows the cell viability of pcDNA3.1 and ARhi cells treated with different GCN2i concentrations.

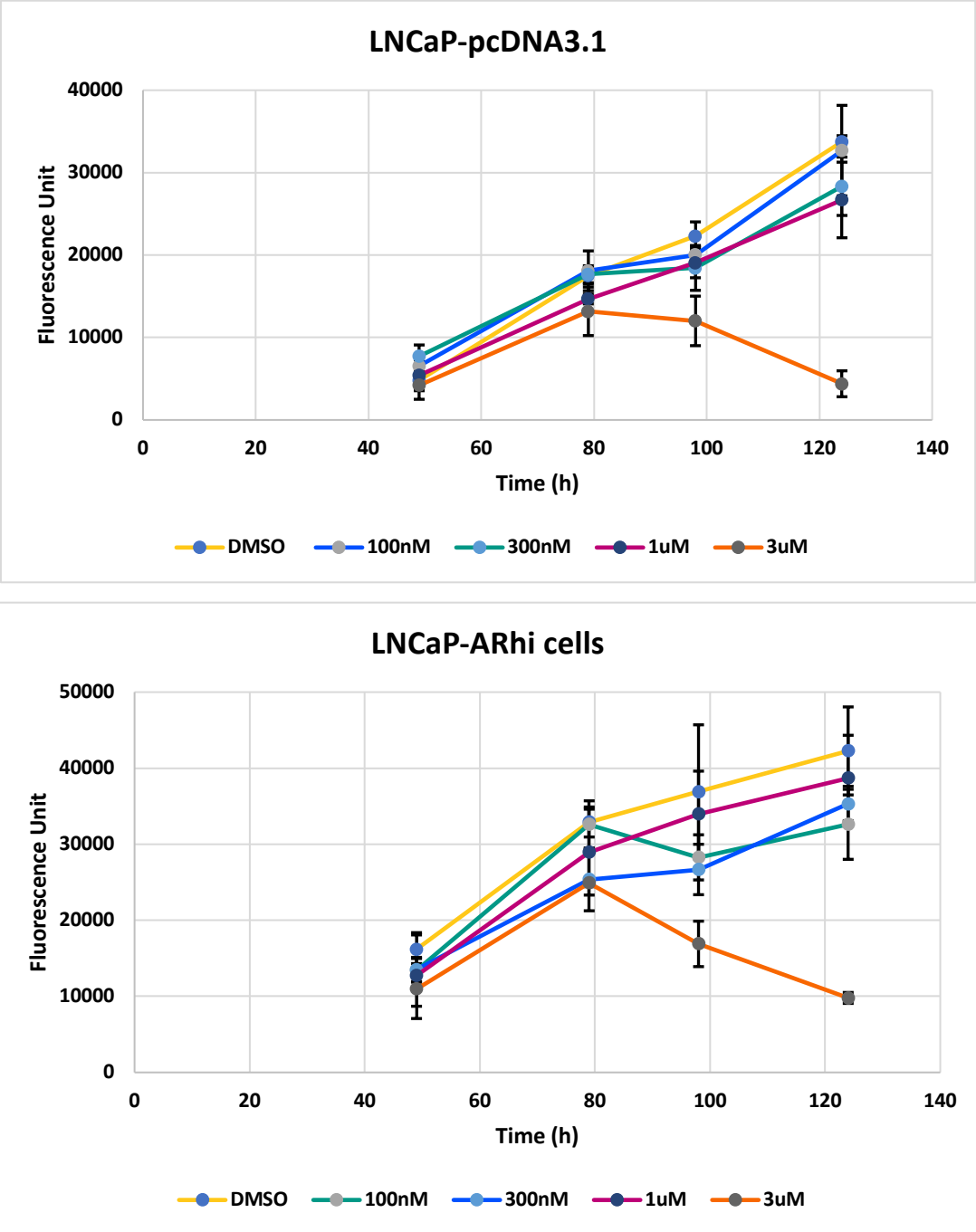

Figure 4.16 Dose and time-dependent survival of pcDNA3.1 and ARhi cells by GCN2i. Scatter plots show cell viability of pcDNA3.1 and ARhi cells that correspond to fluorescence measurement. The fluorescence value of the medium was subtracted as background from all the values.The error bars were calculated using technical triplicates.

Data from figure 4.16 suggested that both cell lines treated with 3 μM GCN2i over the course of 48 hours to 129 hours had a dramatic decrease in cell viability compared to DMSO. Concentrations of the GCN2i between 100nM and 1 μM did show some reduction in viability compared to DMSO treated but did not show significant differences neither between pcDNA3.1 and ARhi cells response.

4.5.4 GCN2i combined with DHT

Next, we repeated the viability experiment performing with even finer titration of GCN2i and culturing the AR model in both red (in full serum) and white media supplemented with 10nM DHT, under the assumption that exposure to androgens would affect levels and dependencies of these cells from GCN2 in a different manner, since we have shown that GCN2 is regulated by AR **figure 4.17** and **table 4.1**, respectively.

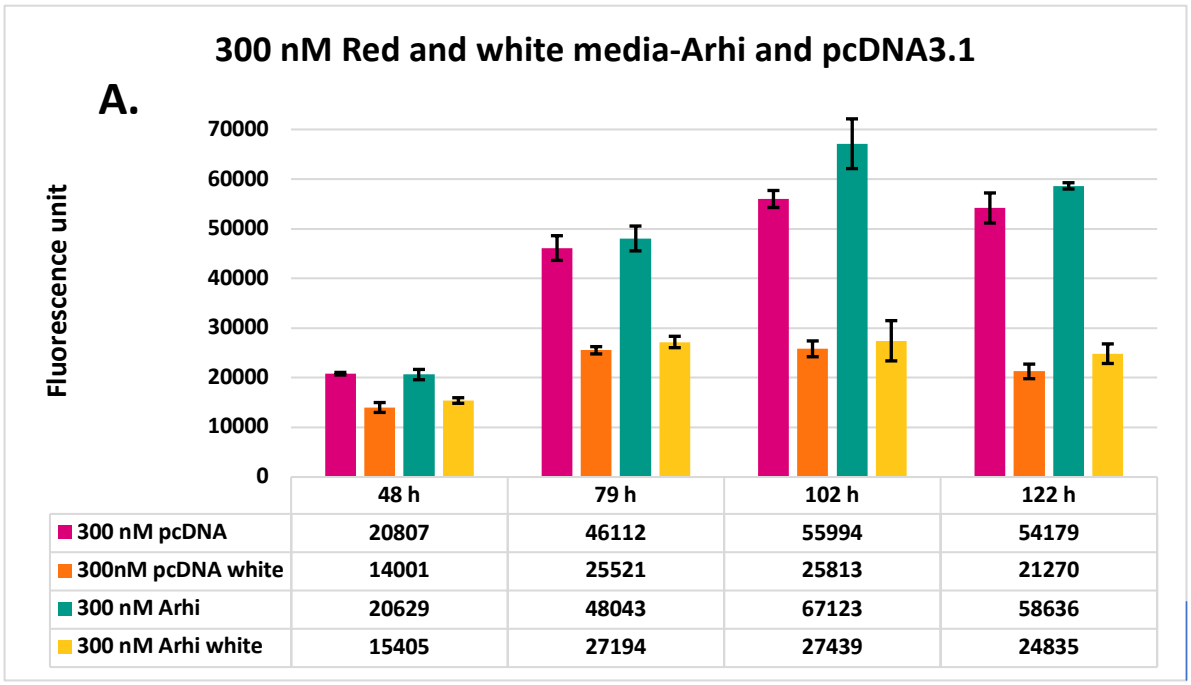

	48 h	79 h	102 h	122 h
300 nM pcDNA	20807	46112	55994	54179
300nM pcDNA white	14001	25521	25813	21270
300 nM Arhi	20629	48043	67123	58636
300 nM Arhi white	15405	27194	27439	24835

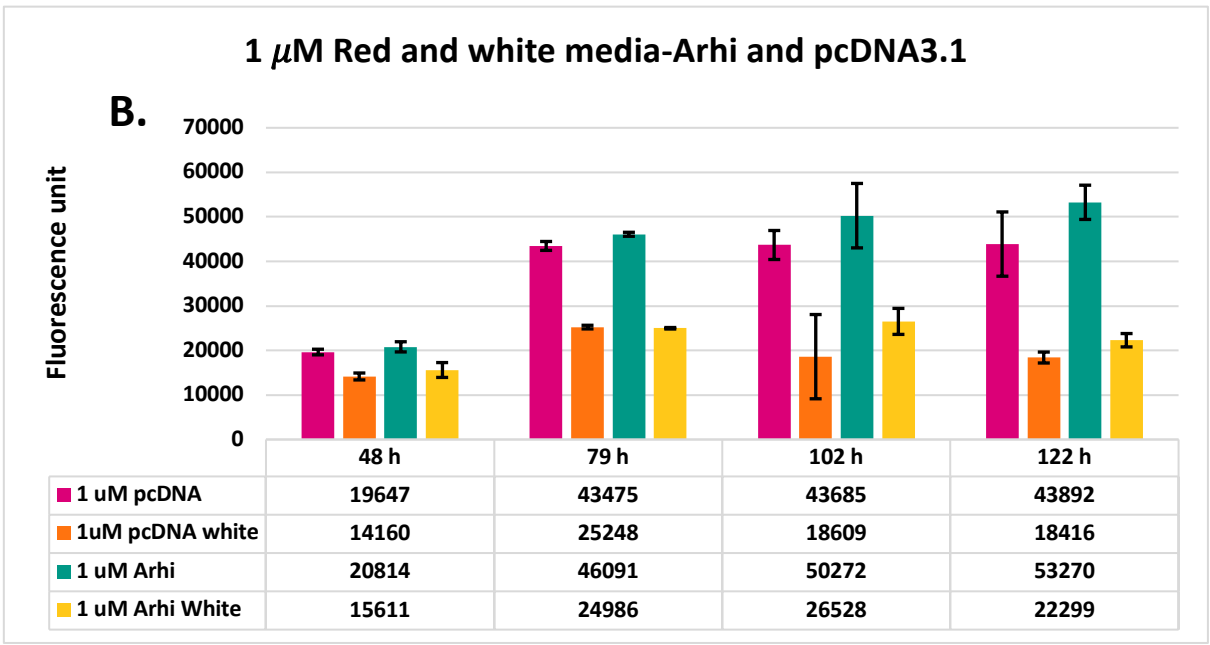

	48 h	79 h	102 h	122 h
1 uM pcDNA	19647	43475	43685	43892
1uM pcDNA white	14160	25248	18609	18416
1 uM Arhi	20814	46091	50272	53270
1 uM Arhi White	15611	24986	26528	22299

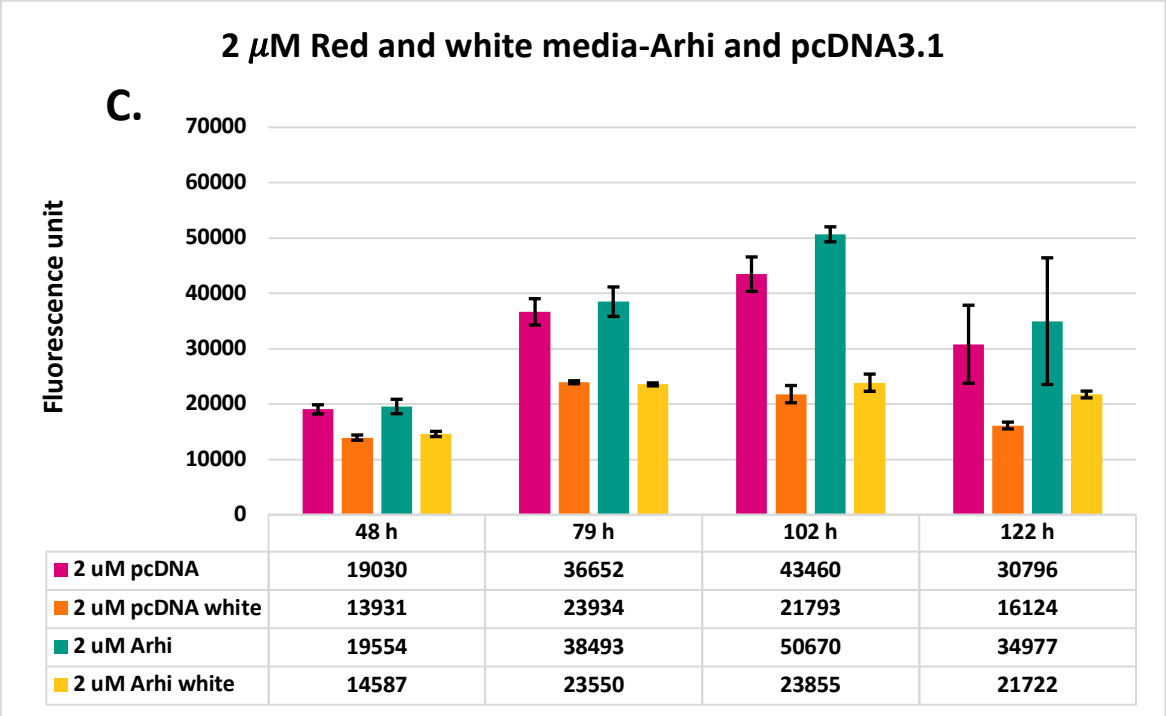

	48 h	79 h	102 h	122 h
2 uM pcDNA	19030	36652	43460	30796
2 uM pcDNA white	13931	23934	21793	16124
2 uM Arhi	19554	38493	50670	34977
2 uM Arhi white	14587	23550	23855	21722

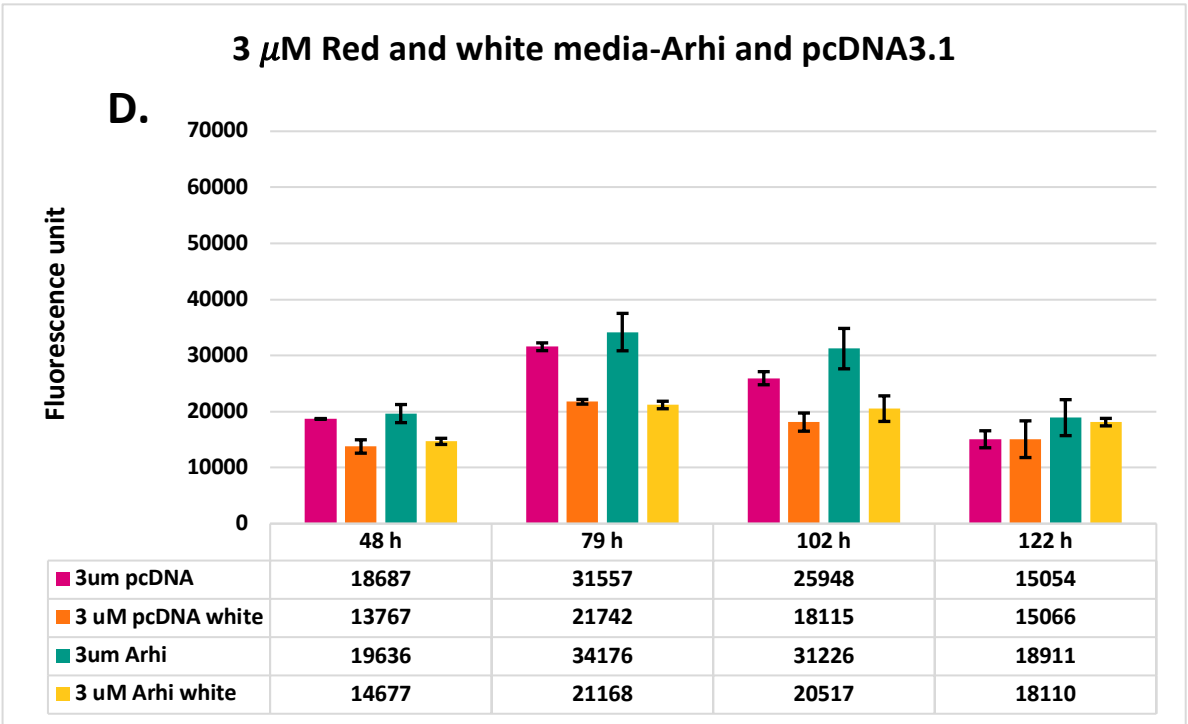

	48 h	79 h	102 h	122 h
3um pcDNA	18687	31557	25948	15054
3 uM pcDNA white	13767	21742	18115	15066
3um Arhi	19636	34176	31226	18911
3 uM Arhi white	14677	21168	20517	18110

Figure 4.17 Growth curves pattern of LNCaP-pcDNA3.1 and LNCaP-ARhi cells treated with GCN2i and DHT. pcDNA3.1 and ARhi cells were seeded in 96 well plates in red and white media with CSFBS, respectively, and incubated for 48 hours. After 48 hours, cells grown in white media were treated with 10 nM DHT. Subsequently, 3 μM DMSO, 3 μM, 2 μM, 1 μM, and 300 nM GCN2i was added accordingly and incubated for 2 hours. Cell viability was measured using the presto blue reagent. Fluorescence was measured over the course of 4 days. Scatter plots shows fluorescence values, and these correspond to viability measurement of pcDNA3.1 and ARhi cells. The fluorescence value of the medium was subtracted as background from all the values. **A)** pcDNA3.1 and ARhi cells treated with 300 nM GCN2i, both in red and white media. **B)** pcDNA3.1 and ARhi cells treated with 1 μM GCN2i, in both media **C)** pcDNA3.1 and ARhi cells treated with 2 μM GCN2i, in both media **D)**

pcDNA3.1 and ARhi cells treated with 3 μM GCN2i, in both media**.** DMSO data is not included in these graphs. The error bars were calculated using technical triplicates.

Table 4.1 LNCaP-pcDNA3.1 and LNCaP-ARhi cells treated with GCN2i and DHT. Represents t-test of LNCaP-pcDNA3.1 and LNCaP-ARhi cultured in different media and treated with GCN2 inhibitor. * = P < 0.05 and ** = P <0.03.

pcDNA3.1 cells in red media versus white media with DHT		
Concentrations	**P- values**	**Significance**
300 nM	0,031	*
1 µM	0,028	**
2 µM	0,028	**
3 µM	0,078	
ARhi cells in red media versus white media with DHT		
Concentrations	**P- values**	**Significance**
300 nM	0,047	*
1 µM	0,034	*
2 µM	0,045	*
3 µM	0,076	

At any concentration of GCN2i pcDNA3.1 and ARhi cells grown in red medium have higher cell viability than cells grown in white media supplemented with DHT, table 4.1 shows the significant differences in cell viability in these cell lines when grown in different media. 300 nM GCN2i has a minimal effect on the viability of both cell lines (figure 4.17 A). On the other hand, we could observe a trend by which AR-overexpressing cells presented more viable cells treated with 1, 2 and 3 μM (figure 4.17 B, C and D), which is consistent with the finding that GCN2 is upregulated in these cells. Taken together these data suggest that increasing concentrations of GCN2i leads to lower survival of PC cells.

5. DICUSSION

This thesis aimed to determine the role and regulation of GCN2 in prostate cancer, with the long-term goal of revealing whether GCN2 will be an effective therapeutic target for the treatment of prostate cancer. However, the role of GCN2s' in PC is unexplored, and consequently, research publications on the topic are non-existing. Thus, due to the lack of previous knowledge on the subject, multiple assessments were made throughout the thesis to establish the path forward. In this section, all the outcomes from the various procedures will be further discussed. The main subject matters include the functionality of GCN2 in PC, regulation of GCN2 and GCN1 proteins by AR and MYC, and functional consequence of GCN2i. In addition, the choice of the cell lines, limitations of the approaches, and future works and prospects are reviewed.

5.1 Choice of the cell lines

The development of CRPC occurs through two main overlapping mechanisms: AR-dependent and AR independent. Thus, the PC cell lines chosen for this study characterize different models of CRPC through signal activation by a range of AR and MYC. C4-2 was the very first cell line used for this thesis based on their independence on androgen. Subsequently, C4-2B was also used based on androgen-independent signaling that exhibits many aspects of bone metastasis of advanced PC. Furthermore, one of the frequently occurring characteristics of CRPC is AR overexpression, and 80% of CRPC display AR amplification, AR mRNA overexpression, or AR protein overexpression (188). Consequently, LNCaP-ARhi and pcDNA3.1 (as control cell line) were excellent models for studying overexpressed AR and the role of GCN2 in these cell lines. In addition, PC become resistant to drug treatment such as enzalutamide, which leads to the progression of CRPC; hence resistance cell lines such as Res-A and Res-B were exceptional cell lines to study the resistant aspect of PC.

Overexpression of *MYC* oncogene in PC leads to partially reprogramming chromatin at the AR locus and progress toward CRPC; interestingly, up to 72% of CRPC exhibit specific amplification of *MYC* gene (189). As discussed later, multiple findings suggested that the

MYC gene regulates GCN2 in PC. Thus, the LNCaP-MYC cell line was the suitable model for studying the interplay between overexpressed MYC and the role of GCN2 in the cell line.

5.2 GCN2 is functional in PC

The cancer microenvironment is very hostile, and one of the most fundamental features of the cancer cell is the adaption to cellular stress through the dysregulation of IRS. GCN2 is one of the regulators of the IRS pathway. As mentioned earlier, several reports have confirmed that GCN2 is essential for cancer cells to survive and thrive in a hostile microenvironment. We hypothesized that since PC cells have to face the same challenges, the IRS and GCN2 is likely to play an important role also in PC. Thus, the practical aspect as the first aim of the study was to determine whether GCN2 is functional in PC.

The novel findings from sections 4.1.1 and 4.1.2 suggest that GCN2 is indeed functional in PC. Cellular stress caused by UV irradiation and amino acid starvation is known to activate GCN2 (114). Cellular stress can activate GCN2 via accumulation of uncharged tRNA; however, it is unknown whether GCN2 is activated similarly upon UV irradiation. Our findings verified that activation of GCN2 through these methods are applicable in AR expressing and androgen-independent C4-2 cells. One of the reasons for the occurrence could be that the accumulation of uncharged tRNAs is faster during treatment with the salt-based starvation medium. Perhaps the UV irradiation dose was too short to observe the same outcome in the C4-2 cell. Or perhaps other unknown mechanism(s) lead to activation of GCN2 in the C4-2 cell line. Curiously, in HeLa cells, activation of GCN2 could not be observed in response to the UV irradiation doses tested, in contrast to previous observations in our group (figure 4.1). The different result might be due to technical reasons, most likely because too many cells were seeded for the experiment.

5.3 AR-mediated regulation of GCN2

The differentiation of normal prostate cells are dependent on the AR, and dysregulation of AR activity plays a crucial role in PC development and the progression towards CRPC. Identifying AR target genes is essential for greater understanding and treatment of CRPC. The data presented in section 4.2.1 showed that GCN2 could be one such AR target gene.

Our findings have suggested that AR activation leads to increased GCN2 activation. Firstly, we have observed a higher level of GCN2-P in the cell lines with higher constitutive AR expression (C4-2 versus LNCaP). Moreover, LNCaP cells treated with enzalutamide, known to inhibit AR, had a low level of GCN2, which suggested that GCN2 is activated in an AR-dependent manner. Lastly, RES-A cells resistant to enzalutamide that targets AR, strong GCN2 activation was seen and lead to the speculation that whether this means that GCN2 status or activity can be relevant in resistance to enzalutamide and other AR inhibitors.

Interestingly these cells were grown at 60-80% confluency, which indicates that these cells persisted in the growing phase and unstressed, this suggests that some other role of GCN2 is relevant here which is not related to ISR. It can also be an indication of the role GCN2 plays in the Warburg effect since it is known that reprogramming cell metabolism is essential for cancer cell survival and growth. Or perhaps the VCP/p97 protein that has a critical role in governing protein homeostasis and a regulator of cellular metabolisms is functionally impaired in these cell lines, enhancing cellular dependency on GCN2 (7). It is also possible that in these cell lines, multiple unknown mechanisms cooperate to activate GCN2 once AR is activated. Therefore, further investigation was needed to confirm whether AR regulates GCN2 in PC.

5.3.1 Transcriptional and protein level regulation

AR and MYC bind to the *GCN2/EIF2AK4* gene locus ChIPseq data from section 4.2.2 further suggested that AR regulates GCN2 expression. We have confirmed that AR regulates GCN2 at the transcriptional and protein levels (figure 4.5 and figure 4.6). We have shown that pcDNA3.1 cells deprived of the hormone had some level of GCN2 expression, but once the cells were treated with DHT had an increasing level of GCN2 mRNA in a time-dependent manner. Consequently, the presence of a low level of androgen leads to more AR activation and subsequently more GCN2 mRNA. However, cells transformed with pcDNA3.1 treated with DHT for 6 hours had a decreasing level of GCN2 mRNA, and the error bars were relatively high, which might be due to one or two of the control samples had a very high value for some technical reasons.

Studies have suggested that overexpression of AR sensitizes cells to a low level of androgen; moreover, overexpression of AR leads to chromatin modification, which then enhances transcription of AR targeted genes (158, 190). Our findings have observed a hormone-dependent increase of GCN2 expression in both cell lines, although at different time points. The different timing might be due to the fact that cells overexpressing AR are sensitized to the DHT, suggesting that more careful time courses will be necessary to get an overview of kinetics.

At the protein level (figure 4.6 B and C), GCN2 seems to correspond to the mRNA trend overserved in RT-PCR. Furthermore, increased GCN2 protein level seems to correlate with increased activity, in these cell lines both in treated and untreated conditions, especially in ARhi cells treated with DHT. Thus, one can speculate that increased AR level correlates with more demands on translation and thus increased GCN2 activity.

Moreover, a study has observed that when the intensity of stress is mild, only a small fraction of GCN2 is phosphorylated as a defense mechanism to protect the cell and increase stress intensity leads to an increased level of phosphorylated GCN2, which then leads to an enhanced GCN2 level (191). Perhaps this is similar in these cell lines; high AR level and altered gene expression of AR target genes mimic a mild stress situation, leading to an increased level of GCN2 activity. As mentioned above, high AR levels are characteristic of PC, giving an advantage to cancer cells. Elevated GCN2 levels might make the cells more resistant to stress, which would provide a selective advantage to the cancer cells.

5.4 The role of GCN1 in PC

As mentioned earlier, GCN1 is a co-activator of GCN2, and studies have shown that in mammalian cells, GCN1 is essential for activation of GCN2-dependent response to stress induced by amino-acid starvation and ultraviolet (UV) irradiation. These findings led to the proposition that GCN1 is might be necessary for GCN2 activation in PC. AR and MYC bind to the *GCN1/GCNL1* gene locus ChIPseq data from section 4.3.1 suggested that GCN1 is regulated by AR, and our findings from section 4.3.2 confirmed that AR regulates GCN1 expression. In both cell lines, under the given conditions, the GCN1 mRNA level seems to

have a similar pattern as for GCN2, except for pcDNA3.1 cells treated with DHT for 24 hours. However, the error bar for that sample is very high, which might be due to one or two of the DHT samples had a very high value for some technical reasons. Despite the error, our data suggested that PC cells that express AR and overexpressing cells tend to regulate GCN1 expression. Furthermore, our data indicate that GCN1 protein level is regulated by AR (figure 4.9).

GCN1 protein had a similar trend as to the level of GCN2 activity (GCN2-P), all the cell lines used for the experiment at section 4.2.1. As discussed earlier that C4-2B and Res-A cell lines had the highest level of GCN2-P; interestingly, the GCN1 level is also very high in these cell lines (figure 4.10). Consequently, most likely, GCN1 in these cell lines contributes to the activation of GCN2 by transferring uncharged tRNAs at the A-site of the ribosome to GCN2 (192).

5.5 MYC regulates GCN2 and GCN1 in PC

The oncogene *c-MYC* contributes to the pathogenesis of a majority of human cancer through the upregulation of transcriptional programs involved in cell division, metabolic adaptation, and survival (193). It has been shown that overexpression of *c-MYC* leads to androgen-independent growth in PC (194), and as mentioned above, 72% of CRPC exhibit specific amplification of the *MYC* gene. Furthermore, discussed earlier, overexpression of c-*MYC* leads to increased protein synthesis, which leads to activation of the ISR pathway through GCN2. Thus, our third aim of the study was to investigate whether MYC regulates GCN2 in PC, moreover, if GCN1 is necessary for activation of GCN2 in the LNCaP-MYC cell.

ChIPseq data from section 4.2.2 suggested that GCN2 is regulated by MYC in PC. Our preliminary data indicated that LNCaP-MYC cells treated with doxycycline that leads to overexpression of MYC had higher GCN2-P (figure 4.11). Furthermore, consistent with the notion that overexpression of *c-MYC* leads to increased protein synthesis, leading to increased demand for amino acids, resulting in intrinsic stress, which can activate the ISR pathway through GCN2. Interestingly, a study has suggested that an antagonist relationship exists between MYC and AR in PC, where overexpression of MYC repressed the expression

of genes that traditionally associate with AR mediated transcriptional pathways (157). Moreover, we have discussed earlier that our findings suggested that GCN2 is regulated by AR in PC. Consequently, it can be speculated that, most likely, GCN2 is co-regulated by MYC and AR in PC.

Furthermore, ChIPseq data from section 4.3.1 suggested that GCN1 is regulated by MYC in PC. We wished to investigate whether MYC affects GNC1 levels and GCN2 activity, both in unstressed and stressed cells. However, due to time limitations, the experiments have only been performed once; therefore, the results are preliminary. Nevertheless, they indicate that GCN1 protein level decreases when LNCaP-MYC cells are treated with doxycycline (figure 4.11). This suggesting that most likely over-expression of MYC leads to a decrease in GCN1 protein level and activation of GCN2 is mediated through other activators known to activate GCN2.

Moreover, GCN1 is essential for activation of GCN2 both in yeast and mammalian cells; when exposed to UV irradiation and starved condition, we have investigated whether GCN2 is regulated by MYC-dependent change in GCN1 protein levels. Our findings suggested that MYC overexpression limits GCN1 protein level both in response to UV and amino acid starvation (figure 4.12 and 4.13). Thus, suggesting that GCN1 is not regulated by MYC in MYC overexpressing PC cell line and activation of GCN2 is mediated through other activators. Unfortunately, the phosphorylated GCN2 activity could not be assessed for this particular experiment due to issues with antibodies.

5.6 GCN2-dependent cell survival

GCN2 is a stress response kinase, and the importance of GCN2 in cancer progression has been increasingly appreciated. As described earlier, GCN2 is essential for cancer cells to survive and thrive in a hostile microenvironment, which makes GCN2 an attractive target for cancer therapy. Thus, the study's fourth and last aim revolves around whether treatment with GCN2 inhibitor could be effective in prostate cancer cells.

Data presented in section 4.5.4 have shown that, even though the difference between the growth curves is very minor, the ARhi cells seem to grow consistently better than pcDNA3.1 cells when exposed to GCN2i at any concentration in both red media with FBS and white media whit 10 nM DHT. One can speculate that due to the high level of AR and altered gene expressions of GCN2, the AR overexpressing cells can better tolerate the inhibitor. In the Appendix B: Western Blot, our data suggested that the inhibitor upregulates GCN1, possibly turning on a feedback loop to restore levels of phosphorylated GCN2.

Even though GCN2i affects survival more severely in the presence of androgen at all concentration tested, it should be noted that a significant difference was observed in cell viability when these cells were grown in red media with FBS versus white media with CSFBS (table 4.1). CSFBS has been absorbed with activated carbon, which removes lipophilic, virus, certain growth factors, hormones, and cytotoxins; in contrast, red media is much more nutritious (195). A poor medium can lead to a starvation response due to limiting factors, which can then activate GCN2; thus, one can speculate that this might be one of the reasons cells grown in white media with CSFBS are more sensitive to GCN2i. Unfortunately, DMSO growth curves could not be shown due to a miscalculation; the DMSO concentration was much higher than that in the cells treated with the inhibitor and was highly toxic to the cells.

5.7 Limitations of the approaches

The scientific findings depend on repeated observations, which can be particularly challenging for immunoblotting. One of the crucial elements of immunoblotting is antibodies that play a crucial role in the reproducibility of the research findings (196). In this study, we had multiple issues with antibodies, especially GCN2-P primary antibody. There are various issues that can result in antibody failure, including the wrong choice of antibody type, dilution mistake, or batch-to-batch variation (197). Thus, multiple experiments could not be performed; moreover, findings from numerous experiments could not be shown in the final effort (Appendix B: Western blot).

Another limitation of this study was that some of the methods performed were not suitable for the cell lines used in this thesis. For instance, UV and starvation methods require media

removal; while performing these methods, we have observed vast loss of cells, even though the dishes were coated with PDL, which aids cells for better attachment to the dish surface (170).

To perform DHT treatment, one has to grow the cells in CSFBS, which is important in the context of GCN2; it is deprived of some growth factors and serum, which might in itself lead to GCN2 activation. A poor medium also means that the number of cells seeded becomes critical since something might become limiting in a poor medium at lower cell numbers, leading to a starvation response. Since these cell lines tend to grow not only in two-dimensional but also on top of each other, estimating confluence was not straightforward, and care was taken to count cells and determine the optimal cell numbers.

6. CONCLUSION

This master thesis aimed to investigate the role and regulation of GCN2 in prostate cancer, with the long-term goal of revealing whether GCN2 will be an effective therapeutic target for the treatment of prostate cancer. Our findings provided new insights into the role and regulation of GCN2; we suggest that GCN2 expression is regulated by both MYC and AR in prostate cancer. In addition, our result indicated that GCN1 is necessary for GCN2 activation in prostate cancer. Moreover, castration resistance prostate cancer resistant to AR signaling inhibitors (such as enzalutamide) has an increased GCN2 activity, which might be at least partly the reason for the resistance –and therefore could be a useful target in combination therapy. Lastly, prostate cancer cell lines exhibiting castration resistant prostate cancer features are sensitive to GCN2 inhibition and led to decrease survival. Taken together, these findings show that targeting GCN2 can be a new and effective therapeutic strategy for castration resistant prostate cancer.

7. FUTURE ASPECTS

Many experiments are still needed to understand the role and regulation of the ISR in PC. We were only able to scratch on the surface of this vast, complicated matter in the given time. Thus, much more extensive work is needed in the future for a better understanding of the activation and regulation of GCN2 and GCN1 in PC.

We have shown that AR regulates GCN2 mRNA and protein levels in pcDNA3.1 and ARhi cells by RT-PCR and immunoblotting. The same approach should be performed in all the other cell lines to observe if GCN2 is also regulated in different prostate cancer cell lines. Data from these findings can further provide a molecular understanding of the GCN2 role in castrate resistance prostate cancer and developing a drug that targets GCN2 and downstream genes.

One of the most interesting findings of our thesis when we have observed a very high level of GCN2-P in Res-A cells resistant to enzalutamide. In the future, immunoblotting should be performed to observe the GCN2-P level in Res-B cells. Moreover, knockdown of GCN2 in these cell lines will provide a better understanding of the interplay between GCN2 and AR, consequently importance of the ATF4 pathway.

Even though we have shown that pcDNA3.1 and ARhi cells are sensitive to GCN2i, further validation is needed. Thus, for the future, GCN2i should be tested on LNCaP-MYC cells and with doxycycline, moreover on LNCaP parental against Res-A. Both cell viability assay and immunoblotting will provide a better understanding of sensitivity towards GCN2i. Furthermore, Poly (ADP-ribose) polymerase (PARP) is a protein that is involved in the DNA repair mechanism (single-strand break) and is important for the maintenance of genomic integrity (198). PARP inhibitors (PARPi) are now FDA approved for the treatment of mCRPC for patients with tumors defective in DNA damage responses (DDR) (199). Thus, PARPi in combination with GCN2i should be tested in all these cell lines to observe whether this leads to growth inhibition of the cells, subsequently, combination with X-ray.

BIBLIOGRAPHY

1. Freddie Bray JF, Isabelle Soerjomataram, Rebecca L. Siegel, Lindsey A. Torre, Ahmedin Jemal. Global Cancer Statistics 2018: GLOBOCAN Estimates of Incidence and Mortality Worldwide for 36 Cancers in 185 Countries. 2018;68(6):394-424.
2. Organization WH. Cancer 2021 [Available from: https://www.who.int/news-room/fact-sheets/detail/cancer
3. Kreft er nå hyppigste dødsårsak i Norge: Folkehelseinstituttet 2018 [Available from: https://www.fhi.no/nyheter/2018/dodsarsakene-2017.
4. Cancer Statistics Cancer Registry of Norway; 2019 [Available from: https://www.kreftregisteret.no/en/The-Registries/Cancer-Statistics/.
5. Key figures on cancer Cancer Registry of Norway; 2019 [Available from: https://www.kreftregisteret.no/en/Temasider/key-figures-on-cancer/.
6. Bruce Alberts AJ, Julian Lewis, David Morgan, Martin Raff, Keith Roberts, Peter Walter. Cancer. Molecular Biology of The Cell. 6th ed: Garland Science 2015. p. 1091-103.
7. A. J. Bruce Alberts JL, David Morgan, Martin Raff, Keith Roberts, Peter Walter. Cells and Genomes. 6th ed: Garland Science; 2015.
8. Wienberg RA. The biology and genetics of Cells and organisms The Biology of Cancer. 2 ed. New York: Garland Science; 2014. p. 1-29.
9. Pecorino L. Introduction. Molecular Biology of Cancer, Mechanisms, Targets, and therapeutics. New York: Oxford University Press 2016. p. 1-16.
10. Winberg RA. Maintenance of genomic Integrity and the development of Cancer. The Biology of Cancer. New York: Garland Science; 2014. p. 511-72.
11. Hanahan D, Weinberg RA. Hallmarks of cancer: the next generation. Cell. 2011;144(5):646-74.
12. Weinberg RA. Growth factors, Receptors and Cancer. The Biology of Cancer. New York Garland Science 2014. p. 131-69.
13. Weinberg RA. p53 and Apoptosis: Master Gurdian and Executioner. The Biology of Cancer. New York: Garland Science; 2014. p. 331-81.
14. Fernald K, Kurokawa M. Evading apoptosis in cancer. Trends Cell Biol. 2013;23(12):620-33.
15. Pecorino L. Angiogenesis. Molecular Biology of Cancer, Mechanisms, Targets, and therapeutics. New York: Oxford University Press; 2016. p. 228-40.
16. Pecorino L. Metastasis Molecular Biology of Cancer, Mechanisms, Targets, and therapeutics. New york Oxford University Press 2016. p. 205-22.
17. Wienberg RA. Moving Out: Invasion and Metastasis. The Biology of Cancer. New York Garland Science 2014. p. 641-711.
18. Pecorino L. Growth Inhibition and tumor supressor genes. Molecular Biology of Cancer, Mechanisms, Targets, and therapeutics. New York: Oxford University Press; 2016. p. 128-47.
19. Wienberg RA. Tumor Suppressor Genes. The Biology of Cancer New York: Garland Science; 2014. p. 231-59.
20. Vinay DS, Ryan EP, Pawelec G, Talib WH, Stagg J, Elkord E, et al. Immune evasion in cancer: Mechanistic basis and therapeutic strategies. Semin Cancer Biol. 2015;35 Suppl:S185-s98.
21. Dean LT, Gehlert S, Neuhouser ML, Oh A, Zanetti K, Goodman M, et al. Social factors matter in cancer risk and survivorship. Cancer Causes Control. 2018;29(7):611-8.

22. Kai H. Hammerich GEA, Thomas M. Wheeler. Anatomy of the prostate gland and surgical pathology of prostate cancer. 2009.
23. McNeal JE. The zonal anatomy of the prostate. Prostate. 1981;2(1):35-49.
24. Alastair D. Lamb AYW, David E. Neal. Pre-malignant Disease in the Prostate. 2014.
25. Timms BG. Prostate development: a historical perspective. Differentiation. 2008;76(6):565-77.
26. Prins GS, Putz O. Molecular signaling pathways that regulate prostate gland development. Differentiation. 2008;76(6):641-59.
27. Brawer MK. Prostatic intraepithelial neoplasia: an overview. Rev Urol. 2005;7 Suppl 3(Suppl 3):S11-8.
28. Tomlins SA, Mehra R, Rhodes DR, Cao X, Wang L, Dhanasekaran SM, et al. Integrative molecular concept modeling of prostate cancer progression. Nat Genet. 2007;39(1):41-51.
29. Wang G, Zhao D, Spring DJ, DePinho RA. Genetics and biology of prostate cancer. Genes Dev. 2018;32(17-18):1105-40.
30. Rao A, Vapiwala N, Schaeffer EM, Ryan CJ. Oligometastatic Prostate Cancer: A Shrinking Subset or an Opportunity for Cure? Am Soc Clin Oncol Educ Book. 2019;39:309-20.
31. Berish RB, Ali AN, Telmer PG, Ronald JA, Leong HS. Translational models of prostate cancer bone metastasis. Nature Reviews Urology. 2018;15(7):403-21.
32. Maurizi A, Rucci N. The Osteoclast in Bone Metastasis: Player and Target. Cancers. 2018;10(7):218.
33. He L, Fang H, Chen C, Wu Y, Wang Y, Ge H, et al. Metastatic castration-resistant prostate cancer: Academic insights and perspectives through bibliometric analysis. Medicine (Baltimore). 2020;99(15):e19760.
34. Grasso CS, Wu Y-M, Robinson DR, Cao X, Dhanasekaran SM, Khan AP, et al. The mutational landscape of lethal castration-resistant prostate cancer. Nature. 2012;487(7406):239-43.
35. Hernández J, Thompson IM. Prostate-specific antigen: a review of the validation of the most commonly used cancer biomarker. Cancer. 2004;101(5):894-904.
36. Thompson IM, Ankerst DP. Prostate-specific antigen in the early detection of prostate cancer. Cmaj. 2007;176(13):1853-8.
37. Litwin MS, Tan HJ. The Diagnosis and Treatment of Prostate Cancer: A Review. Jama. 2017;317(24):2532-42.
38. Hayes JH, Barry MJ. Screening for prostate cancer with the prostate-specific antigen test: a review of current evidence. Jama. 2014;311(11):1143-9.
39. Board CNE. Porstate Cancer: Stages and Grades: Cancer.Net 2020 [Available from: https://www.cancer.net/cancer-types/prostate-cancer/stages-and-grades.
40. Quigley CA, De Bellis A, Marschke KB, el-Awady MK, Wilson EM, French FS. Androgen receptor defects: historical, clinical, and molecular perspectives. Endocr Rev. 1995;16(3):271-321.
41. Tan MHE, Li J, Xu HE, Melcher K, Yong E-l. Androgen receptor: structure, role in prostate cancer and drug discovery. Acta Pharmacologica Sinica. 2015;36(1):3-23.
42. Sullivan WP, Vroman BT, Bauer VJ, Puri RK, Riehl RM, Pearson GR, et al. Isolation of steroid receptor binding protein from chicken oviduct and production of monoclonal antibodies. Biochemistry. 1985;24(15):4214-22.
43. Michmerhuizen AR, Spratt DE, Pierce LJ, Speers CW. ARe we there yet? Understanding androgen receptor signaling in breast cancer. npj Breast Cancer. 2020;6(1):47.

44. Takayama K, Inoue S. Transcriptional network of androgen receptor in prostate cancer progression. Int J Urol. 2013;20(8):756-68.
45. Itkonen H, Mills IG. Chromatin binding by the androgen receptor in prostate cancer. Mol Cell Endocrinol. 2012;360(1-2):44-51.
46. Wang Q, Li W, Liu XS, Carroll JS, Jänne OA, Keeton EK, et al. A hierarchical network of transcription factors governs androgen receptor-dependent prostate cancer growth. Mol Cell. 2007;27(3):380-92.
47. Fujita K, Nonomura N. Role of Androgen Receptor in Prostate Cancer: A Review. World J Mens Health. 2019;37(3):288-95.
48. Mills IG. Maintaining and reprogramming genomic androgen receptor activity in prostate cancer. Nature Reviews Cancer. 2014;14(3):187-98.
49. Wadosky KM, Koochekpour S. Molecular mechanisms underlying resistance to androgen deprivation therapy in prostate cancer. Oncotarget. 2016;7(39):64447-70.
50. Shiv Verma KSP, Prem Prakash Kushwaha, Mohd Shuaib, Atul Kumar Singh, Shashank Kumar, Sanjay Gupta. Resistance to second generation antiandrogens in prostate cancer: pathways and mechanisms. 2020.
51. Romanel A, Gasi Tandefelt D, Conteduca V, Jayaram A, Casiraghi N, Wetterskog D, et al. Plasma AR and abiraterone-resistant prostate cancer. Sci Transl Med. 2015;7(312):312re10.
52. Krongrad A, Wilson CM, Wilson JD, Allman DR, McPhaul MJ. Androgen increases androgen receptor protein while decreasing receptor mRNA in LNCaP cells. Mol Cell Endocrinol. 1991;76(1-3):79-88.
53. Grasso CS, Wu YM, Robinson DR, Cao X, Dhanasekaran SM, Khan AP, et al. The mutational landscape of lethal castration-resistant prostate cancer. Nature. 2012;487(7406):239-43.
54. Jernberg E, Bergh A, Wikström P. Clinical relevance of androgen receptor alterations in prostate cancer. Endocr Connect. 2017;6(8):R146-r61.
55. Azad AA, Volik SV, Wyatt AW, Haegert A, Le Bihan S, Bell RH, et al. Androgen Receptor Gene Aberrations in Circulating Cell-Free DNA: Biomarkers of Therapeutic Resistance in Castration-Resistant Prostate Cancer. Clin Cancer Res. 2015;21(10):2315-24.
56. Waltering KK, Urbanucci A, Visakorpi T. Androgen receptor (AR) aberrations in castration-resistant prostate cancer. Mol Cell Endocrinol. 2012;360(1-2):38-43.
57. Veldscholte J, Ris-Stalpers C, Kuiper GG, Jenster G, Berrevoets C, Claassen E, et al. A mutation in the ligand binding domain of the androgen receptor of human LNCaP cells affects steroid binding characteristics and response to anti-androgens. Biochem Biophys Res Commun. 1990;173(2):534-40.
58. Bryce AH, Antonarakis ES. Androgen receptor splice variant 7 in castration-resistant prostate cancer: Clinical considerations. Int J Urol. 2016;23(8):646-53.
59. Guo Z, Yang X, Sun F, Jiang R, Linn DE, Chen H, et al. A novel androgen receptor splice variant is up-regulated during prostate cancer progression and promotes androgen depletion-resistant growth. Cancer Res. 2009;69(6):2305-13.
60. Sun S, Sprenger CC, Vessella RL, Haugk K, Soriano K, Mostaghel EA, et al. Castration resistance in human prostate cancer is conferred by a frequently occurring androgen receptor splice variant. J Clin Invest. 2010;120(8):2715-30.
61. Hörnberg E, Ylitalo EB, Crnalic S, Antti H, Stattin P, Widmark A, et al. Expression of androgen receptor splice variants in prostate cancer bone metastases is associated with castration-resistance and short survival. PLoS One. 2011;6(4):e19059.

62. Agoulnik IU, Vaid A, Bingman WE, 3rd, Erdeme H, Frolov A, Smith CL, et al. Role of SRC-1 in the promotion of prostate cancer cell growth and tumor progression. Cancer Res. 2005;65(17):7959-67.
63. Taylor BS, Schultz N, Hieronymus H, Gopalan A, Xiao Y, Carver BS, et al. Integrative genomic profiling of human prostate cancer. Cancer Cell. 2010;18(1):11-22.
64. Qin J, Lee HJ, Wu SP, Lin SC, Lanz RB, Creighton CJ, et al. Androgen deprivation-induced NCoA2 promotes metastatic and castration-resistant prostate cancer. J Clin Invest. 2014;124(11):5013-26.
65. Tien JC, Liu Z, Liao L, Wang F, Xu Y, Wu YL, et al. The steroid receptor coactivator-3 is required for the development of castration-resistant prostate cancer. Cancer Res. 2013;73(13):3997-4008.
66. Shiota M, Yokomizo A, Masubuchi D, Tada Y, Inokuchi J, Eto M, et al. Tip60 promotes prostate cancer cell proliferation by translocation of androgen receptor into the nucleus. Prostate. 2010;70(5):540-54.
67. LaTulippe E, Satagopan J, Smith A, Scher H, Scardino P, Reuter V, et al. Comprehensive gene expression analysis of prostate cancer reveals distinct transcriptional programs associated with metastatic disease. Cancer Res. 2002;62(15):4499-506.
68. Chang KH, Li R, Kuri B, Lotan Y, Roehrborn CG, Liu J, et al. A gain-of-function mutation in DHT synthesis in castration-resistant prostate cancer. Cell. 2013;154(5):1074-84.
69. Cheng J, Wu Y, Mohler JL, Ip C. The transcriptomics of de novo androgen biosynthesis in prostate cancer cells following androgen reduction. Cancer Biol Ther. 2010;9(12):1033-42.
70. Braadland PR, Urbanucci A. Chromatin reprogramming as an adaptation mechanism in advanced prostate cancer. Endocr Relat Cancer. 2019;26(4):R211-r35.
71. Toren P, Zoubeidi A. Targeting the PI3K/Akt pathway in prostate cancer: challenges and opportunities (review). Int J Oncol. 2014;45(5):1793-801.
72. Pourmand G, Ziaee AA, Abedi AR, Mehrsai A, Alavi HA, Ahmadi A, et al. Role of PTEN gene in progression of prostate cancer. Urol J. 2007;4(2):95-100.
73. The Molecular Taxonomy of Primary Prostate Cancer. Cell. 2015;163(4):1011-25.
74. Robinson D, Van Allen EM, Wu YM, Schultz N, Lonigro RJ, Mosquera JM, et al. Integrative Clinical Genomics of Advanced Prostate Cancer. Cell. 2015;162(2):454.
75. Taplin ME. Biochemical (Prostate-Specific Antigen) Relapse: An Oncologist's Perspective. Rev Urol. 2003;5 Suppl 2(Suppl 2):S3-s13.
76. King CR, Presti JC, Jr., Gill H, Brooks J, Hancock SL. Radiotherapy after radical prostatectomy: does transient androgen suppression improve outcomes? Int J Radiat Oncol Biol Phys. 2004;59(2):341-7.
77. Stephenson AJ, Kattan MW, Eastham JA, Bianco FJ, Jr., Yossepowitch O, Vickers AJ, et al. Prostate cancer-specific mortality after radical prostatectomy for patients treated in the prostate-specific antigen era. J Clin Oncol. 2009;27(26):4300-5.
78. Aneja S, Pratiwadi RR, Yu JB. Hypofractionated radiation therapy for prostate cancer: risks and potential benefits in a fiscally conservative health care system. Oncology (Williston Park). 2012;26(6):512-8.
79. Quon H, Cheung PC, Loblaw DA, Morton G, Pang G, Szumacher E, et al. Hypofractionated concomitant intensity-modulated radiotherapy boost for high-risk prostate cancer: late toxicity. Int J Radiat Oncol Biol Phys. 2012;82(2):898-905.
80. Jim N. Rose JMC. The role of radiation therapy in the treatment of metastatic castrate-resistant prostate cancer. 2015.

81. Sternberg CN, Petrylak DP, Madan RA, Parker C. Progress in the treatment of advanced prostate cancer. Am Soc Clin Oncol Educ Book. 2014:117-31.
82. Tannock IF, de Wit R, Berry WR, Horti J, Pluzanska A, Chi KN, et al. Docetaxel plus prednisone or mitoxantrone plus prednisone for advanced prostate cancer. N Engl J Med. 2004;351(15):1502-12.
83. Teply BA, Hauke RJ. Chemotherapy options in castration-resistant prostate cancer. Indian J Urol. 2016;32(4):262-70.
84. Westdorp H, Sköld AE, Snijer BA, Franik S, Mulder SF, Major PP, et al. Immunotherapy for prostate cancer: lessons from responses to tumor-associated antigens. Front Immunol. 2014;5:191.
85. Fay EK, Graff JN. Immunotherapy in Prostate Cancer. Cancers. 2020;12(7):1752.
86. Burotto M, Singh N, Heery CR, Gulley JL, Madan RA. Exploiting synergy: immune-based combinations in the treatment of prostate cancer. Front Oncol. 2014;4:351.
87. Madan RA, Arlen PM, Mohebtash M, Hodge JW, Gulley JL. Prostvac-VF: a vector-based vaccine targeting PSA in prostate cancer. Expert Opin Investig Drugs. 2009;18(7):1001-11.
88. Taplin M-E. Biochemical (Prostate-Specific Antigen) Relapse: An Oncologist's Perspective. Reviews in urology. 2003;5 Suppl 2(Suppl 2):S3-S13.
89. Gamat M, McNeel DG. Androgen deprivation and immunotherapy for the treatment of prostate cancer. Endocr Relat Cancer. 2017;24(12):T297-t310.
90. Fizazi K, Faivre L, Lesaunier F, Delva R, Gravis G, Rolland F, et al. Androgen deprivation therapy plus docetaxel and estramustine versus androgen deprivation therapy alone for high-risk localised prostate cancer (GETUG 12): a phase 3 randomised controlled trial. Lancet Oncol. 2015;16(7):787-94.
91. Taylor LG, Canfield SE, Du XL. Review of major adverse effects of androgen-deprivation therapy in men with prostate cancer. Cancer. 2009;115(11):2388-99.
92. Sharifi N, Gulley JL, Dahut WL. Androgen Deprivation Therapy for Prostate Cancer. JAMA. 2005;294(2):238-44.
93. Ahmed A, Ali S, Sarkar FH. Advances in androgen receptor targeted therapy for prostate cancer. J Cell Physiol. 2014;229(3):271-6.
94. Dumas L, Payne H, Chowdhury S. The evolution of antiandrogens: MDV3100 comes of age. Expert Rev Anticancer Ther. 2012;12(2):131-3.
95. Kim W, Ryan CJ. Androgen receptor directed therapies in castration-resistant metastatic prostate cancer. Curr Treat Options Oncol. 2012;13(2):189-200.
96. Clegg NJ, Wongvipat J, Joseph JD, Tran C, Ouk S, Dilhas A, et al. ARN-509: a novel antiandrogen for prostate cancer treatment. Cancer Res. 2012;72(6):1494-503.
97. Chen Y, Clegg NJ, Scher HI. Anti-androgens and androgen-depleting therapies in prostate cancer: new agents for an established target. Lancet Oncol. 2009;10(10):981-91.
98. Osguthorpe DJ, Hagler AT. Mechanism of androgen receptor antagonism by bicalutamide in the treatment of prostate cancer. Biochemistry. 2011;50(19):4105-13.
99. Potter GA, Barrie SE, Jarman M, Rowlands MG. Novel steroidal inhibitors of human cytochrome P45017 alpha (17 alpha-hydroxylase-C17,20-lyase): potential agents for the treatment of prostatic cancer. J Med Chem. 1995;38(13):2463-71.
100. Zhu H, Garcia JA. Targeting the adrenal gland in castration-resistant prostate cancer: a case for orteronel, a selective CYP-17 17,20-lyase inhibitor. Curr Oncol Rep. 2013;15(2):105-12.

101. Dayyani F, Gallick GE, Logothetis CJ, Corn PG. Novel therapies for metastatic castrate-resistant prostate cancer. J Natl Cancer Inst. 2011;103(22):1665-75.
102. Leibowitz-Amit R, Joshua AM. Targeting the androgen receptor in the management of castration-resistant prostate cancer: rationale, progress, and future directions. Curr Oncol. 2012;19(Suppl 3):S22-31.
103. Xu Y, Jiang YF, Wu B. New agonist- and antagonist-based treatment approaches for advanced prostate cancer. J Int Med Res. 2012;40(4):1217-26.
104. Heidegger I, Massoner P, Eder IE, Pircher A, Pichler R, Aigner F, et al. Novel therapeutic approaches for the treatment of castration-resistant prostate cancer. J Steroid Biochem Mol Biol. 2013;138:248-56.
105. Saporita AJ, Ai J, Wang Z. The Hsp90 inhibitor, 17-AAG, prevents the ligand-independent nuclear localization of androgen receptor in refractory prostate cancer cells. Prostate. 2007;67(5):509-20.
106. He S, Zhang C, Shafi AA, Sequeira M, Acquaviva J, Friedland JC, et al. Potent activity of the Hsp90 inhibitor ganetespib in prostate cancer cells irrespective of androgen receptor status or variant receptor expression. Int J Oncol. 2013;42(1):35-43.
107. Kim YS, Kumar V, Lee S, Iwai A, Neckers L, Malhotra SV, et al. Methoxychalcone inhibitors of androgen receptor translocation and function. Bioorg Med Chem Lett. 2012;22(5):2105-9.
108. Sarkar FH, Li Y, Wang Z, Kong D. Novel targets for prostate cancer chemoprevention. Endocr Relat Cancer. 2010;17(3):R195-212.
109. Ahmad A, Kong D, Sarkar SH, Wang Z, Banerjee S, Sarkar FH. Inactivation of uPA and its receptor uPAR by 3,3'-diindolylmethane (DIM) leads to the inhibition of prostate cancer cell growth and migration. J Cell Biochem. 2009;107(3):516-27.
110. Manalo RVM, Medina PMB. The endoplasmic reticulum stress response in disease pathogenesis and pathophysiology. Egyptian Journal of Medical Human Genetics. 2018;19(2):59-68.
111. Pakos-Zebrucka K, Koryga I, Mnich K, Ljujic M, Samali A, Gorman AM. The integrated stress response. EMBO Rep. 2016;17(10):1374-95.
112. Donnelly N, Gorman AM, Gupta S, Samali A. The eIF2α kinases: their structures and functions. Cellular and Molecular Life Sciences. 2013;70(19):3493-511.
113. Deval C, Chaveroux C, Maurin AC, Cherasse Y, Parry L, Carraro V, et al. Amino acid limitation regulates the expression of genes involved in several specific biological processes through GCN2-dependent and GCN2-independent pathways. Febs j. 2009;276(3):707-18.
114. Anda S, Zach R, Grallert B. Activation of Gcn2 in response to different stresses. PloS one. 2017;12(8):e0182143-e.
115. Masson GR. Towards a model of GCN2 activation. Biochem Soc Trans. 2019;47(5):1481-8.
116. Kilberg MS, Pan YX, Chen H, Leung-Pineda V. Nutritional control of gene expression: how mammalian cells respond to amino acid limitation. Annu Rev Nutr. 2005;25:59-85.
117. Dong J, Qiu H, Garcia-Barrio M, Anderson J, Hinnebusch AG. Uncharged tRNA Activates GCN2 by Displacing the Protein Kinase Moiety from a Bipartite tRNA-Binding Domain. Molecular Cell. 2000;6(2):269-79.
118. Wek SA, Zhu S, Wek RC. The histidyl-tRNA synthetase-related sequence in the eIF-2 alpha protein kinase GCN2 interacts with tRNA and is required for activation in response to starvation for different amino acids. Mol Cell Biol. 1995;15(8):4497-506.

119. Castilho BA, Shanmugam R, Silva RC, Ramesh R, Himme BM, Sattlegger E. Keeping the eIF2 alpha kinase Gcn2 in check. Biochimica et Biophysica Acta (BBA) - Molecular Cell Research. 2014;1843(9):1948-68.
120. Wek RC, Jiang HY, Anthony TG. Coping with stress: eIF2 kinases and translational control. Biochem Soc Trans. 2006;34(Pt 1):7-11.
121. UniProt. UniProtKB - Q92616 (GCN1_HUMAN) [Available from: https://www.uniprot.org/uniprot/Q92616.
122. Rakesh R, Krishnan R, Sattlegger E, Srinivasan N. Recognition of a structural domain (RWDBD) in Gcn1 proteins that interacts with the RWD domain containing proteins. Biology Direct. 2017;12(1):12.
123. Sattlegger E, Barbosa JARG, Moraes MCS, Martins RM, Hinnebusch AG, Castilho BA. Gcn1 and Actin Binding to Yih1: IMPLICATIONS FOR ACTIVATION OF THE eIF2 KINASE GCN2*. Journal of Biological Chemistry. 2011;286(12):10341-55.
124. Yamazaki H, Kasai S, Mimura J, Ye P, Inose-Maruyama A, Tanji K, et al. Ribosome binding protein GCN1 regulates the cell cycle and cell proliferation and is essential for the embryonic development of mice. PLoS Genet. 2020;16(4):e1008693-e.
125. Beata Grallert EB. GCN2, an old dog with new tricks. 2013;41(6).
126. Rastogi RP, Richa, Kumar A, Tyagi MB, Sinha RP. Molecular mechanisms of ultraviolet radiation-induced DNA damage and repair. J Nucleic Acids. 2010;2010:592980-.
127. Cutler TD, Zimmerman JJ. Ultraviolet irradiation and the mechanisms underlying its inactivation of infectious agents. Anim Health Res Rev. 2011;12(1):15-23.
128. Powley IR, Kondrashov A, Young LA, Dobbyn HC, Hill K, Cannell IG, et al. Translational reprogramming following UVB irradiation is mediated by DNA-PKcs and allows selective recruitment to the polysomes of mRNAs encoding DNA repair enzymes. Genes & development. 2009;23(10):1207-20.
129. Yang R, Wek SA, Wek RC. Glucose limitation induces GCN4 translation by activation of Gcn2 protein kinase. Molecular and cellular biology. 2000;20(8):2706-17.
130. Baker BM, Nargund AM, Sun T, Haynes CM. Protective coupling of mitochondrial function and protein synthesis via the eIF2α kinase GCN-2. PLoS Genet. 2012;8(6):e1002760.
131. Feng W, Lei T, Wang Y, Feng R, Yuan J, Shen X, et al. GCN2 deficiency ameliorates cardiac dysfunction in diabetic mice by reducing lipotoxicity and oxidative stress. Free Radical Biology and Medicine. 2019;130:128-39.
132. Ron D, Walter P. Signal integration in the endoplasmic reticulum unfolded protein response. Nature Reviews Molecular Cell Biology. 2007;8(7):519-29.
133. Hamanaka RB, Bennett BS, Cullinan SB, Diehl JA. PERK and GCN2 contribute to eIF2alpha phosphorylation and cell cycle arrest after activation of the unfolded protein response pathway. Mol Biol Cell. 2005;16(12):5493-501.
134. Cosnefroy O, Jaspart A, Calmels C, Parissi V, Fleury H, Ventura M, et al. Activation of GCN2 upon HIV-1 infection and inhibition of translation. Cellular and Molecular Life Sciences. 2013;70(13):2411-21.
135. Kloft N, Neukirch C, Bobkiewicz W, Veerachato G, Busch T, von Hoven G, et al. Pro-autophagic signal induction by bacterial pore-forming toxins. Med Microbiol Immunol. 2010;199(4):299-309.
136. Inglis AJ, Masson GR, Shao S, Perisic O, McLaughlin SH, Hegde RS, et al. Activation of GCN2 by the ribosomal P-stalk. Proc Natl Acad Sci U S A. 2019;116(11):4946-54.
137. Krohn M, Skjølberg HC, Soltani H, Grallert B, Boye E. The G1-S checkpoint in fission yeast is not a general DNA damage checkpoint. J Cell Sci. 2008;121(Pt 24):4047-54.

138. Menacho-Marquez M, Perez-Valle J, Ariño J, Gadea J, Murguía JR. Gcn2p regulates a G1/S cell cycle checkpoint in response to DNA damage. Cell Cycle. 2007;6(18):2302-5.
139. Lindahl T, Wood RD. Quality control by DNA repair. Science. 1999;286(5446):1897-905.
140. Nishitani H, Lygerou Z. Control of DNA replication licensing in a cell cycle. Genes Cells. 2002;7(6):523-34.
141. Grallert B, Boye E. The Gcn2 kinase as a cell cycle regulator. Cell Cycle. 2007;6(22):2768-72.
142. Schmidt S, Gay D, Uthe FW, Denk S, Paauwe M, Matthes N, et al. A MYC–GCN2–eIF2α negative feedback loop limits protein synthesis to prevent MYC-dependent apoptosis in colorectal cancer. Nature Cell Biology. 2019;21(11):1413-24.
143. Tameire F, Verginadis II, Leli NM, Polte C, Conn CS, Ojha R, et al. ATF4 couples MYC-dependent translational activity to bioenergetic demands during tumour progression. Nature Cell Biology. 2019;21(7):889-99.
144. Wang Y, Ning Y, Alam GN, Jankowski BM, Dong Z, Nör JE, et al. Amino Acid Deprivation Promotes Tumor Angiogenesis through the GCN2/ATF4 Pathway. Neoplasia. 2013;15(8):989-97.
145. Ye J, Kumanova M, Hart LS, Sloane K, Zhang H, De Panis DN, et al. The GCN2-ATF4 pathway is critical for tumour cell survival and proliferation in response to nutrient deprivation. Embo j. 2010;29(12):2082-96.
146. Ye J, Mancuso A, Tong X, Ward PS, Fan J, Rabinowitz JD, et al. Pyruvate kinase M2 promotes de novo serine synthesis to sustain mTORC1 activity and cell proliferation. Proc Natl Acad Sci U S A. 2012;109(18):6904-9.
147. Martínez-Reyes I, Sánchez-Aragó M, Cuezva JM. AMPK and GCN2-ATF4 signal the repression of mitochondria in colon cancer cells. Biochem J. 2012;444(2):249-59.
148. Munn DH, Sharma MD, Baban B, Harding HP, Zhang Y, Ron D, et al. GCN2 kinase in T cells mediates proliferative arrest and anergy induction in response to indoleamine 2,3-dioxygenase. Immunity. 2005;22(5):633-42.
149. Rashidi A, Miska J, Lee-Chang C, Kanojia D, Panek WK, Lopez-Rosas A, et al. GCN2 is essential for CD8+ T cell survival and function in murine models of malignant glioma. Cancer Immunology, Immunotherapy. 2020;69(1):81-94.
150. Van de Velde LA, Guo XJ, Barbaric L, Smith AM, Oguin TH, 3rd, Thomas PG, et al. Stress Kinase GCN2 Controls the Proliferative Fitness and Trafficking of Cytotoxic T Cells Independent of Environmental Amino Acid Sensing. Cell Rep. 2016;17(9):2247-58.
151. Horoszewicz JS, Leong SS, Kawinski E, Karr JP, Rosenthal H, Chu TM, et al. LNCaP model of human prostatic carcinoma. Cancer Res. 1983;43(4):1809-18.
152. Thalmann GN, Anezinis PE, Chang SM, Zhau HE, Kim EE, Hopwood VL, et al. Androgen-independent cancer progression and bone metastasis in the LNCaP model of human prostate cancer. Cancer Res. 1994;54(10):2577-81.
153. Wu HC, Hsieh JT, Gleave ME, Brown NM, Pathak S, Chung LW. Derivation of androgen-independent human LNCaP prostatic cancer cell sublines: role of bone stromal cells. Int J Cancer. 1994;57(3):406-12.
154. Cunningham D, You Z. In vitro and in vivo model systems used in prostate cancer research. J Biol Methods. 2015;2(1):e17.
155. Das AT, Tenenbaum L, Berkhout B. Tet-On Systems For Doxycycline-inducible Gene Expression. Curr Gene Ther. 2016;16(3):156-67.

156. Ramos-Montoya A, Lamb AD, Russell R, Carroll T, Jurmeister S, Galeano-Dalmau N, et al. HES6 drives a critical AR transcriptional programme to induce castration-resistant prostate cancer through activation of an E2F1-mediated cell cycle network. EMBO Mol Med. 2014;6(5):651-61.
157. Barfeld SJ, Urbanucci A, Itkonen HM, Fazli L, Hicks JL, Thiede B, et al. c-Myc Antagonises the Transcriptional Activity of the Androgen Receptor in Prostate Cancer Affecting Key Gene Networks. EBioMedicine. 2017;18:83-93.
158. Waltering KK, Helenius MA, Sahu B, Manni V, Linja MJ, Jänne OA, et al. Increased expression of androgen receptor sensitizes prostate cancer cells to low levels of androgens. Cancer Res. 2009;69(20):8141-9.
159. Waltering KK, Urbanucci A, Visakorpi T. Androgen receptor (AR) aberrations in castration-resistant prostate cancer. Molecular and Cellular Endocrinology. 2012;360(1):38-43.
160. Handle F, Prekovic S, Helsen C, Van den Broeck T, Smeets E, Moris L, et al. Drivers of AR indifferent anti-androgen resistance in prostate cancer cells. Scientific Reports. 2019;9(1):13786.
161. Aseptic technique: ThermoFisher Scientific [Available from: https://www.thermofisher.com/no/en/home/references/gibco-cell-culture-basics/aseptic-technique.html.
162. Cell Culture Basics Handbook: Gibco Education; [Available from: https://www.thermofisher.com/content/dam/LifeTech/Documents/PDFs/PG1563-PJT1267-COL31122-Gibco-Cell-Culture-Basics-Handbook-Global-FLR.pdf.
163. GlutaMAX Supplement: ThermoFisher Scientific; [Available from: https://www.thermofisher.com/order/catalog/product/35050087?SID=srch-srp-35050087#/35050087?SID=srch-srp-35050087.
164. Trypan Blue Stain (0.4%) for use with the Countess™ Automated Cell Counter: TermoFisher Scientific; [Available from: https://www.thermofisher.com/order/catalog/product/T10282?SID=srch-srp-T10282#/T10282?SID=srch-srp-T10282.
165. BioCision. Snap Freezing Using Dry Ice or Liquid Nitrogen: BioCision; [Available from: http://biocision.com.s219960.gridserver.com/uploads/docs/appnote_snapfreezing_2013.pdf.
166. Baumstark-Khan C. Radiation Biology. In: Gargaud M, Amils R, Quintanilla JC, Cleaves HJ, Irvine WM, Pinti DL, et al., editors. Encyclopedia of Astrobiology. Berlin, Heidelberg: Springer Berlin Heidelberg; 2011. p. 1405-6.
167. Muhammad Uthman FES, Bara'u Gafai Najashi, Ismail Farouk Labran,Abubakar Sadiq Umar, Umar Sani Abdullahi. 5G Radiation and COVID-19: The Non-Existent Connection. 2020;8(2):5.
168. Baskar R, Lee KA, Yeo R, Yeoh K-W. Cancer and radiation therapy: current advances and future directions. Int J Med Sci. 2012;9(3):193-9.
169. Maverakis E, Miyamura Y, Bowen MP, Correa G, Ono Y, Goodarzi H. Light, including ultraviolet. J Autoimmun. 2010;34(3):J247-J57.
170. SEIENTIFIC T. Poly-D-Lysine [Available from: https://www.thermofisher.com/order/catalog/product/A3890401#/A3890401.
171. Bagati A, Koch Z, Bofinger D, Goli H, Weiss LS, Dau R, et al. A Modified In vitro Invasion Assay to Determine the Potential Role of Hormones, Cytokines and/or Growth Factors in Mediating Cancer Cell Invasion. J Vis Exp. 2015(98):51480.

172. Kurien BT, Scofield RH. Western blotting. Methods. 2006;38(4):283-93.
173. MeRCK. Sample Buffer, Laemmli 2× Concentrate: MeRCK; [Available from: https://www.sigmaaldrich.com/catalog/product/sigma/s3401?lang=en&region=NO.
174. Scientific T. Pierce™ BCA Protein Assay Kit.
175. experts BaaE. Western Blotting Principle [Available from: https://www.bosterbio.com/protocol-and-troubleshooting/western-blot-principle.
176. TermoFisher Scientific I. Protein transfer technical handbook [Available from: https://assets.thermofisher.com/TFS-Assets/BID/Handbooks/protein-transfer-technical-handbook.pdf?icid=linchpin2-protein-transfer-technical-handbook.
177. Scientific T. Restore™ Western Blot Stripping Buffer [Available from: https://www.thermofisher.com/order/catalog/product/21063?SID=srch-srp-21063#/21063?SID=srch-srp-21063.
178. Arya M, Shergill IS, Williamson M, Gommersall L, Arya N, Patel HR. Basic principles of real-time quantitative PCR. Expert Rev Mol Diagn. 2005;5(2):209-19.
179. Promega. ReliaPrep™ RNA Cell Miniprep System Technical Manual [Available from: https://no.promega.com/-/media/files/resources/protocols/technical-manuals/101/reliaprep-rna-cell-miniprep-system-protocol.pdf?la=en.
180. NanoDrop. 260/280 and 260/230 Ratios NanoDrop® ND-1000 and ND-8000 8-Sample Spectrophotometers ©2007 NanoDrop Technologies, Inc; [Available from: https://www.bio.davidson.edu/projects/gcat/protocols/NanoDrop_tip.pdf.
181. Quantabio. qScript® cDNA Synthesis Kit [Available from: https://www.quantabio.com/media/contenttype/IFU-024.1_REV_02_95047_qScript_cDNA_Synthesis_Kit.pdf.
182. Biosciences Q. PerfeCTa®SYBR®Green SuperMix: Quanta Biosciences [Available from: https://www.quantabio.com/media/wysiwyg/pdfs/95054%20(PerfeCTa%20SYBR%20Green%20Supermix%20PPS).pdf.
183. Tom Strachan APR. Analyzing the stcture and expression of genes and genomes. Human Molecular Genetics. 5th ed: CRC Press. p. 203-40.
184. Molecular Probes i. PrestoBlue™ Cell Viability Reagent Protocol [Available from: https://tools.thermofisher.com/content/sfs/manuals/PrestoBlue_Reagent_PIS_15Oct10.pdf .
185. Scientific T. PrestoBlue™ HS Cell Viability Reagent [Available from: https://www.thermofisher.com/order/catalog/product/P50200?SID=srch-hj-P50200#/P50200?SID=srch-hj-P50200.
186. Spyrou C, Stark R, Lynch AG, Tavaré S. BayesPeak: Bayesian analysis of ChIP-seq data. BMC Bioinformatics. 2009;10(1):299.
187. Urbanucci A, Waltering KK, Suikki HE, Helenius MA, Visakorpi T. Androgen regulation of the androgen receptor coregulators. BMC Cancer. 2008;8:219-.
188. Crona DJ, Whang YE. Androgen Receptor-Dependent and -Independent Mechanisms Involved in Prostate Cancer Therapy Resistance. Cancers. 2017;9(6):67.
189. Karantanos T, Corn PG, Thompson TC. Prostate cancer progression after androgen deprivation therapy: mechanisms of castrate resistance and novel therapeutic approaches. Oncogene. 2013;32(49):5501-11.
190. Urbanucci A, Marttila S, Jänne OA, Visakorpi T. Androgen receptor overexpression alters binding dynamics of the receptor to chromatin and chromatin structure. Prostate. 2012;72(11):1223-32.

191. Wei C, Lin M, Jinjun B, Su F, Dan C, Yan C, et al. Involvement of general control nonderepressible kinase 2 in cancer cell apoptosis by posttranslational mechanisms. Molecular biology of the cell. 2015;26(6):1044-57.
192. Sattlegger E, Hinnebusch AG. Polyribosome binding by GCN1 is required for full activation of eukaryotic translation initiation factor 2{alpha} kinase GCN2 during amino acid starvation. J Biol Chem. 2005;280(16):16514-21.
193. Delmore JE, Issa GC, Lemieux ME, Rahl PB, Shi J, Jacobs HM, et al. BET bromodomain inhibition as a therapeutic strategy to target c-Myc. Cell. 2011;146(6):904-17.
194. Bernard D, Pourtier-Manzanedo A, Gil J, Beach DH. Myc confers androgen-independent prostate cancer cell growth. The Journal of clinical investigation. 2003;112(11):1724-31.
195. Scientific T. Charcoal Stripped Fetal Bovine Serum [Available from: https://www.thermofisher.com/no/en/home/life-science/cell-culture/mammalian-cell-culture/fbs/specialty-serum/charcoal-stripped-fbs.html.
196. Pillai-Kastoori L, Heaton S, Shiflett SD, Roberts AC, Solache A, Schutz-Geschwender AR. Antibody validation for Western blot: By the user, for the user. The Journal of biological chemistry. 2020;295(4):926-39.
197. Voskuil J. Commercial antibodies and their validation. 2014.
198. Helleday T. The underlying mechanism for the PARP and BRCA synthetic lethality: clearing up the misunderstandings. Mol Oncol. 2011;5(4):387-93.
199. Administration USFaD. FDA approves niraparib for first-line maintenance of advanced ovarian cancer [Available from: https://www.fda.gov/drugs/drug-approvals-and-databases/fda-approves-niraparib-first-line-maintenance-advanced-ovarian-cancer.

APPENDIX

Appendix A: Material

Cell culture: All the cell lines were provided by Dr. Alfonso Urbanucci and Dr. Beata Grallert.

Cell culture medium and sterile solutions

Type	Product	Reference number	Supplier
Growth media	RPMI -1640 medium without L-glutamine and sodium bicarbonate, liquid sterile filtered	RNBJ9375	SIGMA life science
	RPMI 1640 medium, no phenol red	11835030	Gibco™
	RPMI-1640 medium	R8758-6	Merck life science
Sterile solutions	Phosphate Buffered Saline PBS, pH 7.2	20012068	ThermoFisher
	Trypsine –EDTA (0.25%) phenol red	25200056	ThermoFisher
Supplements	Fetal Bovine Serum, FBS	RNBH0548	ThermoFisher
	Glutamax	A1286001	ThermoFisher
	Hyclone FBS	SH30070.03	ThermoFisher
	Penicillin-Streptomycin (PS)	15140122	ThermoFisher
	Geneticin	ant-gn-1	InvivoGen
	Enzalutamide (MDV3100)	HY-70002	MedChemExpress
	Dihydrotestosterone (DHT)	S4757	Selleckchem
	Dimethyl sulfoxide DMSO	D8418-250 mL	Merck Sigma
	Doxocycline	D9891-5G	Merck

	GCN2-IN-1, GCN2i	HY-100877	MedChemExpress

Antibody

Antibody		Dilution	Reference number	Supplier
Primary	GCN2 phospho (GCN2-P) antibody	1:1000	94668	Cell signalling
	GCN2 total (GCN2-T) antibody	1:1000	3302	Cell signalling
	GCN1L1 antibody	1:500	PA5-54043	ThermoFisher
	eIF2-α-total antibody	1:1000	701640	ThermoFisher
	eIF2-α-phospho antibody	1:1000	44-728G	Life technologies
	ATF4-antibody	1:500	11815	Cell signalling
	Anti-γ-tubulin Antibody	1:50 000	T6557	Sigma-Aldrich
Secondary	Anti-Mouse IgG	1:5000	7076S	Cell signaling
	Anti-Rabbit IgG	1:5000	7074S	Cell signaling

Materials and kits used in various methods

RNA isolation and PCR	Reference Number	Supplier
ReliaPrep RNA Cell Miniprep System	PAZ6011	Promega
qScript® cDNA Synthesis Kit	95047-025	Quantabio
PerfeCTa® SYBR® Green super mix kit	95054-100	Quanta Biosciences
Tubes, 0.2 mL, flat cap	AB0620	ThermoFisher
Cell culture		
35 mm Cell Culture Dish, Falcon®	734-0005	VWR
60 mm Cell Culture Dish, Falcon®	734-0007	VWR

T25 filter cap Nunc™ Cell Culture Treated EasYFlasks™	734-2064	VWR
T75 filter cap Nunc™ Cell Culture Treated EasYFlasks™	734-2066	VWR
96 Well Black Polystyrene Microplate	CLS3603-48EA	Merck
96-well microplate, flat-bottom: Transparent:	734-2097	VWR
96-well, semi-skirted, flat deck	AB1400	ThermoFisher
Countess™ Cell Counting Chamber Slides	C10228	ThermoFisher
Pasteur pipets, glass	612-1702	VWR
Disposable Serological Pipets, 5 mL	13-676-10H	Fisher Scientific
Disposable Serological Pipets, 10 mL	13-676-10J	Fisher Scientific
Disposable Serological Pipets, 25 mL	13-676-10K	Fisher Scientific
Culture tubes, round bottom, sterile, 17x100 mm	60818-667	VWR
Immunoblotting		
BCA™ Protein Assay Kit	23225	ThermoFisher
Criterion™ TGX™ Precast Gels, 4-15 %	5671084	BioRad
Trans-Blot Turbo RTA Transfer Kit, PVDF	1704273	BioRad
Cell scraper	179693	ThermoFisher
Precision Plus ProteinTM Dual Color Standards	1610374	BIO-RAD
Cell viability assay		
PrestoBlue™ Cell Viability Reagent	A13261	Invitrogen

Reagents used in various methods

Reagent	**Reference number**	**Supplier**
Trypan Blue Stain (0.4%)	T10282	ThermoFisher
Re-BlotPlus Mild Antibody Stripping Solution	2502	Sigma-Aldrich
Immobilon® Western Chemiluminescence HRP Substrate	WBKLS0500	Sigma-Aldrich

Skim Milk Powder	70166-500G	Sigma-Aldrich
Absolute ethanol		VWR
BSA, DTT, EDTA, glycerol, $MgCl_2$, MTT, NaCl, SDS, Tris-base, Tris-HCl, Triton-X-100, Tween-20		ThermoFisher

Instruments

Instrument	Supplier
AE31 Trinocular Microscope	Motic
Allegra X-12R Centrifuge	VWR
Autoflow IR direct heat CO_2 incubator with HEPA filter ISO class 5	VWR
Bio Wizard Golden line GL-130 Laminar flow hood class II	KOJAIR
Biofuge Fresco refrigerating centrifuge	Heraeus
CFX connect real-time PCR detection system	BIO-RAD
ChemiDoc™ MP Imaging System	BIO-RAD
Countess™ II Automated Cell Counter	Invitrogen
Criterion™ Vertival Electrophoresis Cell	BIO-RAD
Engine Tetrad® 2 Thermal Cycler	BIO-RAD
Fume hood with UV lamp and protection glass	ADDVISE
Grant GD100 Stirred Water Batch	Keison Products
Heating block Grant Boekel	BBD
Integra Pipetboy	IBS Biosciences
Lab water purification system for Milli-Q water	ELGA
Modulus Microplate Multimode reader	Turner BioSystems
Multiscan FC microplate photometer	TermoFisher
NanoDrop spectrophotometer	ThermoFisher
PowerPac 300 Electrophoresis Power Supply	BIO-RAD
Trans-Blot® Turbo™ Transfer System	BIO-RAD
Universal Refrigerated Centrifuge Model 5910	Kubota
Universal Refrigerated Centrifuge Model 5930	Kubota

Vortex MSI Minishaker IKA®	Sigma-Aldrich
VWB18 water bath	VWR
X-ray 225	Precision Xray Inc

Buffers

Buffer/ solution	Components	Concentration
Laemmli Buffer 2X	Tris-HCl, pH = 6.8	65.8 mM
	Glycerol	26.3 %
	SDS	2.1 %
	Bromophenol blue	0.01 %
	Milli-Q H_2O	To desired volume
Loading buffer	DTT	100 mM
	Laemmli Buffer 2X	1X
	Lysate	To desired volume
Running buffer 10X	Tris-base	30.2 g/ L
	Glycine	144 g/ L
	Milli-Q H_2O	To desired volume
Running buffer	Running buffer 10X	1X
	SDS	10 %
	Milli-Q H_2O	To desired volume
Transfer buffer	Transfer buffer 5X (BIO-RAD)	1X
	Absolute EtOH	20 %
	Milli-Q H_2O	To desired volume
TBS (10X)	Tris-HCl, pH = 7.5	200 mM
	NaCl	80 g
	Milli-Q H_2O	To desired volume
TBS-Tween	TBS 10X	1X
	Tween 20	0.1 %
	Milli-Q H_2O	To desired volume

Primers

Name	Direction	Sequence	Supplier
GCN1	Forward	CCAGGCAATTGTCAACCTCC	Integrated DNA technologies IDT
GCN1	Reverse	CTCGTTCAGCACCTCCAAAC	Integrated DNA technologies IDT
GCN2	Forward	ATGGCAGAGAAGCTTCCGAT	ThermoFisher
GCN2	Reverse	GGCAAGGGAGGTCTGAAGTC	ThermoFisher
KLK3 or PSA	Forward	CAGCATTGAACCAGAGGAG	Integrated DNA technologies IDT
KLK3 or PSA	Reverse	GTCGTAACTTGGTCTCCTC	Integrated DNA technologies IDT
TBP	Forward	GGGGAGCTGTGATGTGAAGT	Integrated DNA technologies IDT
TBP	Reverse	CCCCTCGACACTACACTTCA	Integrated DNA technologies IDT

Software used in different methods

Software	Developer
Image Lab	BIO-RAD
Office Excel 2016	Microsoft
Office PowerPoint 2016	Microsoft
Office Word 2016	Microsoft
NanoDrop1000 software	Thermo Scientific
Bio-Rad CFX Manager	BIO-RAD

Appendix B: Western Blot

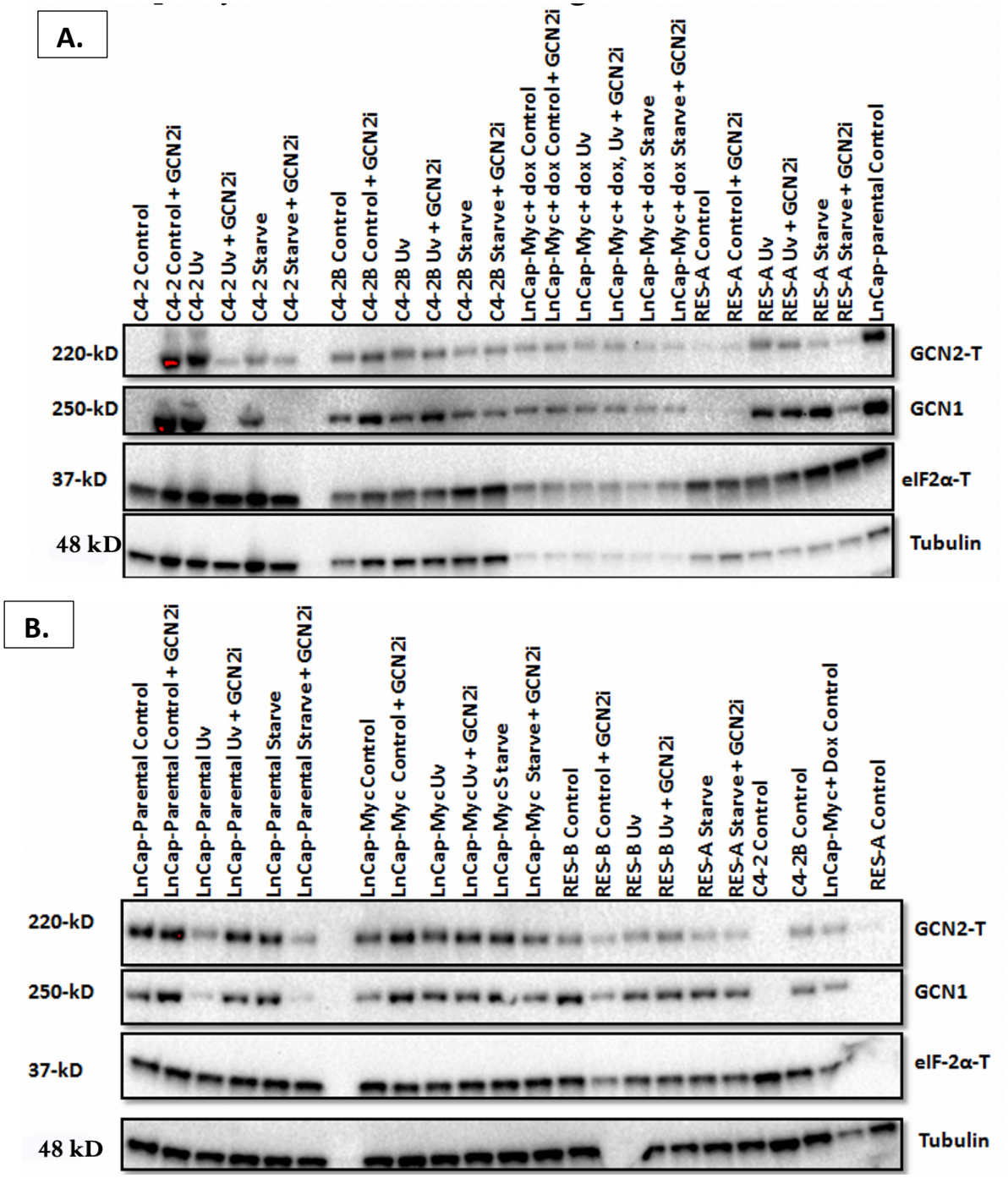

Figure B1: GCN2 and GCN1 protein in various PC cell lines. A) and B) Western blot image representation of six PC cell lines. C4-2, C4-2B, LNCaP-parental, LNCaP-MYC, RES-A, RES-B cells were seeded in PDL coated 35 mm dishes, resistance cells were grown in red media containing 10μM enzalutamide and half of the LNCaP-MYC cells were treated with 2µg/mL doxycycline. All the cells were incubated for 36 hours, after 36 hours these cells were incubated with 3 μM GCN2i for 2 hours. After incubation these cells were either UV irradiated or treated with salt-based starvation media. Western blot image shows GCN2-total (GCN2-T, 220 kD), GCN1 (250 kD), eIF2-α-total (eIF2-α-T, 37 kD) and γ-tubulin (48-kD).

Appendix C: GCN2 and GCN1 primers

A.

```
File Name       20210215_test_old_template_2012-GCN2-483-4_585-6_ATAD2_TBP_with_BCat_series_samples-2013.pcrd
Created By User admin
Notes
ID
Run Started     15.02.2021 15:50:49 UTC +01:00
Run Ended       15.02.2021 17:17:52 UTC +01:00
Sample Vol      10
Lid Temp        105
Protocol File Name      Standard protocol.prcl
Plate Setup File Name   Quick Plate_96 wells_SYBR Only.pltd
Base Serial Number      BR001734
Optical Head Serial Number      788BR01890
CFX Manager Version     3.0.1224.1015.

Well group      All Wells
Amplification step      3
Melt step       6
```

Well	Fluor	Target	Content	Sample	Cq	Starting Quantity (SQ)		Melt Temperature
C01	SYBR		Std		25,22	1.000E+03		81,00
C02	SYBR		Std		25,47	1.000E+03		81,00
C03	SYBR		Std		27,34	2.000E+02		81,00
C04	SYBR		Std		27,07	2.000E+02		81,00
C05	SYBR		Std		29,31	4.000E+01		81,00
C06	SYBR		Std		29,06	4.000E+01		81,00
C07	SYBR		Std		32,20	8.000E+00		81,00
C08	SYBR		Std		32,01	8.000E+00		81,00
C09	SYBR		Std		33,85	1.600E+00		81,00
C10	SYBR		Std		34,15	1.600E+00		81,00
C11	SYBR		Unkn		24,13	2.061E+03		81,00
C12	SYBR		Unkn		24,44	1.648E+03		81,00
D01	SYBR		Unkn		24,38	1.722E+03		81,00
D02	SYBR		Unkn		N/A	N/A	None	
D03	SYBR		Unkn		24,13	2.063E+03		81,00
D04	SYBR		Unkn		24,23	1.909E+03		81,00
D05	SYBR		Unkn		24,34	1.770E+03		81,00
D06	SYBR		Unkn		24,35	1.753E+03		81,00
D07	SYBR		Unkn		24,02	2.224E+03		81,00
D08	SYBR		Unkn		24,05	2.183E+03		81,00
D09	SYBR		Unkn		24,28	1.848E+03		81,00
D10	SYBR		Unkn		24,31	1.803E+03		81,00
D11	SYBR		Neg Ctrl			N/A	N/A	None
D12	SYBR		Neg Ctrl			N/A	N/A	None

B.

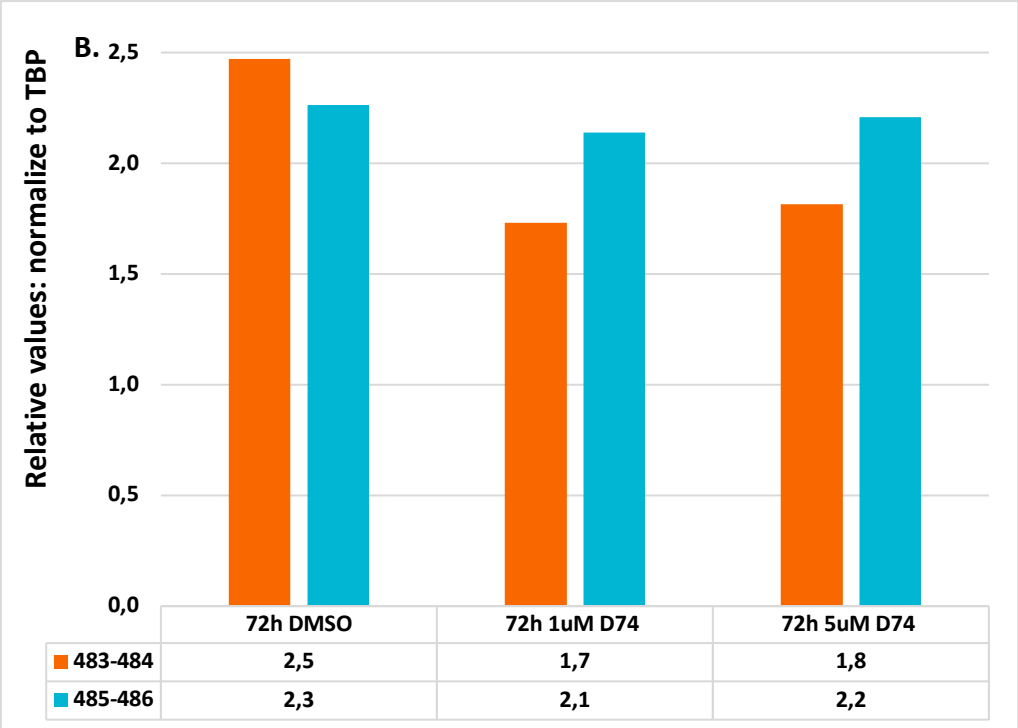

	72h DMSO	72h 1uM D74	72h 5uM D74
483-484	2,5	1,7	1,8
485-486	2,3	2,1	2,2

C.

File Name 2021-03-16_First_biological_sample_GCN1_psA_AND_tBP_BR001734.pcrd
Created By User admin
Notes
ID
Run Started 16.03.2021 18:09:56 UTC +01:00
Run Ended 16.03.2021 19:36:22 UTC +01:00
Sample Vol 10
Lid Temp 105
Protocol File Name Standard protocol.prcl
Plate Setup File Name Quick Plate_96 wells_SYBR Only.pltd
Base Serial Number BR001734
Optical Head Serial Number 788BR01890
CFX Manager Version 3.0.1224.1015.

Well group All Wells
Amplification step 3
Melt step 6

Well	Fluor	Target	Content	Sample	Cq	Starting Quantity (SQ)			Melt Temperature	
A01	SYBR		Std		20,33	1.000E+03		82,50	270,47	
A02	SYBR		Std		20,48	1.000E+03		82,50	265,95	
A03	SYBR		Std		22,49	2.000E+02		82,50	251,76	
A04	SYBR		Std		22,16	2.000E+02		82,50	260,57	
A05	SYBR		Std		24,84	4.000E+01		82,50	252,86	
A06	SYBR		Std		24,82	4.000E+01		82,50	275,60	
A07	SYBR		Std		27,44	8.000E+00		82,50	243,62	
A08	SYBR		Std		27,81	8.000E+00		82,50	186,25	
A09	SYBR		Std		29,30	1.600E+00		82,00	225,76	
A10	SYBR		Std		29,79	1.600E+00		82,00	196,79	
A11	SYBR		Std		33,73	3.200E-01		82,00	107,23	
A12	SYBR		Std		31,93	3.200E-01		82,00	195,42	
B01	SYBR		Unkn		24,33	6.298E+01		82,50	251,39	
B02	SYBR		Unkn		23,88	8.437E+01		82,50	242,09	
B03	SYBR		Unkn		23,19	1.318E+02		82,50	270,58	
B04	SYBR		Unkn		22,95	1.540E+02		82,50	294,99	
B05	SYBR		Unkn		24,10	7.296E+01		82,50	289,63	
B06	SYBR		Unkn		22,31	2.333E+02		82,50	300,84	
B07	SYBR		Unkn		23,58	1.026E+02		82,50	282,36	
B08	SYBR		Unkn		24,40	5.994E+01		82,50	262,53	
B09	SYBR		Unkn		22,94	1.550E+02		82,50	309,68	
B10	SYBR		Unkn		23,04	1.449E+02		82,50	292,01	
B11	SYBR		Unkn		22,98	1.508E+02		82,50	251,46	
B12	SYBR		Unkn		22,23	2.461E+02		82,50	255,30	
C01	SYBR		Unkn		22,11	2.660E+02		82,50	300,54	
C02	SYBR		Unkn		22,36	2.258E+02		82,50	283,48	
C03	SYBR		Unkn		23,27	1.252E+02		82,50	319,06	
C04	SYBR		Unkn		23,08	1.417E+02		82,50	345,53	
C05	SYBR		Unkn		22,51	2.051E+02		86,00	210,49	
C06	SYBR		Unkn		21,11	5.087E+02		86,00	195,60	
C07	SYBR		Unkn		22,29	2.373E+02		86,00	205,78	
C08	SYBR		Unkn		20,00	1.050E+03		86,00	201,97	
C09	SYBR		Unkn		22,23	2.459E+02		86,00	194,83	
C10	SYBR		Unkn		19,80	1.200E+03		86,00	213,75	
C11	SYBR		Unkn		21,07	5.253E+02		86,00	201,77	
C12	SYBR		Unkn		19,46	1.493E+03		86,00	177,01	
D01	SYBR		Unkn		26,83	1.234E+01		77,50	235,03	
D02	SYBR		Unkn		26,27	1.773E+01		77,50	255,67	
D03	SYBR		Unkn		28,06	5.555E+00		77,50	187,65	
D04	SYBR		Unkn		26,26	1.790E+01		77,50	253,71	
D05	SYBR		Unkn		25,90	2.260E+01		77,50	287,13	
D06	SYBR		Unkn		26,25	1.797E+01		77,50	313,18	
D07	SYBR		Unkn		25,15	3.686E+01		77,50	328,85	
D08	SYBR		Unkn		25,98	2.149E+01		77,50	312,71	
D09	SYBR		Neg Ctrl			38,13	7.910E-03		75,50	131,85
D10	SYBR		Neg Ctrl			N/A	N/A	None	None	
D11	SYBR		Unkn		N/A	N/A	None	None		
D12	SYBR		Unkn		N/A	N/A	None	None		

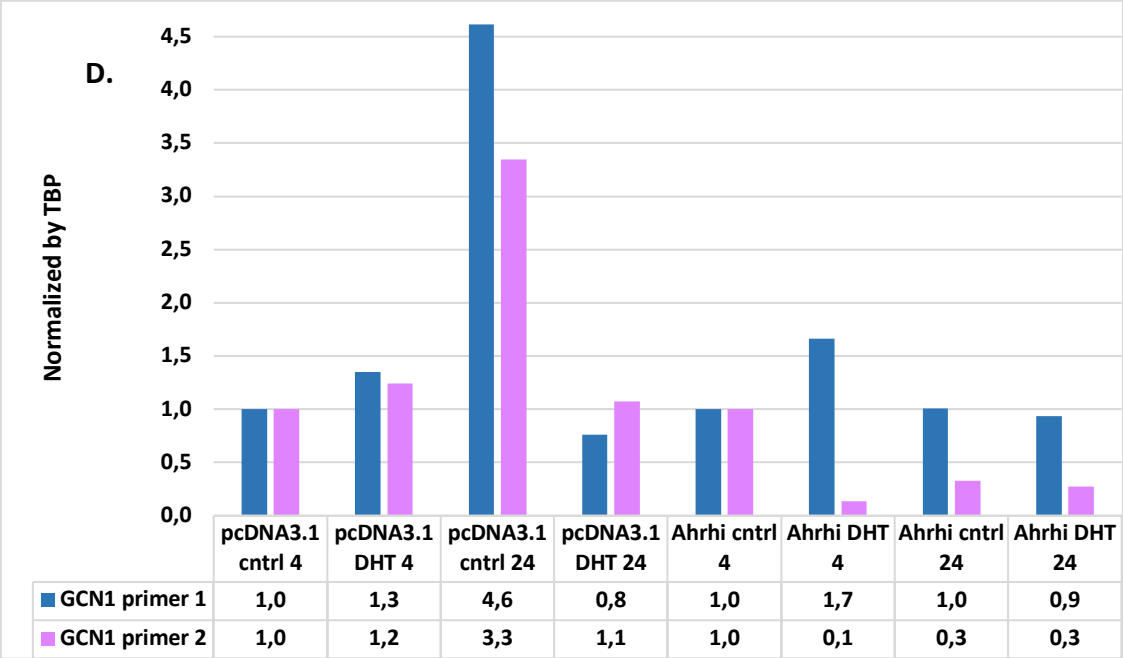

	pcDNA3.1 cntrl 4	pcDNA3.1 DHT 4	pcDNA3.1 cntrl 24	pcDNA3.1 DHT 24	Ahrhi cntrl 4	Ahrhi DHT 4	Ahrhi cntrl 24	Ahrhi DHT 24
GCN1 primer 1	1,0	1,3	4,6	0,8	1,0	1,7	1,0	0,9
GCN1 primer 2	1,0	1,2	3,3	1,1	1,0	0,1	0,3	0,3

Figure C1: Testing GCN2 and GCN1 primer. A) Representation of CFX Maestro software datasheet of GCN2 primer sets 483-484 and 485-486. **B)** Bar graph representation of mean relative values of three samples normalize to TBP. These samples were provided by Dr. Alfonso Urbanucci. **C)** Representation of CFX Maestro software datasheet of GCN1 primer sets, AU37-AU38 and AU39 and AU40. **D)** Bar graph represents relative values of eight samples normalize to TBP and then normalize to 4-hour control in each cell lines at different time points. These values were measured using primer set 1 (AU37-AU38) and primer set 2 (AU39-AU40). Bar graphs represents mean values of two technical repeats.